N_2O Production and Removal in Streambed Sediments: Understanding Physicochemical Influences on N_2O Fluxes from Agricultural Streams on the Eastern Shore of Virginia

Anne Elaine Dunckel
San Antonio, Texas

B.S. University of Texas, 2009

A Thesis presented to the Graduate Faculty
of the University of Virginia in Candidacy for the Degree of
Master of Science

Department of Environmental Sciences

University of Virginia
May, 2014

_____

_____

_____

_____

Abstract

N_2O production and removal within sediments of gaining, low-relief coastal streams proximal to agricultural fields was examined in the context of how changes in temperature, NO_3^- concentration, and pore water velocity can affect the concentration of N_2O in the groundwater and efflux of N_2O from the sediment. Sediment cores extracted from Cobb Mill Creek (CMC), a 2nd order stream, on the Eastern Shore of Virginia were used as vertical-flow columns and operated under conditions that varied, in turn, each of the aforementioned parameters systematically, resulting in 36 scenarios. Pore water samples were extracted after equilibration in each scenario from ports in the columns and were analyzed for major anions and N_2O. Nitrate concentration was the strongest control on N_2O efflux followed by temperature, where increasing NO_3^- concentration and temperature each resulted in an increase of N_2O efflux and N_2O yield. As NO_3^- concentration increased from 3.5 to 18 mg N L^{-1}, mean N_2O fluxes increased from 91 to 284 µg N m^{-2} h^{-1} and N_2O yield increased from 0.15% to 1.75%, respectively. Pore water velocity had minimal effect on N_2O efflux due to a net balance of production and removal along the flow path and advection rates. Within the columns distinct areas of N_2O production followed by areas of removal were observed. These zones were positioned deeper in the column at higher temperature and at slower pore water velocities. The overall mean N_2O flux for all 36 environmental scenarios was 156 µg N m^{-2} h^{-1}. In addition to the column study, N_2O efflux and production at depth was studied *in situ* at CMC for each season of 2013. Denitrification was found to occur prior to the shallow biologically active zone in the sediments causing a buildup of N_2O at 70 cm depth. A seasonal lag in groundwater temperature resulted in warm groundwater temperatures in the winter which coincided with

increased denitrification and mean N_2O fluxes of 568 µg N m^{-2} h^{-1}. All other mean seasonal fluxes were between 4 and 8 µg N m^{-2} h^{-1}. On average, concentrations of N_2O were less at 5 cm depth than at 70 cm, indicating N_2O removal along a vertical flow path. Despite overall removal of N_2O, singular locations of concentrated N_2O production at the sediment surface were found to contribute 37 to 97% of the N_2O efflux to the surface water. Overall, projected increases in groundwater NO_3^- in agricultural areas suggest that there could be significant impacts to enhancing N_2O emissions from biologically active streambed sediments, especially when coupled with projected temperature increases.

Table of Contents

List of Figures

List of Tables

1 Introduction

1.1 Overview

Some streams draining agricultural areas on the Eastern Shore of Virginia provide a significant ecosystem service by removing nitrate contamination in the groundwater as it passes through active denitrification zones in streambed sediments (Galvotti, 2004; Mills *et al.*, 2008; Flewelling, 2009). However, this service comes with a cost. Nitrous oxide (N_2O), a significant greenhouse gas, is a byproduct of denitrification (Smith, 1997; Galloway *et al.*, 2004; Beaulieu *et al.*, 2007). Currently, there are no estimates or measurements of N_2O emissions from streams on the Eastern Shore where significant denitrification has been observed. This study seeks to fill this gap in knowledge by measuring N_2O production in sediment cores taken from a stream on the Eastern Shore and incubated under controlled conditions along with measuring of N_2O efflux in the field over four seasons. The major objective of this study was to explore how varying environmental factors including temperature, nitrate concentration, and pore water velocity, affect N_2O fluxes from streambed sediments.

1.2 N_2O

Over the past four decades, attention has been drawn to the increasing concentration of N_2O in the atmosphere and emissions of N_2O are predicted to increase from 12 Tg N per year in 2000 to 16 Tg N per year 2050 (Bouwman, 2013). Initially concern was brought over the increasing concentration of N_2O in conjunction with other ozone-depleting pollutants that destroy significant amounts of stratospheric ozone (Crutzen, 1981). N_2O is fairly stable in the troposphere with a residence time of ~100 years (Wuebbles, 2009). As a result N_2O emitted in the troposphere is able to persist and transfer into the stratosphere where it is the principle source of stratospheric NO_x radicals that destroy ozone in catalytic cycles (Wayne, 2000). Before the

Montreal Protocol (MP) was globally enacted, N_2O was less important to the depletion of ozone in comparison to chlorofluorocarbons (CFCs). However, recently, through the success of the MP in regulating CFCs and bromine-containing halocarbons, N_2O has risen to become the most important ozone-depleting substance emitted and will remain in that position throughout the 21st century (Ravishankara *et al.*, 2009).

In addition, recent concerns focus on N_2O as one of the major greenhouse gasses in our atmosphere today (Bouwman, 1996). N_2O has a global warming potential (GWP) of 298, which is a measure of the ability of a green-house gas to trap infrared radiation in the atmosphere relative to that of carbon dioxide over a 100-year time period factoring in the gas's residence time in the atmosphere (Forster *et al.*, 2007), i.e., the GWP of CO_2 is 1. Today, N_2O is present in the atmosphere at trace levels of 325 ppb. However, due the long residence time of N_2O in the atmosphere and the resulting high GWP, N_2O is seen as a significant factor in global warming over an extended period. Currently, roughly 6% of the observed greenhouse effect is attributed to the traces of N_2O that are currently in the atmosphere (Forster *et al.*, 2007).

N_2O is emitted from many different anthropogenic and natural processes. Industrial production such as manufacturing of nitric acid and nylon in addition to fossil fuel combustion are the leading abiotic anthropogenic sources of N_2O. Naturally, as part of the nitrogen cycle, N_2O is produced during the microbial processes of denitrification and nitrification, and to a minor extent through fungal and nitrifier denitrification, and dissimilatory nitrate reduction (Hynes & Knowles, 1984). Nitrification is the aerobic oxidation of ammonia to nitrate through a multiple step process that produces N_2O as a byproduct (Hynes & Knowles, 1984) (Equation 1-1). Denitrification is the anaerobic reduction of nitrate to the non-reactive form N_2 (Equation 1-2). During denitrification, N_2O is produced as an intermediate product, and, whereas, in closed

systems it will be entirely reduced to N_2, in open systems, some of the N_2O often escapes before being fully reduced. Additionally, if conditions inhibit N_2O reduction, N_2O will remain as the terminal product (Tiedje, 1988). Soils contain a matrix of oxic and anoxic microsites that provide environments for both nitrification and denitrification leading to N_2O production to occur, often simultaneously. However, in anoxic environments such as saturated stream bed sediments, nitrification is non-existent, and denitrification is the dominant process producing N_2O (Knowles, 1982; Groffman, 1994).

Nitrification

$$\begin{array}{ccccccc} & & N_2O & & N_2O & & \\ & & \uparrow & & \uparrow & & \\ NH_4^+ & \rightarrow & NH_2OH & \rightarrow & NO_2^- & \rightarrow & NO_3^- \end{array}$$

Equation 1-1

Denitrification

$$NO_3^- \rightarrow NO_2^- \rightarrow NO \rightarrow N_2O \rightarrow N_2$$

Equation 1-2

N_2O emissions have increased by about 40 to 50% over pre-industrial levels as a result of human activity and disruption of the natural nitrogen cycle (Hirsch *et al.*, 2006). Most notably modern agriculture is the single largest anthropogenic source of N_2O as a byproduct of the use of synthetic nitrogen fertilizer, increases in nitrogen fixing crops, land use change, and increased manure application (Galloway *et al.*, 2004). The creation of the Haber-Bosch process in 1913 was an immense boon to agriculture and food stocks all over the globe as it doubled the amount of reactive nitrogen (Nr) available for plant production. The resulting growth of population and the positive feedback give incentive for increasing agricultural intensity which has perpetuated the increase of Nr in the environment to 187 Tg N per year in 2005 (Smith *et al.*, 2010). This has not come without negative impacts following the cascade of Nr through terrestrial and aquatic

systems (Galloway *et al.*, 2003). Excess Nr in ecosystems causes eutrophication leading to anoxic dead zones, soil and water acidification, declines in marine fisheries, increases air pollution, stratospheric ozone depletion, global warming, and reduces biological [*Galloway et al.*, 2003; *Nixon*, 1995; *Tilman*, 1987; *Vitousek et al.*, 1997, *and references therein*].

As the population on earth and the concomitant demand for food grows, there will likely be a continued increase in the amount of nitrogen fertilizer used for agricultural applications as well as the use of nitrogen fixing plants. It is estimated that roughly 1% of all added Nr in the form of nitrogen fertilizers or waste deposited from farm animals will be converted to N_2O directly at the application site (Eggleston *et al.*, 2006). However, an estimated 30 to 50% of added Nr to agricultural lands is leached in the form of NO_3^- through surface water runoff or groundwater flow and is discharged into ditches, streams, rivers, and estuaries. Along this pathway N_2O is emitted as NO_3^- is denitrified. N_2O emitted from these indirect sources is estimated to be 0.75% of leached nitrogen (Eggleston *et al.*, 2006). As the amount of fertilizer use grows, the amount of N_2O in the atmosphere will continue to climb from both direct and indirect sources. Currently, however, the uncertainty associated with estimating indirect emissions is almost two orders of magnitude larger than any uncertainty for estimates of other N_2O sources at 1.6 Tg N per year with an estimate range of 0.13 to 7.7 Tg N per year (Nevison, 2000). This range of estimates accounts for half the uncertainty in the Intergovernmental Panel on Climate Change (IPCC) calculations of agricultural contributions to global N_2O budgets (Nevison, 2000; Reay *et al.*, 2005; Eggleston *et al.*, 2006). While our inability to fully model and predict N_2O emissions from agricultural activities persists, we will be unable to balance the global N_2O budget. Research focused on quantifying the heterogeneity of N_2O emissions from

indirect sources is essential to closing this budget and to better constrain our predictions of global N_2O emissions as a result of agricultural intensification.

1.3 Controls on N_2O Production and Denitrification Inefficiency

The molar fraction of N_2O produced during denitrification in comparison to that of N_2 is of much interest in the overall understanding of how much N_2O is emitted from nitrate-contaminated environments. This ratio is the common methodology used to determine the denitrification efficiency of a particular system. In other words, denitrification efficiency quantifies how the current or changing environmental parameters effect to what extent denitrification goes to completion resulting in N_2 or terminates early at N_2O. Numerous soil studies have investigated how the N_2/N_2O ratio changes with varying environmental parameters such as the fraction of water-filled pore space, soil texture, temperature, O_2, pH, different carbon sources, and more. Soil studies have been on the front line of this issue and dominate the available literature. Denitrification in terrestrial soils is the largest land based process for nitrogen removal at 124 Tg N per year; less than 50 Tg N per year is removed from groundwater, lakes, and rivers individually (Seitzinger *et al.*, 2006). As a result, direct soil emissions of N_2O additively account for a significant proportion of the total terrestrial N_2O flux occurring over a large surface area of agricultural fields, forests, and grasslands (Bouwman *et al.*, 2010).

In soils, denitrification efficiency increases with increasing water-filled pore space (Nommik, 1956; Weier *et al.*, 1993). Larger wetted areas means that any N_2O produced from denitrification has to travel a longer path for before it can escape being fully reduced to N_2, thus reducing the amount of N_2O that is able to escape. Increasing NO_3^- concentration decreases denitrification efficiency in soils (Nommik, 1956; Blackmer & Bremner, 1978; Weier *et al.*,

1993). NO_3^- is found to have an inhibitory effect on denitrifiers and is hypothesized to be caused by high concentrations of NO_3^- suppressing the transcription of N_2O reducing enzymes thus allowing N_2O to accumulate while NO_3^- is continued to be reduced (Bergaust *et al.*, 2011). In addition, the denitrification efficiency of a soil decreases with decreasing pH due to the inhibitory effect of pH on the full reduction of N_2O or other indirect effects (Nommik, 1956; Šimek & Cooper, 2002). Nommik [1956], in his seminal work on denitrification efficiency found that below a pH of 6 roughly equal parts N_2O and N_2 were being produced and at a lower pH N_2O was the dominant nitrogen gas produced. Overall, N_2O production is relatively higher under conditions that are suboptimal for denitrification (Hefting *et al.*, 2003).

Although increasing temperature is widely known to increase the N_2/N_2O ratio, an increase in temperature does not necessarily mean a decrease in N_2O emissions. Warmer temperatures result in an overall increase in denitrification rates and ultimately an increase in both N_2 and N_2O production as temperature-induced increase in respiration results in an increase in the anaerobic volume (Smith, 1997; Holtan-Hartwig *et al.*, 2002). A review of Q_{10} values for N_2O from both field and laboratory soil experiments shows a range of positive values from 1 to 23 (Smith, 1997). The studies that showed the largest Q_{10} values were all from fertilized grasslands versus lower values of Q_{10} (1-5) that were predominantly from laboratory studies and a variety of field environments (Smith, 1997). Indeed, field studies have shown a seasonal trend in increased N_2O emissions corresponding with warmer spring and summer seasons (Hefting *et al.*, 2003).

1.4 N_2O Emissions from Riparian Zones, Streams, and Rivers

While soil studies provide a foundation of understanding how N_2O production is affected by environmental parameters in static closed flasks or unsaturated field conditions, they cannot

fully predict what we will observe in saturated sediments under advective processes. At the moment, few studies have focused on understanding how environmental factors alter N_2O emissions in advective and saturated systems. While soils are responsible for a large portion of denitrification within a watershed on a per-area basis, denitrification rates are ~75 mmol N m^{-2} per year compared to ~900 mmol N m^{-2} per year found in river ecosystems (Seitzinger *et al.*, 2006). Denitrification in aquatic habitats is of extreme importance as anthropogenic loading of Nr into aquatic systems is predicted to increase from the 1990's level of 1.05 Tg N per year to 3.22 Tg N per year by 2050 (Seitzinger *et al.*, 2000). Worldwide, rivers show the highest denitrification rates, up to 3.72 mol N m^{-2} per year when compared to coastal areas, estuaries, and lakes, with the highest rates occurring during the summer months (Piña-Ochoa & Álvarez-Cobelas, 2006).

Rivers and their surrounding riparian zones are prime locations for denitrification to occur and often provide a valued ecosystem service of removing excess NO_3^- in contaminated waters (Tesoriero *et al.*, 2000; McClain *et al.*, 2003; Ocampo *et al.*, 2006). Most NO_3^--contaminated aquifers are void of large amounts of organic carbon, and they often remain fairly oxic at depth. Therefore they lack sufficient denitrification capacity to remove excess NO_3^- (Lowrance *et al.*, 1997). Aquifers beneath riparian zones and rivers, on the other hand, often contain substantial amounts of carbon, and thus shallow groundwater beneath these surface features can become anoxic and can support denitrification (Groffman, 1994; Hill, 1996; Hedin *et al.*, 1998; Ocampo *et al.*, 2006; Seitzinger *et al.*, 2006). Groundwater flow through these areas can follow two major flow paths. A shallow riparian-influenced flow path passes through the biologically active area below the riparian root zone and the water chemistry is altered through biological uptake and evapotranspiration (Mulholland & Hill, 1997; Gu *et al.*, 2008a; Flewelling,

2009). A deeper flow path that discharges directly into the stream or river bypasses the chemical alterations of the near-surface portions of the riparian zone and usually delivers higher concentrations of NO_3^- to surface water (Mulholland & Hill, 1997). Both flow paths experience an increased potential for denitrification whether it be in the root zone or in near-streambed sediments where ample organic-carbon sources exist (Hedin *et al.*, 1998; Gu *et al.*, 2007; Flewelling, 2009). As increased levels of NO_3^- are leached to aquifers and flow through nearby riparian zones and streambeds characterized by significant denitrification capacity we should expect to see a concomitant increase in the ability of these areas to emit N_2O.

Recently, researchers have been deriving reach-scale N_2O fluxes from streams and rivers using NO_3^- and gas tracers in combination with wind models (Cole & Caraco, 2001; Clough *et al.*, 2006; Beaulieu *et al.*, 2011). The largest study of this type, the Lotic Intersite Nitrogen eXperiment (LINX II) studied N_2O fluxes resulting from water column processes in 72 streams across 3 land-use categories. They found that, on average, the streams emitted a total of 37 µg N_2O-N $m^{-2}h^{-1}$. Only 27% of the flux could be attributed to water column processes while 27 µg N_2O-N $m^{-2}h^{-1}$ was estimated to come from unmeasured sources such as groundwater (Beaulieu *et al.*, 2011). The LINX II study points to the existence of a significant undefined source of N_2O in streams that results in waters supersaturated with respect to N_2O. A sediment-column study investigating hyporheic exchange effects on benthic N_2O fluxes found similar values of 7.5 to 124 µg N_2O-N $m^{-2}h^{-1}$ (Silvennoinen *et al.*, 2008a).

Both these studies focus on water column and hyporheic processes much like the other few studies that exist on N_2O emissions from streams and rivers (Cole & Caraco, 2001; Clough *et al.*, 2006; Beaulieu *et al.*, 2011). These studies only look at the processing of stream water NO_3^- concentrations within the water column and through exchange with the hyporheic zone

where NO_3^- concentrations have already been largely reduced due to previous denitrification along groundwater flow paths. There have been no studies to my knowledge that have investigated the production of N_2O derived from denitrification along the flow path of groundwater discharging into streams and rivers. There is a paucity of work quantifying the amount of N_2O emitted from river and stream bed sediments across all scales, including small, low-relief agricultural streams such as those found on Virginia's Eastern Shore.

1.5 Nitrate Pollution and Denitrification on the ESVA

On the Eastern Shore of Virginia, where roughly 37% of land is agricultural, heavy fertilizer use has contaminated the shallow unconfined Columbia aquifer to levels 2 to 3 times the USEPA drinking water limit of 10 mg NO_3^--N L^{-1} (Debrewer *et al.*, 2007a; Mills *et al.*, 2008; USDA, 2009). Given that there is very little biological activity in the sandy unconfined aquifer receiving the fertilizer N, these high levels of NO_3^- threaten to discharge into nearby riparian areas and streams. These streams ultimately empty into seaside lagoons and the Chesapeake Bay, where eutrophication problems can occur (Nixon, 1995). However, most streams on the seaside of the Eastern Shore often contain NO_3^- levels below USEPA drinking water limits; concentrations are most commonly around 2-7 mg NO_3^--N L^{-1} (Mills *et al.*, 2008, 2011). This drastic difference between groundwater and surface water NO_3^- concentrations alludes to efficient NO_3^--removal mechanisms within the groundwater-surface water interface. Multiple investigations at Cobb Mill Creek (CMC) have shown that the denitrification potential in these sediments averages 1.1 mg N L^{-1} h^{-1} (Galvotti, 2004; Gu *et al.*, 2007), a value that ranks moderately high compared to denitrification rates in aquatic systems (Piña-Ochoa & Álvarez-Cobelas, 2006). Hypothetically, if the N_2O yield range of 0.3% to 1.0% from the LINX II study

(Beaulieu *et al.*, 2011) was applied to the CMC denitrification rate we would estimate an N_2O flux of 3.3 to 11 μg N L^{-1} h^{-1}, which, over time, would represent a notable emission of N_2O.

Like other agriculturally intensive areas, the Delmarva Peninsula has also experienced increased applications of nitrogen fertilizers since the 1950s (Böhlke & Denver, 1995; Phillips *et al.*, 2003). Dated groundwater samples from wells across the Delmarva Peninsula show an increasing trend of nitrate concentrations with more recent recharge dates (Phillips *et al.*, 2003). In addition, some work has shown that the NO_3^- flux to groundwater increased by a factor of 3-6 from the 1940s to 1980s (Böhlke & Denver, 1995). Average residence times for groundwater in the area are estimated between 10 to 20 years in Eastern Delaware (Böhlke & Denver, 1995). Flewelling [2009] found that at CMC if nitrogen fertilizers were to maintain at current levels it would take close to 40 years for the mean catchment NO_3^- concentration to level off. Ultimately projecting that model into the future predicts groundwater levels of NO_3^- reaching 25 mg N L^{-1} by 2050 (Flewelling, 2009).

1.6 Importance of This Study

As agriculture intensifies we expect to see increasing amounts of nitrogen fertilizers applied to fields every year (Galloway *et al.*, 2004). However, we will not see the effects of that intensification within groundwater for another 10 to 40 years (Böhlke & Denver, 1995; Flewelling, 2009). While it is apparent that riparian areas are significant zones of denitrification, it is uncertain to what extent they will be able to help reduce the increasing levels of NO_3^- contamination. In addition, we are equally uncertain of how these increasing NO_3^- loads will affect denitrification inefficiency and ultimately N_2O emissions from riparian areas, rivers, and streams.

This study aims to understand better how N_2O emissions change over varying environmental conditions including increasing NO_3^- concentration, temperature, and varying pore water velocity. These environmental parameters were chosen for this study because not only are there projected increases in NO_3^- loading to aquifers, stream water temperature correlated to air temperature has been shown to be increasing (Kaushal *et al.*, 2010) which could have significant implications for increasing biological activity. Gu [2007] showed that pore water velocity played a significant role in denitrification in streambed sediments due to the kinetically controlled nature of the system. By using the resident carbon of streambed sediments in order to maintain natural distribution and structure we are able to show how changing NO_3^- concentrations and temperature will alter denitrification rates and N_2O emissions under a variety of groundwater flow conditions. A dualistic approach involving both field and laboratory measurements provides a suite of data needed in order to better predict N_2O emissions from streambed sediments near agricultural fields. Modelers are unanimous in stating that N_2O emission models cannot be adequately calibrated and validated without more temporal and spatial observational data (Boyer *et al.*, 2006; Groffman *et al.*, 2009a). These emission models continue to grow in complexity and are increasingly used for greenhouse gas policy decision making. The results discussed in this thesis are important in filling a significant gap in observational N_2O emission data as well as for predicting future environmental N_2O emission scenarios.

2 Materials and Methods

2.1 Field Methodology

2.1.1 Field Site Description

This field study was conducted at Cobb Mill Creek (CMC) located in Northampton County on the Eastern Shore of Virginia (ESVA) which is the southernmost county on the Delmarva Peninsula (37°17'25.59"N, 75°55'44.91"W) (Figure 2.1). The seaside portion of the ESVA has an area of 1540 km^2 and is a part of the Virginia Coast Reserve Long Term Ecological Research site (VCR-LTER). The topography of the ESVA is of relatively flat relief and does not exceed the 15 m topographic divide which runs north to south in the middle of the peninsula and is approximated by the highway US13. Land use on the ESVA is roughly 38% agriculture, 32% forest, 27% wetlands, and 2% developed. Agriculture in the area is dominated by soybean, corn, tomato, wheat, cotton, and other vegetables (USDA, 2009).

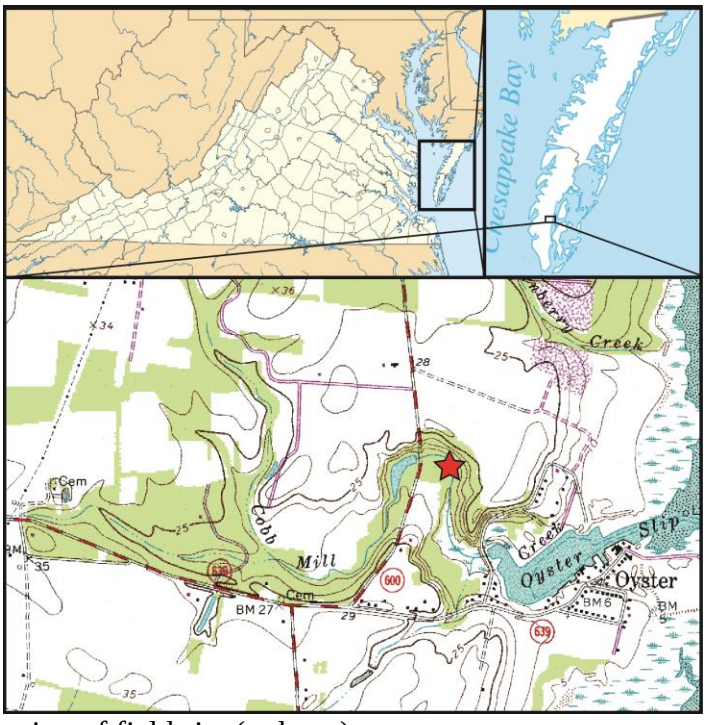

Figure 2.1 Map of location of field site (red star).

The ESVA is underlain by a series of aquifers and confining units; the uppermost portion is the shallow unconfined Columbia aquifer followed by a series of confining units and the Yorktown-Eastover aquifer upper, middle, and lower sections (Richardson, 1994). The Columbia aquifer is composed of Pleistocene-aged, unconsolidated sands 8 to 30 m thick (Sinnott & Tibbitts, 1968). This aquifer is recharged locally and due to the proximity of a confining layer near the surface at about 8m BMSL at this location, groundwater flow is dominantly lateral from the topographic divide to streams, marshes, lagoons, and to the Atlantic Ocean and Chesapeake Bay (Richardson, 1994).

Historical use of fertilizer on agricultural land has led to elevated levels of nitrate within the Columbia aquifer. A survey of the water quality of the Columbia aquifer on the Delmarva Peninsula found a median NO_3^- content of 5.4 mg N L^{-1}; about one third of the samples had concentrations above the EPA maximum contaminant level (MCL) for drinking water of 10 mg N L^{-1}, and a maximum concentration of 37.5 mg N L^{-1} was found in one well (Debrewer *et al.*, 2007a).

Cobb Mill Creek is a second-order tidal creek that drains into Oyster Harbor with a total catchment area of 4.96 km^2. Within the CMC watershed, land use is 62% forested, 34% agricultural, and 4% developed (Gu *et al.*, 2008b). Upland soils comprise the well-drained Bojac sandy loam and the Molena loamy sand are found along Cobb Mill Creek (Cobb & Smith., 1989). The location this study focuses on at CMC is located above tidal influence, is bounded by a hill slope on one side, flatter topography on the other, and is surrounded by a forested riparian buffer zone roughly 150 m on either side. Water levels in CMC range seasonally from 10 to 40 cm with an average flow of 900 m^3 day^{-1} [un-published raw data].

2.1.2 Fieldwork and Sample Collection

Field investigations were performed once in each season during the 2013 calendar year at the CMC experimental hill slope located near the Anheuser-Busch Coastal Research Center in Oyster, VA. Sampling dates were as follows:

Table 2-1. List of sampling seasons

Season	Date	Creek	# of Samples	Notes
Winter	1/11/2013	CMC	74	some light rain during sampling
Spring	5/8/2013	CMC	75	light rain overnight
	5/9/2013	CMC		continuation of sampling
Summer	8/20/2013	CMC	50	Water level down, only did two transects of 3 points
Fall	10/25/2013	CMC	50	Water level down, only did two transects of 3 points

During each field investigation, water samples were collected from the surface water and at incremental depths beneath the stream sediment surface. Either two (summer and fall) or three (winter and spring) stream length transects (left bank, center, right bank) were performed with 3 points (upstream, center stream, downstream) set 1 to 1.5 meters distant. Samples were collected at 5, 10, 20, 30, 40, 50, 60, and 70 cm below the sediment surface in addition to samples of surface water from the stream (Figure 2.2). Sampling at depth was achieved by using a drive-point piezometer made of 1" electrical conduit pipe sealed and pointed at the tip with small perforations just above the base. The piezometer was pounded into the sediment such that the perforations were at the selected depth below the surface. Tygon tubing was run from the base of the drive-point to a peristaltic pump to extract the sample (details below). After sampling, the tubing was removed and the piezometer was driven to the next depth to be sampled.

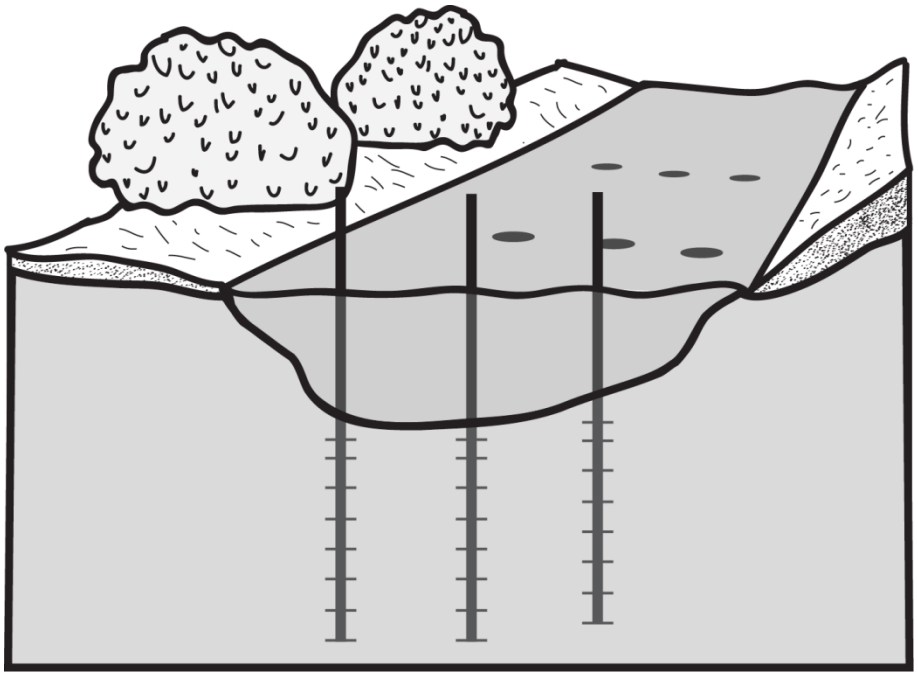

Figure 2.2. Illustration of field sampling design. Notches on the rods represent depths to which the sampler was, incrementally, driven. Circles represent other sampling points. A single sampling tube was used for all the collections.

Before sampling, each serum vial was poisoned with mercuric chloride by drying 50 µL of a 1% $HgCl_2$ solution on the bottom of 20-mL serum vials under a ventilated hood and then capping the vials with Parafilm. In the field, each sample was collected by driving the piezometer so the openings were at the correct depth, inserting the Tygon tubing, then pumping and disposing of three well-volumes of water, and finally collecting a sample in a 20-mL vial containing $HgCl_2$, and sealing it with clear PTFE-lined gray butyl septum secured with an aluminum crimp seal. All samples were filled to the top with no headspace or air bubbles present. Samples were then placed top down in a cooler filled with ice water and were transported to the laboratory at the University of Virginia in Charlottesville, VA for analysis within 48 hours of collection. During sampling, dissolved oxygen was measured for each sample using a rapid pulse polarographic DO probe on an YSI 600XLM Sonde with a 650 MDS.

Temperature was measured in the surface water and was also measured for each sampling depth, 0, 10, 20, 30, 40, and 50 cm.

2.1.3 Sample Analysis

Samples remained upside down in the cooler with ice water until they were withdrawn, one at a time, for N_2O analysis. As each sample was removed from the ice water, a headspace of 5 mL of pure (99.9%) N_2 gas was added to the serum vial with a gas-tight syringe while 5 mL of sample was withdrawn and subsequently disposed in a hazardous waste container. The sample was then placed upside down in a water-bath incubator for 30 minutes at 25 °C. After incubation, the sample was removed and was shaken vigorously for 30 seconds followed by a 30-second period of rest. While the sample was resting, a 1-mL gas-tight syringe (SGE. Inc. Austin, TX) was cleaned with N_2 gas. A 0.5-mL sample of the headspace gas was then taken using the gas-tight syringe and immediately injected into a Varian CP-3800 gas chromatograph (GC). The GC was operated under the following conditions: the model 1177 injector was run at 50 °C with a split ratio of 1:1; the column oven was operated isothermally at 25°C with a 30m-long HP/Plot Q column of 0.530 mm diameter and 40-µm film thickness;, and the ^{65}Ni electron capture detector was set to 300 °C.

The amount of N_2O present in samples spanned four orders of magnitude, thus two calibration curves were needed to capture the range of measurements, one for peak areas of 0-25 µg mL^{-1} N_2O-N and the other for 25.01 to 5500 µg mL^{-1} N_2O-N. Calibration curves were made using incremental volumes of injections from two Scott air tanks of calibration gas at 5% and 10.1 ppm N_2O with N_2 make up gas. A quadratic equation was chosen as the best fit for each curve.

$$M = aA^2 + bA + c$$ Equation 2-1

Where M is the mass of N_2O in µg and A is the peak area in mV*s. The coefficients and R^2 are as follows:

Table 2-2. Coefficients for quadratic equations for N_2O calibration curves

coefficient	**peak area < 5 mV*s**	**peak area > 5 mV*s**
a	1.90E-02	4.00E-04
b	2.53E-02	5.39E-02
c	2.10E-03	6.10
R^2	0.9904	0.9963

Total N_2O (M) in the sample is then calculated using the Bunsen absorption coefficient of 0.544 at 25 °C according to the following equation (Tiedje, 1994):

$$M = C_g\left(V_g + V_l \cdot \alpha\right)$$ Equation 2-2

where M is the total amount of N_2O in the water plus gas phases (nmol), C_g is the concentration of N_2O in gas phase (nmol mL^{-1}), V_g is volume of gas phase (mL), V_l is the volume of liquid phase (mL) and α is the Bunsen absorption coefficient (Wilhelm *et al.*, 1977).

Immediately after GC analysis, samples were filtered through 0.45-µm pore size nitrocellulose filters into glass liquid-scintillation vials and stored in a refrigerator at 4°C. Anion analysis was performed on all samples to determine chloride, sulfate, nitrate, nitrite, and phosphate, using a Dionex ICS-2300 ion chromatograph. The IC was operated with an AS/DV

auto sampler, using KOH eluent and a Dionex IonPac AS18 column. Calibration standards were run with each run of 40 samples.

2.1.4 Temperature Derived Pore Water Velocity & Flux

Temperature measurements made at each vertical profile at depths 0, 10, 20, 30, 40, and 50 cm were used to derive pore water velocity values using the Bredehoeft and Papadopilos [1965] method for steady vertical groundwater flow. The solution is as follows:

$$\frac{T - T_o}{T_L - T_o} = \frac{\exp\left(\frac{\beta x}{L}\right) - 1}{\exp(\beta) - 1} \qquad \text{Equation 2-3}$$

Where L is the maximum depth of measurement, T_o is the temperature at the top of the profile, and T_L is the temperature at the maximum depth(z), and β is a non-dimensional parameter defined as,

$$\beta = c_o \rho_o v_z L / \kappa \qquad \text{Equation 2-4}$$

Where c_o is the specific heat, ρ_o is the density of water, κ is the thermal conductivity of the bulk fluid-porous medium, and v_z is the vertical velocity of groundwater. The value for κ was estimated (κ = 2.4 W m^{-1} K^{-1}) based on published values for saturated sandy sediments (Woodside & Messmer, 1961). Temperature values at 50, 30, and 0 cm were used for T_L, T, and T_o respectively. The Bredehoeft equation is implicit; therefore the iterative method of MATLAB's **fzero** function was used to calculate v_z. Flewelling [2009] showed that estimates of specific discharge derived from the Bredehoeft method were linearly related to estimates from seepage meters deployed in CMC with a slope close to one. Therefore, this method has been

shown to accurately estimate groundwater velocities using temperature measurements at this site. During the spring field campaign only 3 of 9 temperature profiles were taken as a result of some equipment breaking in the field. An average pore water velocity of 1.58 cm hr^{-1} was derived for the three temperature profiles and was used for calculating fluxes at all 9 sample locations.

Solute and dissolved gas fluxes were derived using a 1-dimensional vertical solute transport equation. Pore water velocity values derived from the Bredheoft method showed only upward flow, such that all flux was assumed to be vertical and upward. The advective flux is defined as:

$$J = C \times v \qquad \text{Equation 2-5}$$

Where the flux (J) is in mg m^{-2} hr^{-1} and C is the solute concentration (mg L^{-1}) and v is pore water velocity (m hr^{-1}). Values of C for the depth of 5 cm were used to derive fluxes of NO_3^- and N_2O from the groundwater-surface water boundary to the surface water.

2.1.5 Statistics

The data collected failed to meet the assumptions of an ANOVA investigation. The data did not satisfy the assumption of homogeneity using Levene's test. Also, if did not satisfy the assumption of normality, failing in most cases to reject the null hypothesis of the Shapiro-Wilk test for normality Therefore, differences in seasonal concentrations and fluxes of NO_3^-, N_2O, DO, and Cl^- were investigated using the method of the Kruskal-Wallis non-parametric ANOVA using MATLAB's statistical package (MATLAB **kruskalwallis)**. This test compares ranked means of two or more groups with the null-hypothesis that all the samples are drawn from the same population. In addition, a multiple comparison procedure (MATLAB **multcompare)** using

the Dunn–Šidák correction for multiple pairwise comparisons was used in order to identify significantly different groups using the following equation:

$$\alpha' = 1 - (1 - \alpha)^{1/k} \qquad \text{Equation 2-6}$$

Where α' is the adjusted alpha value and k is the number of comparison tests being performed.

2.2 Experimental Column Methodology

2.2.1 Core Retrieval and Preparation

Two sediment cores were extracted from streambed sediments of CMC on November 18, 2012 for use in an environmental-parameter laboratory experiment. Cores were extracted by driving a length of 3" diameter PVC pipe that was sharpened on one end into the sediment until a core length greater than 60 cm of sediment was obtained. The depth to sediment inside and outside the core was measured to determine compaction which was ~2 cm for both cores. The top of the core tube was filled with water and capped with a rubber stopper that was sealed with waterproof plumbing caulk (GOOP®). After the caulk had dried for 20-30 min, the cores were pulled from the sediment, the bottom subsequently capped and caulked, and both cap ends were sealed with duct tape for additional security. Cores were kept upright and transferred to the lab at the University of Virginia where they were kept in a refrigerator at 4 °C until they were needed.

Hydraulic conductivity (K_s) of each sediment core was found using the falling head method. K_s is calculated as:

$$K_s = \frac{L}{t}\ln(\frac{h_1}{h_2}) \qquad \text{Equation 2-7}$$

Where *L* is the column length, *t* is the time taken for the head to drop, h_1 is the initial head, and h_2 is the final head.

The cores were then prepared for the experimental runs in a manner similar to that used by Gu et al. (2007). The ends of the PVC pipe were cut to within 2" of the sediment of the core and the open space was filled with polyester wool. The ends of the cores were capped with covers that each had a small outlet installed and sealed in place with Goop®. Small holes were then drilled at 0, 10, 20, 30, 35, 40, 45, 50, 55, and 60 cm from the bottom of the sediment. A B-D 16G1½" needles with a luer-lock end were then placed in each hole and were secured and sealed in place with Goop®. A three-way stopcock was attached to each needle end, and the entire outside of the connection was sealed with Goop®. Once all the caulk on the ports had dried, the two columns were attached to a stand in a vertical position and secured with hose clamps. The column stand was then placed in a Conviron 4030 environmental chamber where steady temperature could be set and monitored. Masterflex 06509-13 tubing was then attached to the inlet and outlet of each column. The outlets were run into plastic 2000 mL Erlenmeyer flasks so that the effluent volume could be monitored. The tubing leading to both inlets were anchored to the bottom with a rubber weight at the bottom of large Nalgene reservoir that contained artificial groundwater (AGW). The following AGW recipe was used (per liter of deionized water): 60 mg $MgSO_4 \cdot 7H_2O$, 20 mg KNO_3, 36 mg $NaHCO_3$, 36 mg $CaCl_2$, 35 mg $Ca(NO_3)_2$ and 25 mg $CaSO_4 \cdot 2H_2O$ (Bolster, 2000). The inlet tubing then ran through a Cole-Parmer MasterFlex peristaltic pump with two rotary heads attached before connecting to the

inlets of the columns. The connections with the tubing at the inlets and outlets were secured in place and sealed with Goop® to prevent any leaks (Figure 2.3).

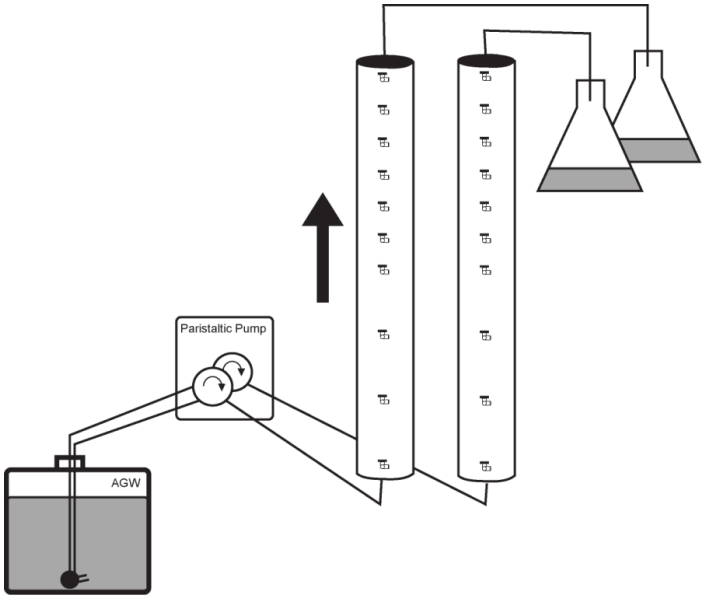

Figure 2.3. Column design with Erlenmeyer flasks at outlets. A fraction collector replaced the flasks at the outlets for the Cl^- tracer experiments.

2.2.2 Experimental Design & Sample Analysis

The following factorial experimental design was implemented on both columns at the same time, altering flow rates within a set temperature and NO_3^- concentration, then altering the NO_3^-, then finally altering the temperature in the series:

Table 2-3. Experimental factorial design for sediment column experiments in an environmental chamber with 2 replicates for each 36 scenarios

		Temperature											
		5 °C				15 °C				25 °C			
Pore water Velocity (cm hr^{-1})		0.5	1.25	2.5	4.5	0.5	1.25	2.5	4.5	0.5	1.25	2.5	4.5
NO_3^- (mg N L^{-1})	3.5	2	2	2	2	2	2	2	2	2	2	2	2
	10	2	2	2	2	2	2	2	2	2	2	2	2
	18	2	2	2	2	2	2	2	2	2	2	2	2

Each scenario was run on both columns at the same time until 3 pore volumes had passed through each column, allowing the columns to reach a steady state. Pore water samples were taken from each port using a 60-mL syringe. From each port, 10 mL was removed and placed in a 10-mL labeled serum bottle and capped with a clear PTFE lined grey butyl septa and aluminum crimp cap. These serum bottles were then placed upside down in a cooler of ice water. After each sample was drawn, another 10 mL of pore water was drawn from the port and placed into a cup, and the DO probe was immersed in the sample until a steady DO reading was obtained. Samples remained upside down in the cooler with ice water until they were withdrawn one at a time for N_2O analysis. Samples taken from the columns were processed within 3 hours of collection. Each sample was removed from the ice water one by one and a headspace of 2.8 mL of pure (99.9%) N_2 gas was added with an air tight syringe while 2.8 mL of sample was withdrawn and disposed. Water analysis was performed n the same fashion as in section 2.1.3.

2.2.3 Cl^- Breakthrough Curves & Denitrification Rate

In order to determine the denitrification rate occurring under each set of conditions it was necessary to determine the effective dispersivity of the columns. This was done by performing Cl^- tracer tests. Four times the amount of Cl^- was added to a separate AGW reservoir and pumped into a column. The flasks at the outlet of the column was replaced with a fraction collector that collected 25 mL (0.025 pore volumes) in each test tube A total of 130 tubes (3.25 pore volumes) were collected and every fourth sample was run on the IC for anion analysis. A 1-D non-reactive advection-dispersion model was fit to the breakthrough data with CXTFIT 2.0 (Toride *et al.*, 1995). A breakthrough curve analysis was completed for each pore water velocity in order to determine if dispersion was independent of changes in velocity and if the Peclet numbers ranged from 10-20, showing that the columns behaved as advection-dominated

sediments. The denitrification rate, R, was derived from the advection dispersion equation assuming steady state reactive transport and assuming dispersion was insignificant:

$$R = -\bar{v}\,\frac{\partial C}{\partial x} \qquad \text{Equation 2-8}$$

Where R is the denitrification rate ($\partial C/\partial t$), and $\bar{v}$ is the average linear pore velocity. N_2O yield, which is a measure of the percentage of NO_3^- that is not fully reduced to N_2, but terminates at N_2O, was calculated along the flow path of the columns using the following equation:

$$N_2O\ yield = \frac{N_2O \cdot N\ (at\ 0\ cm)}{NO_3^- \cdot N(at\ 60\ cm) - NO_3^- \cdot N(at\ 0\ cm)} \times 100 \qquad \text{Equation 2-9}$$

2.2.4 Sediment Analysis

After all the environmental scenarios were run on the columns, the sediment was sampled at each port by boring a hole next to each port and using a truncated 10 mL syringe as a mini-corer. The samples were then weighed to determine their wet mass, and oven dried at 105 °C for 24 hours. The sediment samples were then reweighed to determine porosity. In order to determine total organic matter, loss upon ignition was employed by placing the samples in a muffle furnace at 500 °C for 24 hours and weighing the samples for a final time.

2.2.5 Column Model of NO_3^- and N_2O

Denitrification was estimated for the whole column using a first order kinetic equation as a function of residence time and an exponential temperature relationship. NO_3^- is assumed to be at saturated concentrations and does not have an impact of the denitrification rate within this

model. The following equation was used to estimate the concentration of NO_3^- at the outlet of the column:

$$[NO_3^-] = N_o e^{(-\frac{L}{v} \cdot Ae^{\left(-\frac{C}{T}\right)})} \quad \text{Equation 2-10}$$

Where N_o is the initial input NO_3^- concentration (mg L^{-1}), residence time is represented by L/v where L is the length of the column (cm), v is the pore water velocity (cm h^{-1}), T is the temperature (K), A (h^{-1}) and C (K) are reaction constants. N_2O is produced and removed within the column at various depths dependent on temperature and pore water velocity resulting in net gains N_2O if the column remains open and advective. We assume that the concentration of N_2O at the outlet is the net production of N_2O which is a function of initial NO_3^- concentration, pore water velocity, and the amount of NO_3^- removed as shown in equation 2-11. N_2O yield which is the measure of how much N_2O is produced for unit NO_3^- removed was estimated using the following multiple linear regression:

$$N_2O_{yield} = 10^{(\beta_N \log(N_o) + \beta_r t_r + \varepsilon)} \quad \text{Equation 2-11}$$

Where β_N and β_r are regression constants associated with initial NO_3^- concentration (N_o) and residence time (t_r), respectively. N_2O_{yield} is then used to estimate the concentration of N_2O as a function of the amount of NO_3^- removed within the column:

$$[N_2O] = N_2O_{yield}\ (N_o - NO_3^-) \quad \text{Equation 2-12}$$

3 Results

3.1 Fieldwork Results

3.1.1 Patterns in Sediment Profiles of NO_3^-

The deepest sample point in each sampling profile was 70 cm. Concentrations at this depth are assumed to be initial values along a vertical flow path traveling from 70 cm to the sediment surface. NO_3^- values at the deepest sample point of 70 cm for all seasons, except fall, had mean values ~8.7 mg N L^{-1}. Values of NO_3^- at 70 cm in the fall had the lowest mean of 6.30 mg N L^{-1}. There was not a significant difference between input values of NO_3^- at 70 cm between any of the seasons ($p=0.03$, $\alpha=0.009$). Values of NO_3^- at 5 cm below the sediment are assumed to represent the concentration of NO_3^- prior to fluxing into the surface water. There were no significantly different concentrations of NO_3^- at 5 cm for each season ($p=0.28$, $\alpha=0.009$). Mean values of NO_3^- at 5 cm are listed in Table 3-1. Assuming a direct flow path along the sampling profile, percent loss was calculated for each sampling location using the following equation:

$$\frac{NO_3^-\text{-N (at 70 cm)} - NO_3^-\text{-N (at 5cm)}}{NO_3^-\text{-N (at 70 cm)}} * 100 \qquad \text{Equation 3-1}$$

There was more denitrification observed in the winter than in the fall. The percent loss of NO_3^- at the time of sampling in the winter was significantly more than during the fall ($p=0.003$, $\alpha=0.009$) (Table 3-1).

Table 3-1. Mean values of NO_3^--N at 70 and 5 cm and the % loss between those two points.

Season	n	NO_3^- at 70 cm (mg N L^{-1})	NO_3^- at 5 cm (mg N L^{-1})	Amount Lost (mg N L^{-1})	Percent Loss
Winter	9	8.65	3.80	4.85	54.23
Spring	9	8.80	5.09	3.71	38.49
Summer	6	8.69	5.50	3.19	38.12
Fall	6	6.30	5.50	0.80	11.27

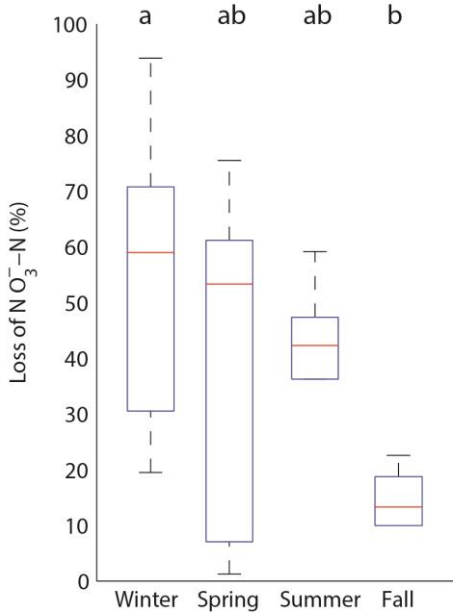

Figure 3.1 Percent loss of NO_3^--N along an upwards flow path from 70 cm to 5 cm below the sediment surface. Letters above groups represent significantly different ranked means defined by the Kruskal-Wallis test and a Dunn-Šidák correction for pairwise comparisons (α=0.009). The red line represents the median value, the boxes define the inner quartile range (IQR), whiskers define 1.5*IQR, and any other points are defined as outliers. This boxplot convention is used for all following boxplots.

Fluxes of NO_3^- in the spring were significantly larger than in the fall (p=0.002, α=0.009). Mean fluxes in the spring were 79.43 mg m^{-2} hr^{-1} while mean fluxes in the fall were 21.30 mg m^{-2} hr^{-1}. Maps of NO_3^- flux for all four seasons indicate a pattern of a higher NO_3^- flux coming from the upstream right side of the stream (Figure 3.2). The spring yielded the broadest range of fluxes. The highest flux values in the spring occurred along the full length of the right side of the

stream bed and the lowest were observed in the center of the sampling space. The highest values of flux in the winter, summer, and fall were detected in the upstream right side of the sample space. The largest value of NO_3^- flux in the upper right portion of the sample space occurred in the summer the smallest fluxes occurred in the fall. Profiles of NO_3^- concentration at depth reveal changes of NO_3^- along the flow paths within the streambed sediment (Figure 3.3). Kruskall-Wallis mean rank tests with Dunn-Šidák corrections for pairwise comparisons were performed at each depth value in order to determine significant differences among values of NO_3^- at depth within each season. In the winter, NO_3^- at 5 cm was significantly lower than at 50 and 70 cm depth ($p<0.001$, $\alpha=0.002$). There were no significant differences in values of NO_3^- among depths for samples taken during the spring, summer, and fall field campaigns ($p=0.038$, 0.39 and 0.69, respectively, $\alpha=0.0018$). For the spring samples, there are two measurements of surface water NO_3^- concentration due to a small storm that occurred the morning of the second day of sampling. The base flow stream water NO_3^- concentration before the spring storm was 9.43 mg N L^{-1} which dropped dramatically after the storm passed to 0.97 mg N L^{-1}.

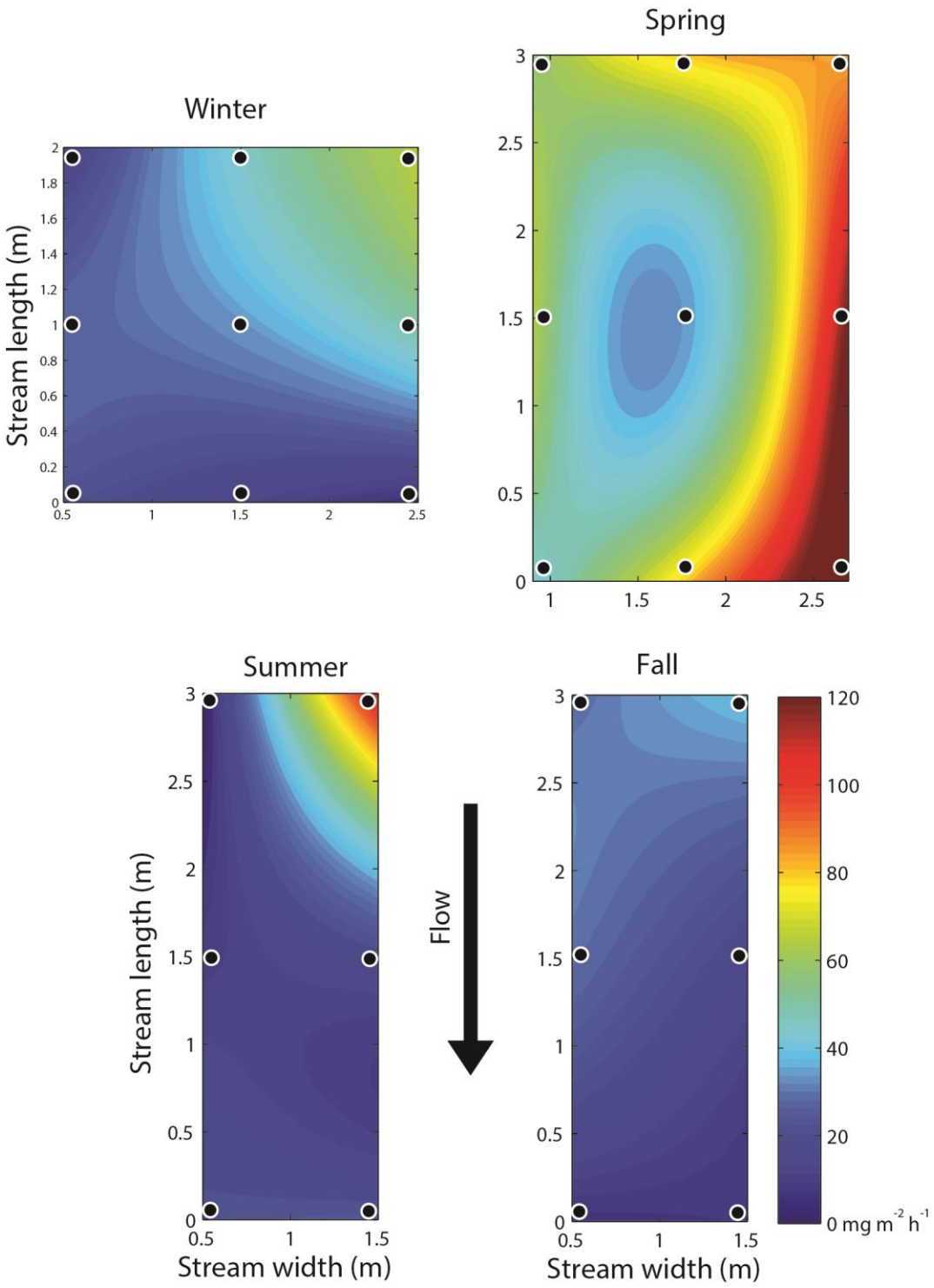

Figure 3.2 Birds eye view maps of NO_3^--N flux for each season in mg m^{-2} hr^{-1}. Sample locations are marked with black points with a white outline.

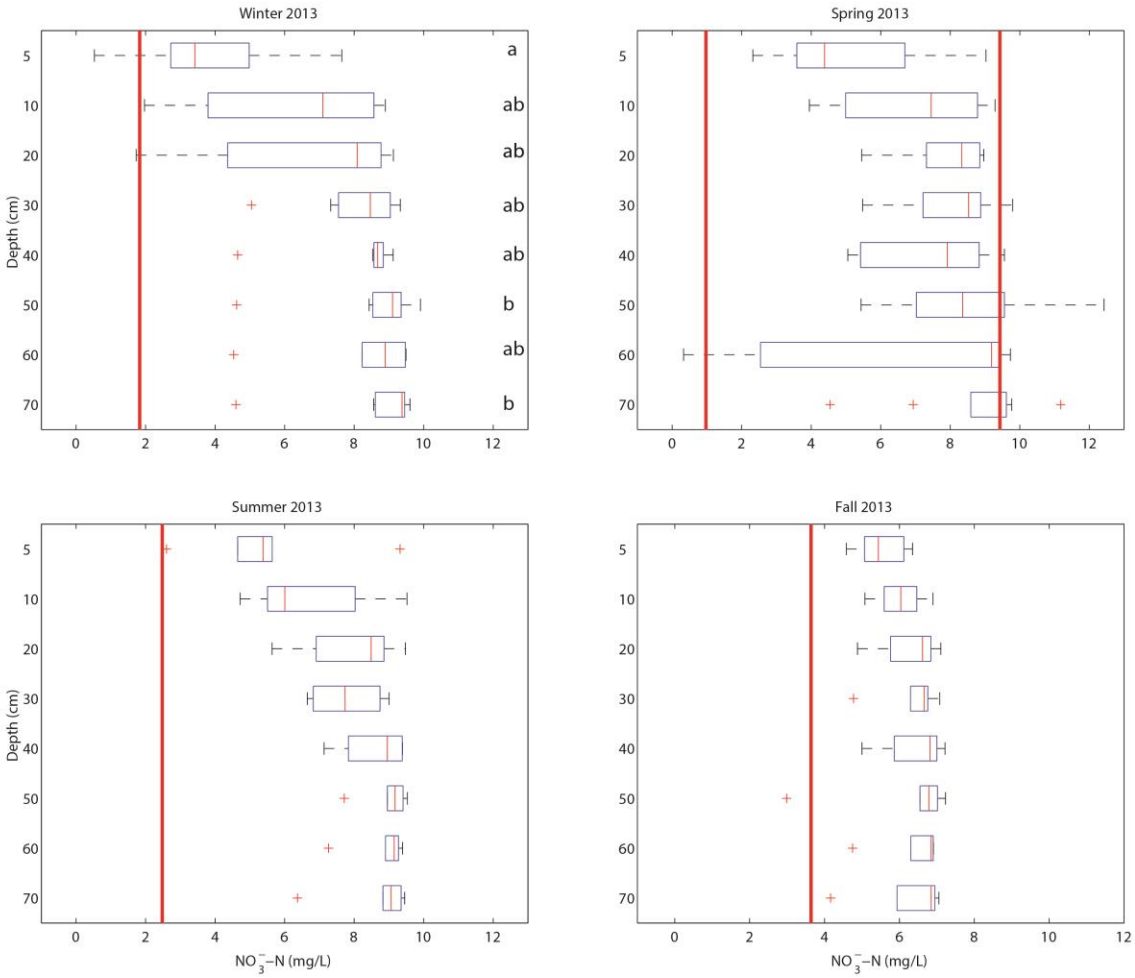

Figure 3.3 Boxplots of NO_3^--N at all sample depths for each season. Letters represent statistically different ranked mean values (α=0.002). Red vertical lines represent the concentration of the surface water. The two red lines in the spring indicate base flow conditions at 9.43 mg N L^{-1} and after a small morning storm at 0.97 mg N L^{-1}.

Change in NO_3^- with depth in the sediment was calculated assuming gaining conditions (i.e., upward flow) along a direct flow path within the sampling profile. Aggregated change in NO_3^- is shown in Figure 3.4. In winter, summer, and fall, all the profiles showed decreases in NO_3^- from 5 cm depth to the surface water. For all seasons, the largest loss in NO_3^- concentration occurred in the 10- to 5-cm interval. Other regions dominated by NO_3^- loss were observed between 30 and 10 cm for each season. Median values of change in NO_3^- are near 0 for depths 70 to 30cm for winter, summer, and fall, indicating minimal denitrification or NO_3^- inputs

at these deeper depths. In the spring, there were highly variable changes in NO_3^- concentration from 70 to 30 cm. Between 70 and 60 cm there was a median loss of NO_3^-, however from 60 to 30 cm the median values represent gains in NO_3^- concentration along the flow path.

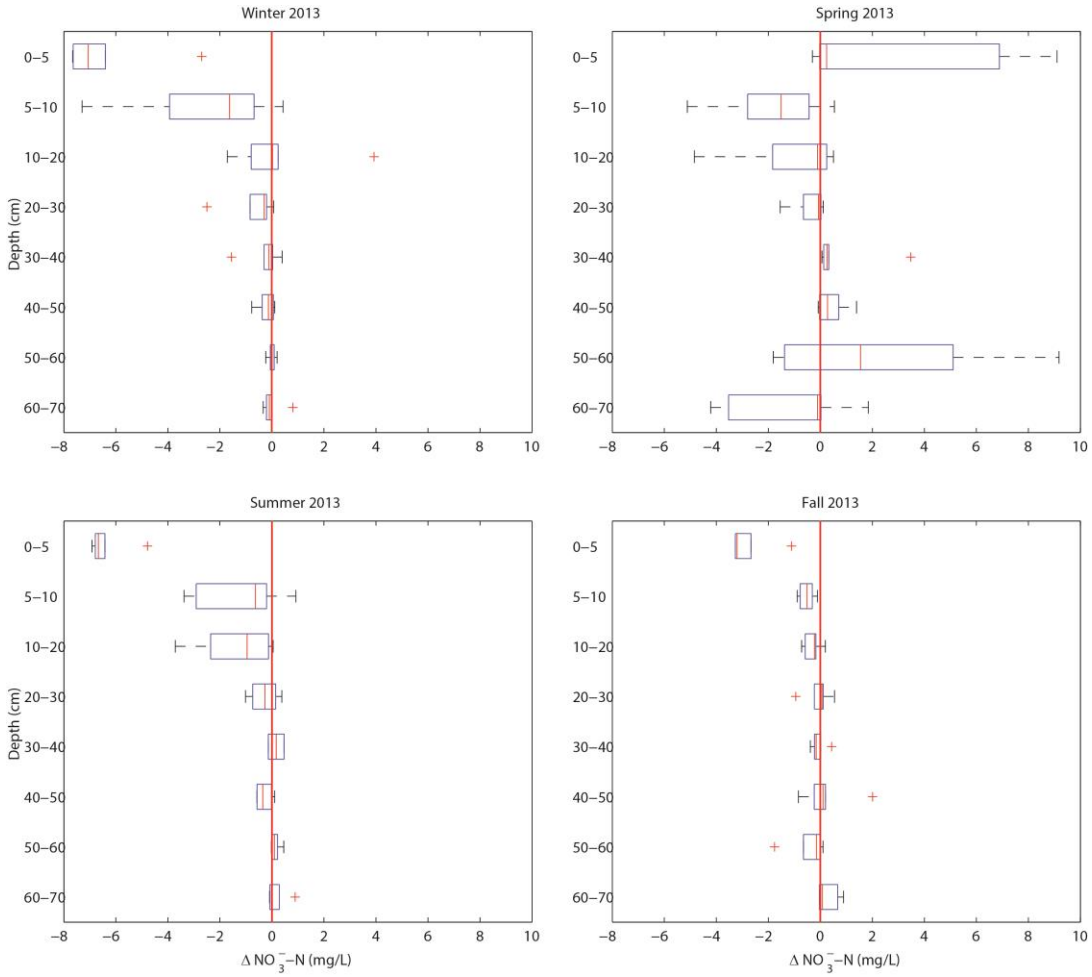

Figure 3.4 Change in NO_3^--N concentration from 70 to 5 cm at 10 cm intervals for all seasons. Surface water values are represented by 0 cm. The red line marks zero change in NO_3^--N concentration.

3.1.2 Patterns in Sediment Profiles of N_2O

N_2O concentrations at the deepest sampling point (70 cm) were significantly lower in the spring than in the winter and the fall ($p=0.002$, $\alpha=0.009$) (Figure 3.5). The lowest input concentrations of N_2O were observed in the spring with a mean value of 0.38 µg N L^{-1} and the highest occurred

in the fall with a mean value of 3.40 µg N L^{-1}. N_2O concentrations at 5 cm were significantly higher in the winter than in the spring (p=0.008 , α=0.009). A summary of mean values of N_2O concentrations at 5 and 70 cm and median percent loss for all seasons is displayed in Table 3-2. Percent loss is the percent difference in concentration between 70 cm and 5 cm over the initial concentration at 70 cm. The median value of percent loss is reported here due to a few large outliers in each season that skew the mean. The median values of percent loss best represent the overall trend in the percentage of change in N_2O concentrations along the flow path.

Table 3-2 Summary of mean values of N_2O-N at 70 and 5 cm below the sediment surface and the median percent loss between those two depths for 4 seasons in 2013.

Season	n	N_2O at 70 cm (µg N L^{-1})	N_2O at 5 cm (µg N L^{-1})	Percent Loss (%)
Winter	9	1.78	49.30	0.74
Spring	9	0.38	0.50	0
Summer	6	1.31	0.90	41.79
Fall	6	3.40	1.34	32.21

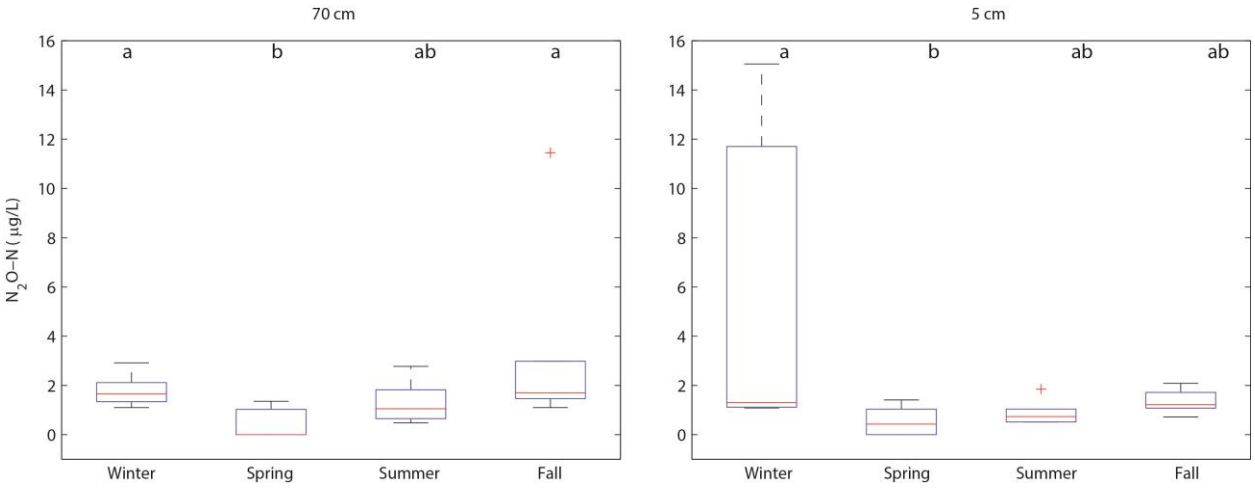

Figure 3.5 N_2O-N concentrations at depths of 70 cm (left) and 5 cm (right) for all seasons. The letters above groups signify statistically significant differences among the groups (α=0.009).

There was no significant difference in the percentage change in N_2O concentrations going from 70 cm to 5 cm in any of the 4 seasons (Figure 3.6). However, all seasons except spring had a positive median percentage loss in N_2O concentrations from 70 to 5 cm. Therefore in winter, summer, and fall we observed a majority decrease in N_2O concentrations along each flow path. There was a median loss in the spring of 0% which represents a balance of increasing and decreasing N_2O concentrations on the flow path. There is one sample taken at 5 cm depth in the winter that yielded an extremely large concentration of N_2O. This large value skewed the results of percentage loss of N_2O in winter as seen in the large variance in Figure 3.6. The positive median value of 0.74%, however, revealed a close balance of percent loss and percent gain in N_2O concentrations along the flow paths.

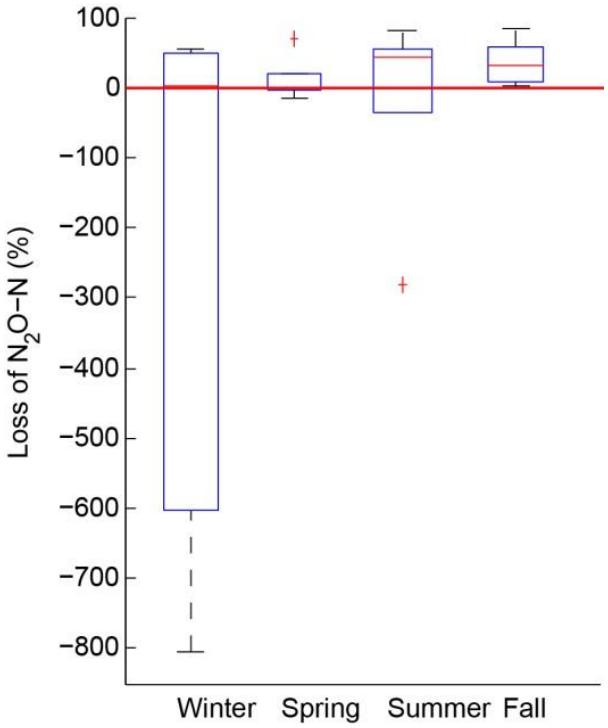

Figure 3.6 Percent loss of N_2O-N from 70 to 5 cm for each season. Negative values represent an increase in concentration of N_2O from 70 to 5 cm. Positive values represent a decrease in concentration of N_2O from 70 to 5 cm.

Fluxes of N_2O proved not to be significantly different among the seasons as there was high variability for each season (p=0.069, α=0.009) (Figure 3.7). The highest mean fluxes of N_2O-N were observed in the winter with a mean of 568.20 µg m^{-2} hr^{-1} and the lowest fluxes occurred in the summer with a mean of 4.19 µg m^{-2} hr^{-1}. Bird's eye view maps of N_2O fluxes for each season reveal the heterogeneity of N_2O flux at the sediment water interface (Figure 3.9). In the winter located at the downstream right-bank side of the stream, fluxes were 2 orders of magnitude higher than all other flux values measured. Fluxes in the spring were also highly localized near the upstream right bank as well as near the downstream left bank. However, the largest values of flux in the spring were much lower than the maxima observed in the winter fluxes.

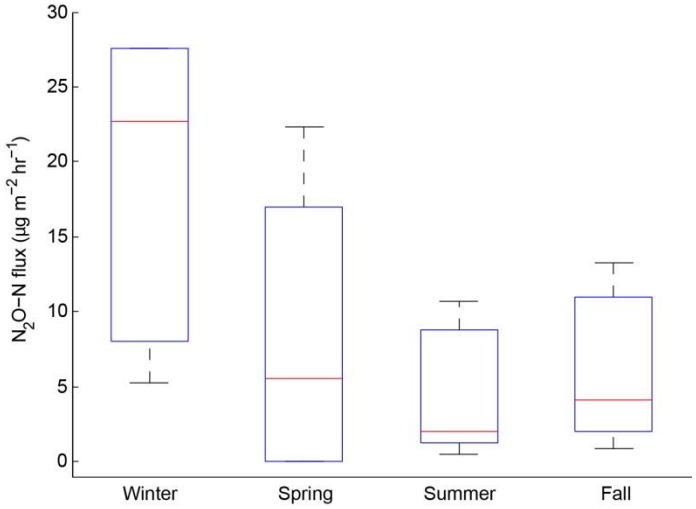

Figure 3.7 N_2O-N fluxes for all seasons in 2013. Winter is not significantly different from the summer (p=0.025, α=0.009).

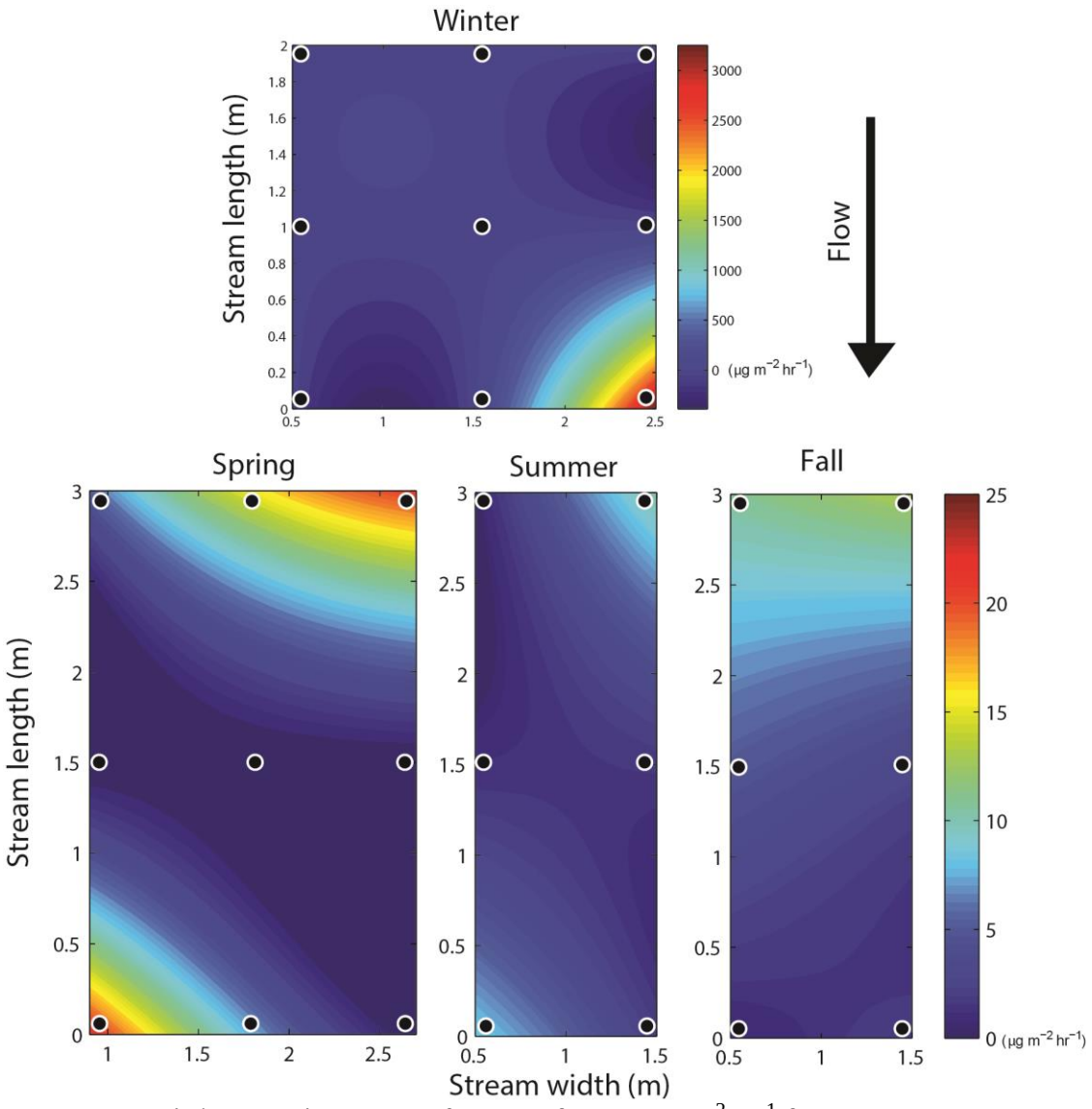

Figure 3.8 Bird's eye view, map of N_2O-N flux in µg m^{-2} hr^{-1} for all 4 seasons in 2013. Each scale corresponds to each row. Black dots with white outlines signify the approximate sampling location. Stream flow is from the top to the bottom of each map.

Profiles of N_2O at each sample point reveal the vertical distribution of N_2O for each season (Figure 3.9). As before, there was a large concentration of N_2O at the 5-cm-sample depth in the winter which skews the distribution of all samples at that depth. There were not any significantly different N_2O concentrations observed at depth for all seasons (p ranged from 0.2 to 0.8). Samples collected during the fall had the highest surface water concentration of 1.88 µg N L^{-1} N_2O and also yielded the largest variability of N_2O-N at the deeper depths, from 50 to 70 cm.

The lowest values of N_2O concentrations tended to occur at 20 to 40 cm depth for all seasons except winter. Concentrations observed in each season followed a general trend of high N_2O at the deepest sample points (70 to 60 cm) to lower concentrations at the middle sample points (40 to 20 cm) and then to higher concentrations again just below the sediment surface (5 to 10 cm). Most often, as shown in Figure 3.6, there was a general trend of overall loss of N_2O along the flow path from deeper groundwater to the groundwater surface water interface. The exception was in the spring when the changes in N_2O were relatively stable, although there was an overall increase in median N_2O along the flow path.

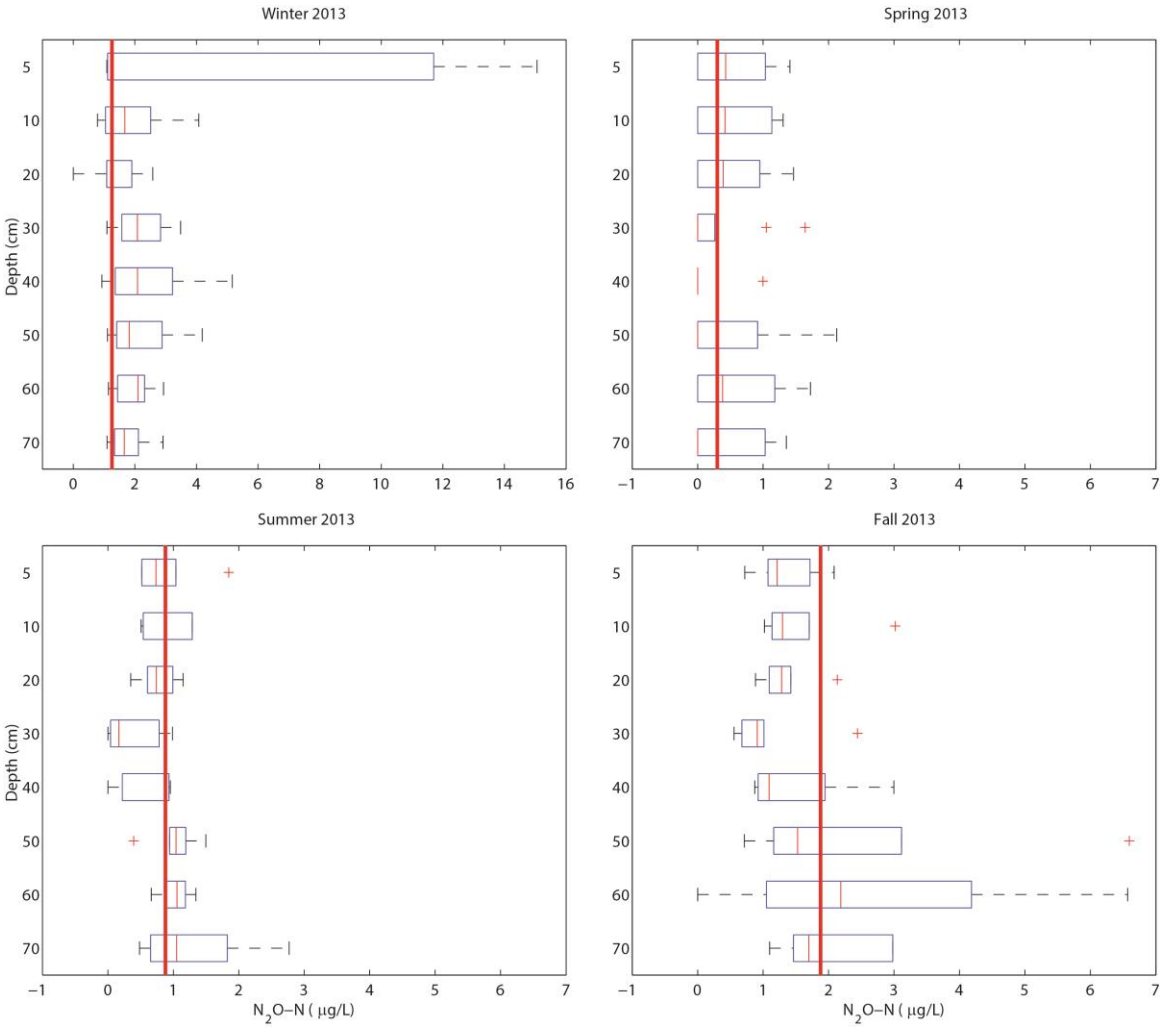

Figure 3.9 N_2O-N at depth for all seasons. The red vertical line represents surface water concentrations of N_2O-N.

Changes in N_2O at each depth indicate areas of N_2O production and removal along the flow path (Figure 3.10). In the winter, changes with depth were balanced around 0 as consistent concentrations were observed along the flow path from 70 to 30 cm depth (Figure 3.9). There was a zone of N_2O removal from 30 to 20 cm prior to an area of production along the flow path (20 to 5 cm). There was then an overall loss of concentration at the transition from the sediment at 5 cm to the surface water indicating higher concentrations of N_2O in the sediment than in the surface water. Profiles in the summer and the fall had distinct zones of N_2O removal at depths of 70 to 40 cm, overlain by an area of production or overall gain in the median concentration of N_2O from 30 to 10 cm depth. However, in the top 10 cm of sediment there was an overall decrease in N_2O concentration from 10 cm to the surface water concentrations. Unlike spring and summer, fall and winter both had high variability in changes of N_2O concentrations along the flow paths. Changes in N_2O were balanced around 0 change along the full length of the sampled flow path.

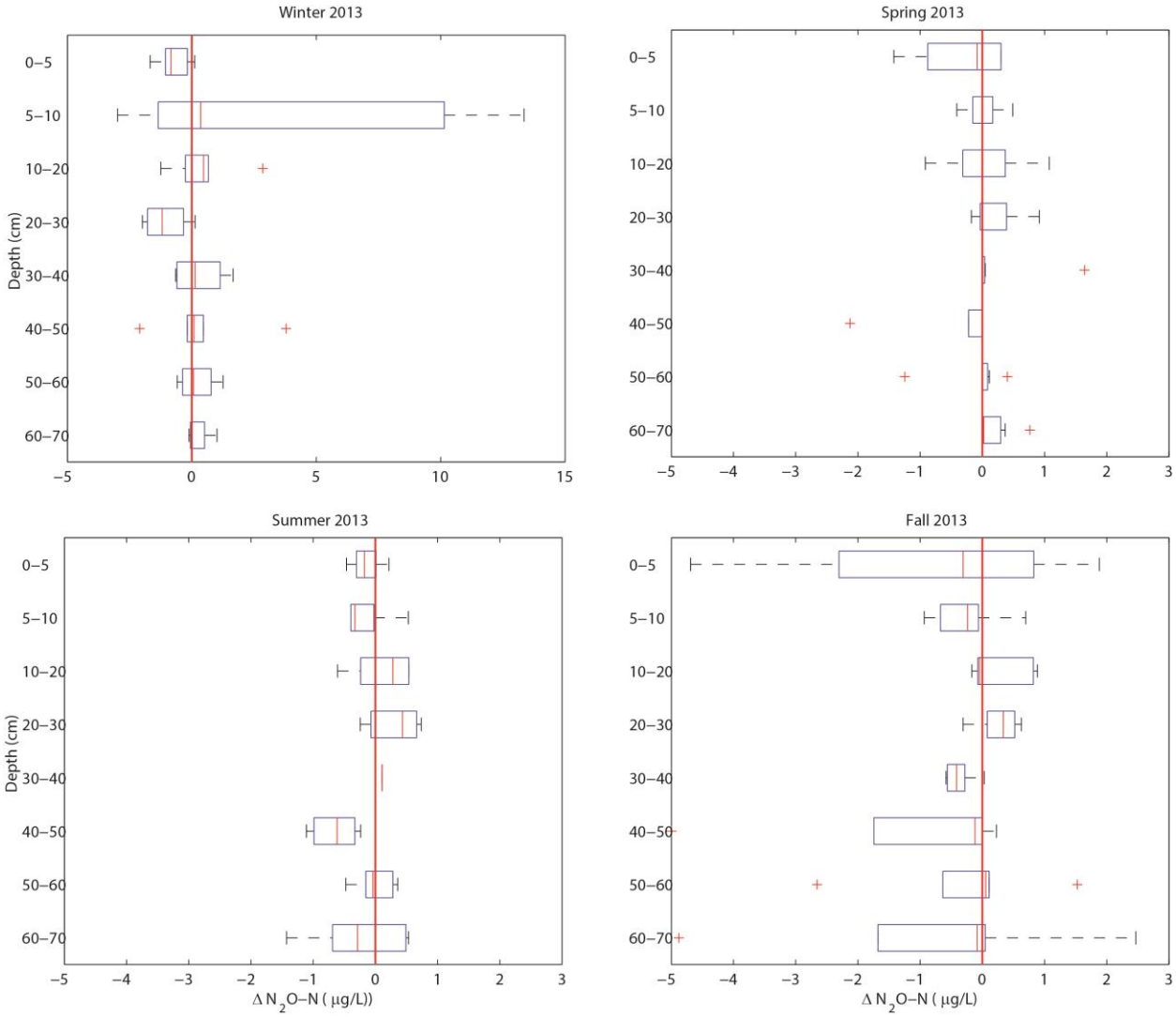

Figure 3.10 Change in N_2O-N along a gaining flow path for each 4 seasons. The red line is centered on 0.

3.1.3 Seasonal Groundwater Temperature & N_2O at Depth

Temperature was measured at the surface, 10, 20, 30, 40, and 50 cm depth at each sample location for each season. Deep groundwater in the winter and fall was found to be warmer than the surface water (Figure 3.11). In the spring and summer deep groundwater was cooler than the surface water. There appears to be a seasonal lag in groundwater temperature, where the thermal signal of groundwater samples taken in the spring might be indicative of surface water temperatures in the winter, and groundwater temperatures in the fall might be indicative of surface water temperatures during the summer. The concentration of N_2O at 50 cm was found to

have a significant correlation with temperature where warmer temperatures were associated with higher concentrations of N_2O in the same groundwater samples ($r=0.46$ $p<0.001$) (Figure 3.12). Thus, there appears to be a seasonal lag associated with the concentration of N_2O beneath the shallow biologically active zone.

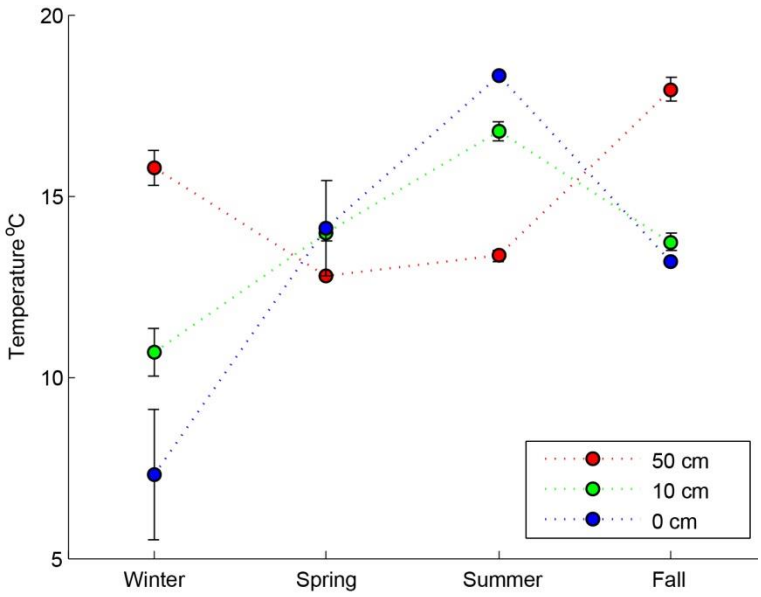

Figure 3.11 Temperature of the surface water (0cm), 10 cm, and 50 cm within the sediment for each season. Error bars represent the standard error of the mean.

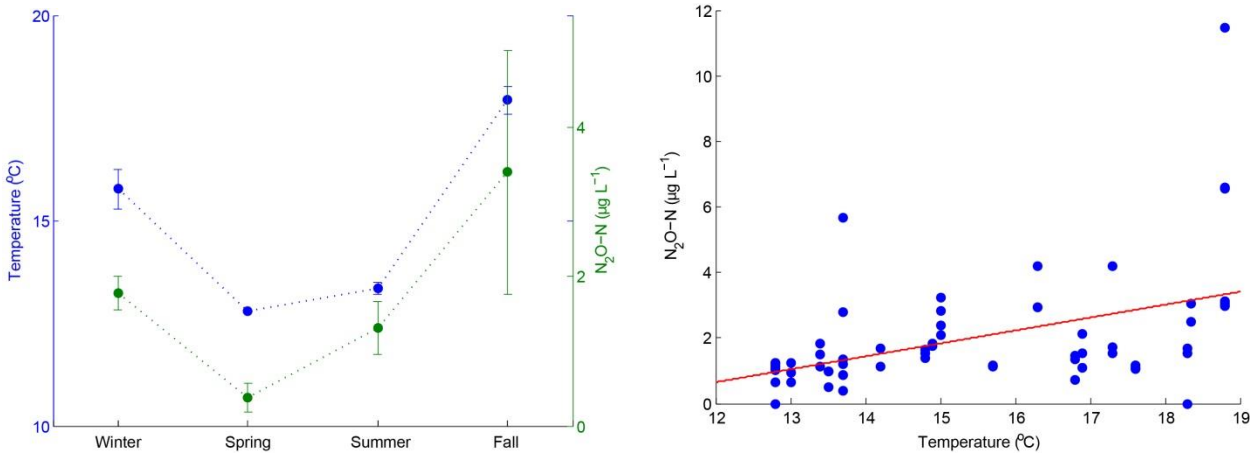

Figure 3.12 (Left) Temperature at 50 cm depth (blue), and N_2O at 50 cm depth (green). (Right) Correlation between temperature and N_2O at 50 cm depth ($r=0.46$, $p<0.001$).

3.1.4 Dissolved Oxygen Patterns

Dissolved oxygen (DO) was not measured during the winter field campaign due to equipment malfunctions, therefore DO measurements are only reported for the spring, summer, and fall field campaigns of 2013. DO at the deepest sampling location of 70 cm was not significantly different for each season ($p=0.61$). However, there was a significantly greater DO concentration at 5cm in the fall than in the spring ($p<0.001$, $\alpha=0.017$) (Figure 3.13).

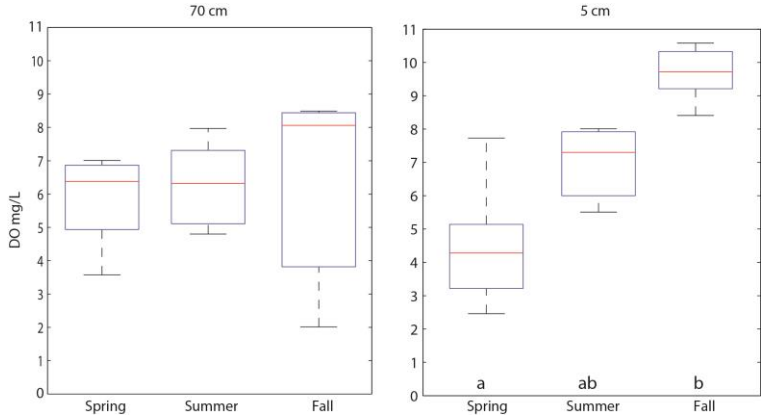

Figure 3.13 DO at depth 70 (left) and 05 cm (right) for 3 seasons. Letters at the bottom indicate significantly different groups ($\alpha=0.017$).

Change in DO concentration at each depth illuminates areas where DO concentrations decreased and increased along the flow path (Figure 3.14). There were no significant differences in changes in DO concentrations for each season (p ranges from 0.06 (spring) to 0.66). In the spring, there was a decrease in DO concentrations from 70 to 60 and 40 to 10 cm, whereas DO concentrations increased from 60 to 40 and 10 cm to the surface water. In the summer, the dominant trend is increasing concentration of DO with decreasing depth along the flow path. However in the summer there is a location of decreasing DO concentration at 50 to 30 cm depth. The fall profiles followed a trend similar to that of the spring samples. There was a decrease in DO concentrations in the fall midway through the profile from 40 to 20 cm, however at all other depths there was an increase in DO concentration along the upward flow path.

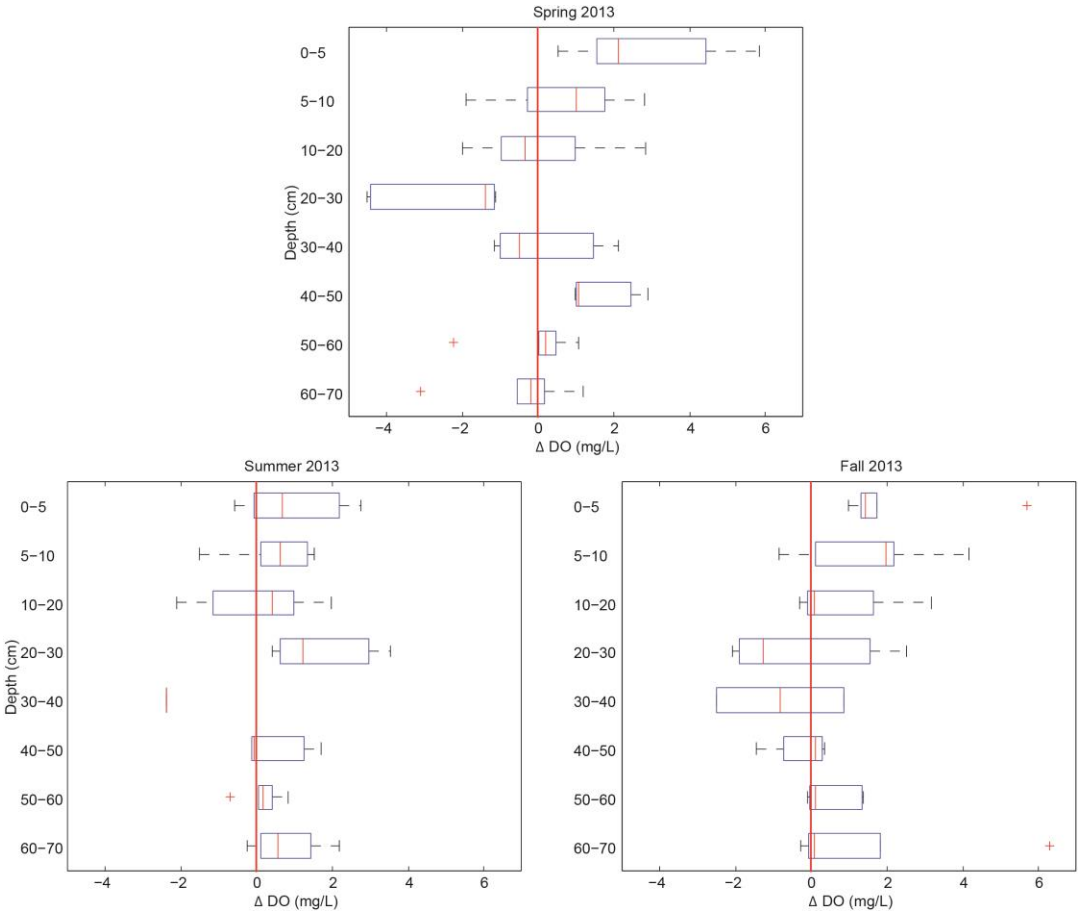

Figure 3.14 Change in DO concentration along the upward flow path for the 3 seasons for which data were obtained.

3.1.5 Cl^- Patterns

Concentrations of Cl^- at depth for all seasons did not vary along the sampling profiles. There are no significantly different concentrations of Cl^- for any season ($p=0.42$). Cl^- concentrations at 5 cm have the highest values for all seasons, but they are not significantly higher than at any other depth (Figure 3.15). A histogram of Cl^- concentrations at the deepest sampling location of 70 cm shows a normal distribution with a mean of 24.82 mg L^{-1} (Figure 3.16). A clump of 5 samples at the higher end between 28 to 31 mg L^{-1} represents a higher Cl^- input versus the two samples below 18 mg L^{-1} which represent a relatively lower input concentration. There is a significant negative correlation between NO_3^- and Cl^- concentrations at

70 cm depth (R=-0.44, p=0.008). As input NO_3^- concentrations increase input Cl^- concentrations decrease (Figure 3.17).

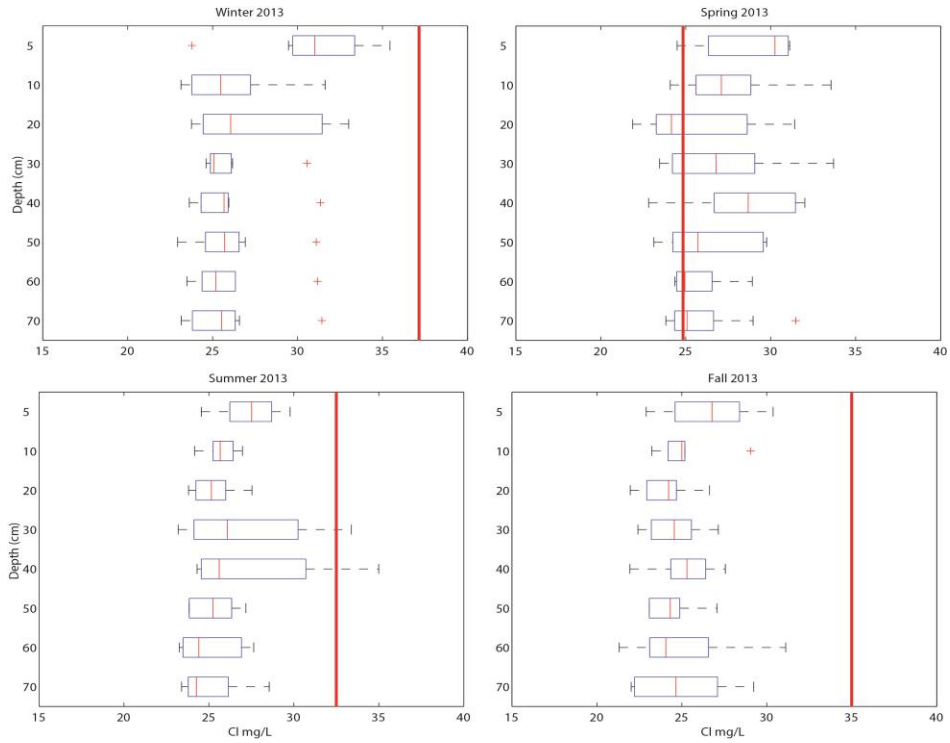

Figure 3.15 Cl^- concentrations at depth for 4 seasons in 2013. The red lines represent surface water Cl^- concentrations.

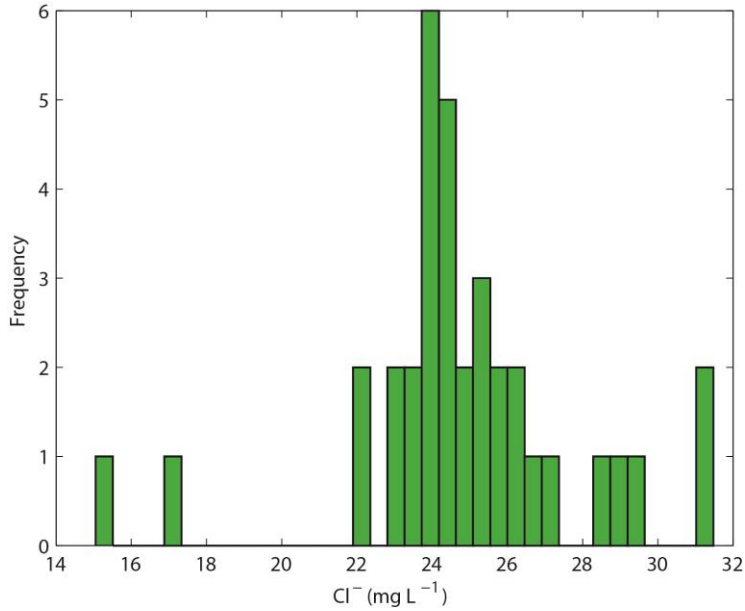

Figure 3.16 Histogram of Cl^- concentrations at 70cm sampling depth

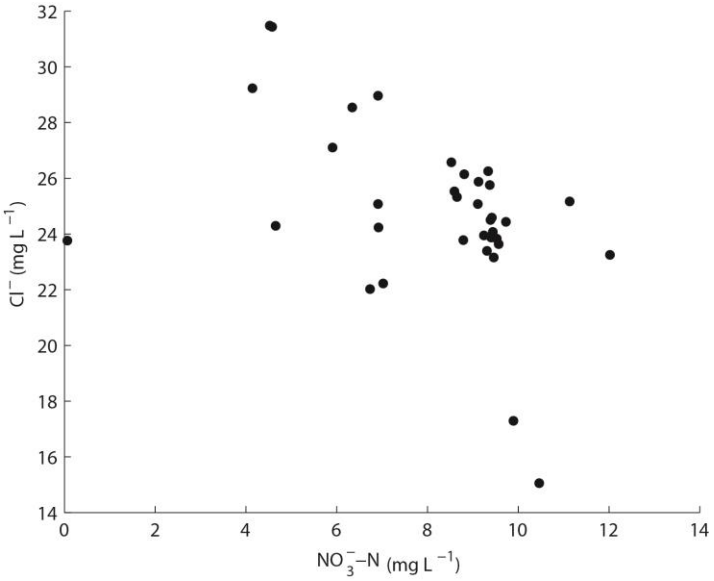

Figure 3.17 Correlation of NO_3^--N to Cl^- at 70 cm sampling depth

3.1.6 NO_2^- Patterns

NO_2^- was found at small concentrations of 0 to 0.28 mg/L at all sampling depths for each season (Figure 3.18). There was a similar trend in NO_2^- concentrations for winter, spring, and summer of increasing NO_2^- with decreasing sample depth. There were no significant differences in NO_2^- concentrations at different sample depths for each season (α=0.0018) Samples taken in the fall do not show any statistically different NO_2^- concentrations at depth (p=0.95) and do not reflect the general trend of increasing NO_2^- with decreased depth. Concentrations of NO_2^- at depth in the fall are highly variable and do not have any noticeable changes in with depth.

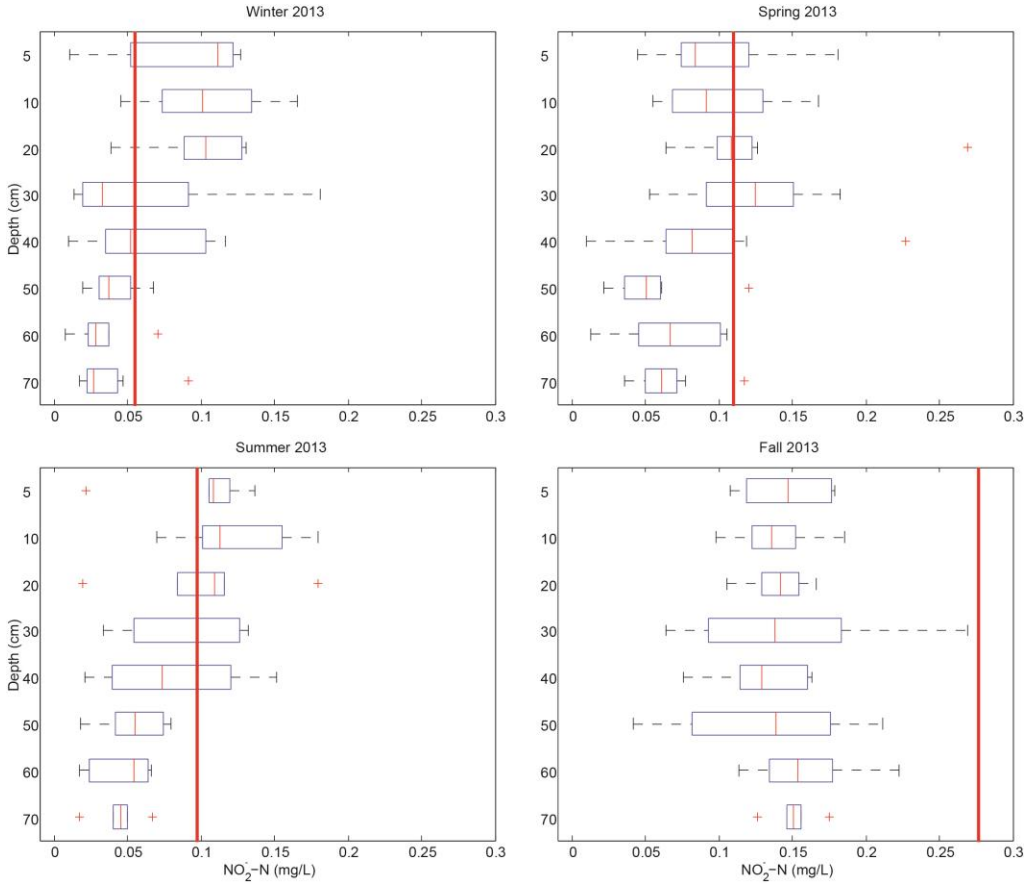

Figure 3.18 NO_2^--N concentration profiles for 4 seasons in 2013. Vertical red lines represent NO_2^- concentrations in the surface water.

3.1.7 Patterns in N_2O Production and Removal

N_2O production zones can be shown through the percent N_2O yield. N_2O yield is defined as the percentage of denitrified N released as N_2O (

Figure **3.19**). Instances within the columns where an there was a gain in N_2O associated with a loss in NO_3^- concentrations are categorized as locations of N_2O yield and represented 28% of all samples from all depths. For all seasons, there were peaks in mean N_2O yield of 1 to 40% from 30 to 5 cm. At depths 70 to 40 cm, N_2O yield did not exceed an average of 0.3%. All seasons, except summer, had relatively low N_2O yields ranging from 0 to 1.44%. In contrast,

summer had an extreme active zone at 20 to 10 cm where an average of 42.28% N_2O yield occurred.

Preferential removal of N_2O is defined as the percentage of N_2O removed of the total of N_2O and NO_3^- lost along an interval in the sampling profile. Instances of preferential removal of N_2O along the flow path represent 39% of all samples. There was an increasing trend of preferential N_2O removal from 70 to 40 cm with an average peak of 2.18% between 50 and 40 cm (Figure 3.20). In addition, at shallower depths of 10 cm to the sediment surface (0 cm) there was increased preferential removal of N_2O. There is a minimum in preferential N_2O removal from 20 to 10 cm which mirrors an increase in N_2O yield at this interval for all seasons except winter.

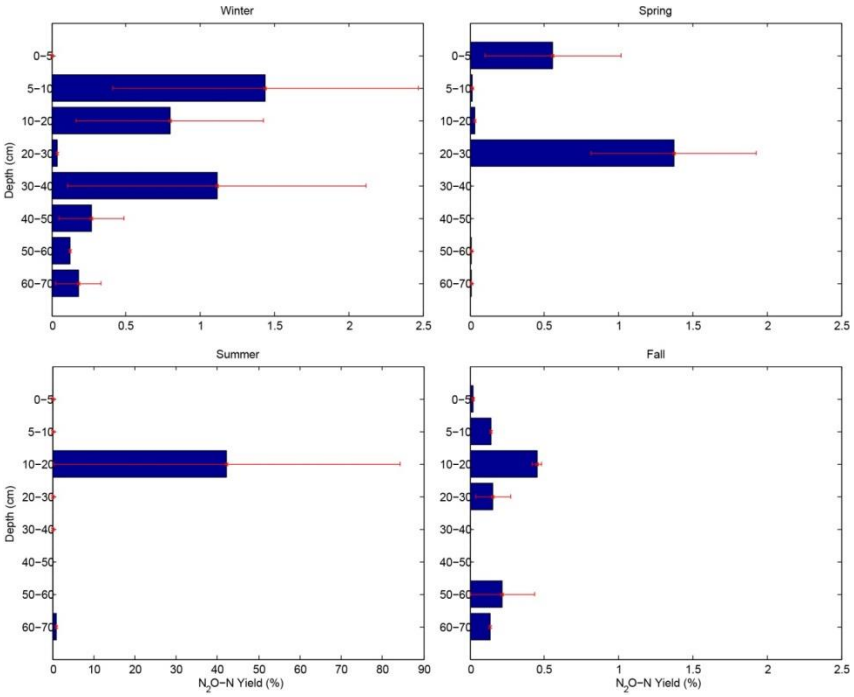

Figure 3.19. N_2O yield upwards along sampling profiles for all seasons. N_2O yield is defined as the percentage of N_2O-N produced for amount of NO_3^--N removed along each interval of the flow path.

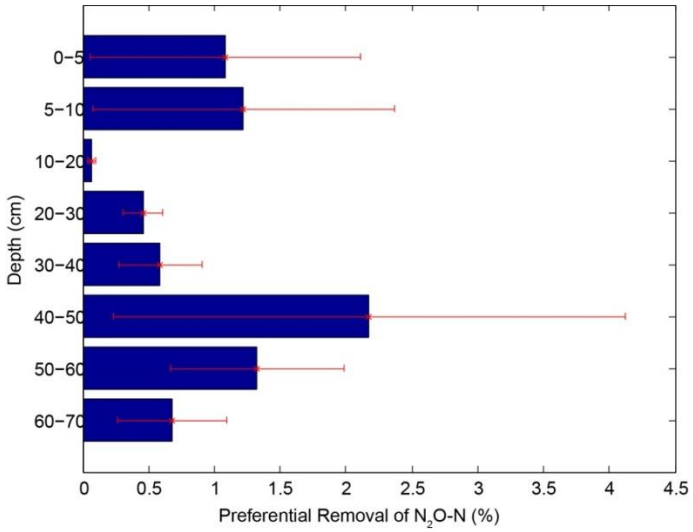

Figure 3.20. Preferential removal of N_2O upwards along sample profiles for all seasons. Preferential removal of N_2O is defined as the percentage of N_2O-N removed of the sum of N_2O-N and NO_3^--N removed in an interval along the flow path.

3.1.8 Correlation and Regression Relationships

Pearson correlation coefficients were calculated for most environmental parameters monitored during field work. No significant correlations were discovered for N_2O concentrations. However, numerous significant correlations with NO_3^- concentration were found with Cl^- concentration, depth, SO_4^{-2} concentration, lateral stream location (X), NO_3^- input concentration at 70 cm, N_2O input concentration at depth 70 cm, and pore water velocity (υ). There was a consistent correlation between Cl^- concentration and NO_3^- concentration as shown previously in Figure 3.17 for both anions at depth 70 cm. For all samples there was a smaller correlation coefficient of -0.28 confirming decreasing NO_3^- with increasing Cl^- at all depths and seasons ($p<0.001$). As shown in boxplots of NO_3^- at depth in Figure 3.3, there was a positive correlation coefficient of 0.45 ($p<0.001$). NO_3^- concentrations decreased with decreasing depths across all season samples. X represents lateral sample location in the stream from 1 to 3 for left bank to right bank. There was a positive correlation of increasing NO_3^- concentrations from

samples taken closer to the right bank (R=0.24, p<0.001). The right bank of the stream is bounded by a hill slope whereas the left bank is defined by relatively flat terrain.

There was a strong positive correlation between NO_3^- concentrations at 70 cm and the concentrations of NO_3^- at all other depths for each sample profile (R=0.5, p<0.001) (Figure 3.21). There was a small amount of scatter for profiles that have 8.5 to 10 mg N L^- NO_3^- at 70 cm indicating noticeable changes in NO_3^--N concentrations. However most other profiles hover around the initial value of NO_3^- found at 70 cm depth indicating minimal changes from the input NO_3^- concentration.

Table 3-3. Correlation table of Pearson linear pairwise correlations. Bolded values are significant at the α=0.05 level. Values with a * are significant to the α=0.01 level.

	$[N_2O]$	**$[NO_3^-]$**	**$[Cl^-]$**	**[DO]**	**T**	**Depth**	**$[NO_2^-]$**	**$[SO_4^{2-}]$**	**X**	**$[NO_3^-]$ @ 70 cm**	**$[N_2O]$ @ 70 cm**	**υ**	**NO_3^- Flux**	**N_2O Flux**
$[N_2O]$														
$[NO_3^-]$	-0.06													
$[Cl^-]$	0.00	**-0.28***												
[DO]	-0.03	-0.07	0.01											
T	0.01	0.00	-0.16	0.18										
Depth	-0.10	**0.45***	**-0.31***	0.00	0.11									
$[NO_2^-]$	0.02	**-0.32***	**-0.20***	0.15	0.04	**-0.24***								
$[SO_4^{2-}]$	0.05	**-0.36***	**0.68***	**-0.20**	-0.11	**-0.20***	**-0.31***							
X	-0.04	**0.24***	-0.04	**0.22**	0.11	-0.01	0	**-0.29***						
$[NO_3^-]$ @ 70 cm	0.02	**0.50***	-0.09	-0.07	-0.14	-0.01	**-0.14**	**-0.40***	**0.29***					
$[N_2O]$ @ 70 cm	-0.03	**-0.32***	0.04	0.06	0.02	0.00	0.00	**0.31***	**-0.21***	**-0.59***				
υ	0.04	**-0.20***	-0.05	**0.43***	0.15	0.00	**0.16**	-0.01	**-0.28***	**-0.44***	**0.31***			
NO_3^--N Flux	-0.08	**0.29***	0.08	**-0.33***	-0.11	0.00	-0.11	-0.04	**0.36***	**0.38***	**-0.29***	-0.75		
N_2O-N Flux	**0.17**	0.02	0.01	**-0.35***	-0.03	0.00	-0.05	-0.13	**0.20***	0.06	-0.04	-0.04	**-0.21***	

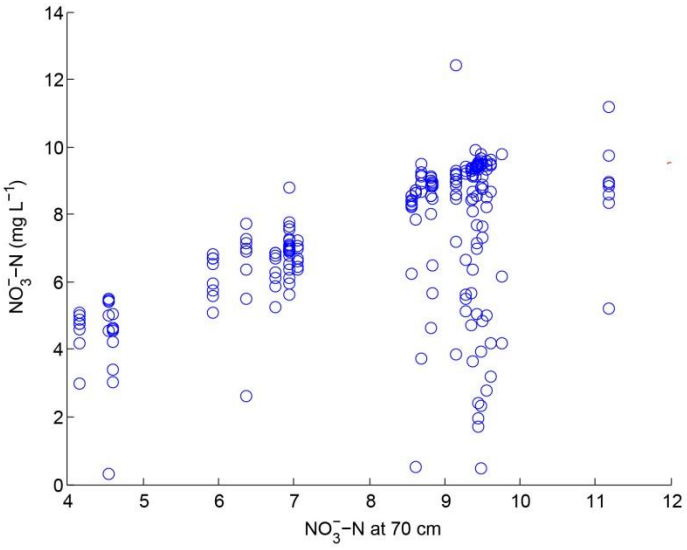

Figure 3.21. Correlation of NO_3^--N at depth 70 cm and NO_3^--N concentrations along the sampling profile**.**

Cl^- had a strong correlation with SO_4^{2-} where increasing Cl^- values correspond to increasing SO_4^{-2} concentrations at all depths for all seasons (R=0.68, p<0.001). Cl^- concentrations tended to decrease with increasing depth (R=-0.31, p<0.001). This correlation indicated that there were higher concentrations in the shallowest sediment and surface water compared to lower Cl^- concentrations in the deepest sediments.

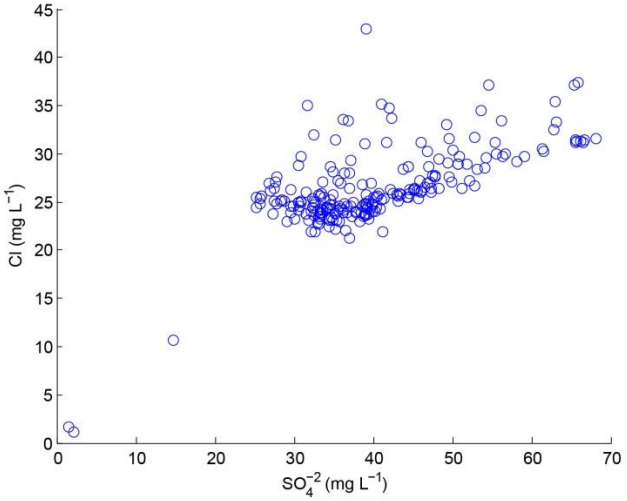

Figure 3.22. Correlation of SO_4^{2-} and Cl^- at all sample locations for all seasons.

DO had a strong correlation with pore water velocity, where increasing pore water velocity (gaining velocities are represented by negative values) coincided with decreasing DO concentrations at all depths and seasons ($R=0.43$, $p<0.001$). Similarly DO had a strong correlation to NO_3^- and N_2O fluxes at the surface. Increasing DO concentrations coincided with similar decreases in NO_3^- and N_2O fluxes with correlation coefficients of -0.33 and -0.35 respectively ($p<0.001$). A regression analysis of DO versus NO_3^- and N_2O fluxes found that DO concentrations result in negative slopes of -6.07 and -1.16 and cause 10.8 and 12.4 percent of the variance of NO_3^- and N_2O fluxes respectively ($p<0.001$). Temperature had no significant correlations with any of the measured parameters.

While there was not a strong correlation between NO_3^- and N_2O for all samples and all seasons, when observing a correlation of only NO_3^- and N_2O values at 70 cm we find a significant correlation with a coefficient of -0.59 ($p<0.001$). This correlation revealed that at a depth of 70 cm larger concentrations of NO_3^- coincided with smaller concentrations of N_2O and the reverse is true (Figure 3.23). A line of best fit fitted to NO_3^--N versus N_2O-N each at 70 cm, resulted in an R^2 of 0.35, where the concentration of NO_3^--N at 70 cm described 35 percent of the variance in the concentration of N_2O-N at 70 cm ($p<0.001$). NO_3^- at 70 cm had a negative correlation with pore water velocity with a coefficient of -0.44 ($p<0.001$). Gaining pore water velocity is represented as a negative value therefore a negative correlation means that with increasing pore water velocity there was a coinciding increase in NO_3^- concentration at 70 cm. The reverse was true for N_2O at 70 cm depth. There was a decrease in concentrations of N_2O at 70 cm with increasing pore water velocity ($R=0.31$, $p<0.001$).

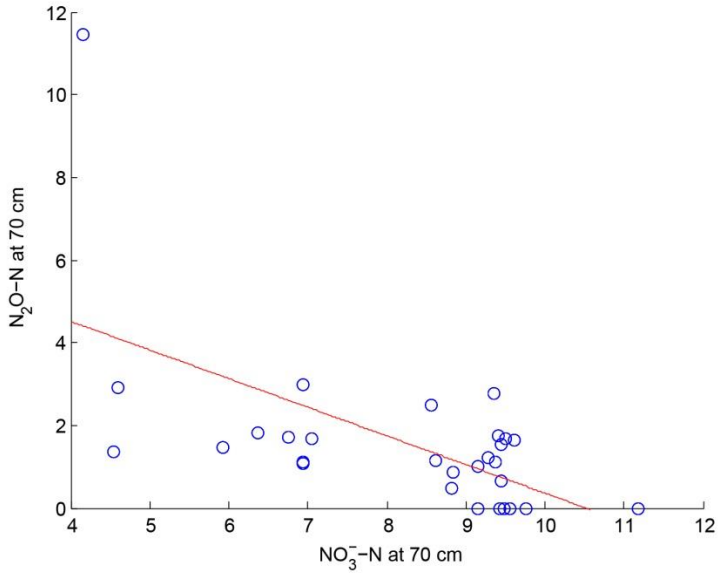

Figure 3.23 Regression of NO_3^--N versus N_2O-N at 70 cm for all four seasons. R^2=0.35 p<0.001

Fluxes of NO_3^- and N_2O increased from the left bank to the right bank of CMC towards the hill slope (R=0.36, 0.20; p<0.001, p=0.003). There was a positive correlation of NO_3^- concentrations at the sample depth of 70 cm and NO_3^- flux at the sediment surface (R=0.38, P<0.001). A regression analysis of NO_3^- at 70 cm versus the NO_3^- flux indicated that the concentration of NO_3^- at 70 cm was able to estimate 14.7 percent of the variance in NO_3^- flux for all seasons (p<0.001) (Figure 3.24). Lastly, there was a negative correlation between values of NO_3^- flux and of N_2O flux (R=-0.21, p=0.002). For all seasons, increasing fluxes of NO_3^- coincided with decreased fluxes of N_2O.

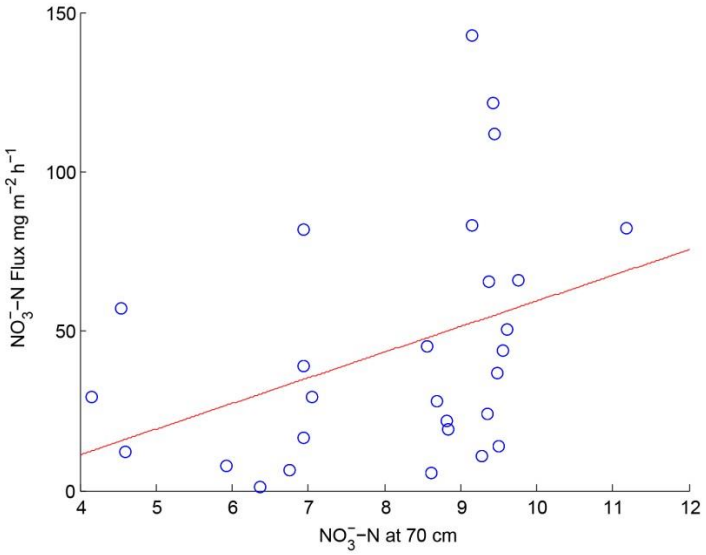

Figure 3.24. Regression of NO_3^--N at 70 cm and NO_3^--N flux. R^2=0.15 p<0.001

Two forms of linear regressions were used for a regression analysis to match the one performed on the column data. A simple multiple linear regression was used to identify the overarching controls of each variable on the resultant dependent variable and a stepwise multiple linear regression was used to investigate interactions of independent variables on the resultant dependent variable. Independent variables were temperature, NO_3^-, and pore water velocity for NO_3^- and N_2O concentrations within the column. Pore water velocity was removed as an independent variable in the models of NO_3^- and N_2O flux, however there were not significant models found for NO_3^- and N_2O flux. All the estimated coefficients reported are significant to the p<0.05 level and are defined by the following equations:

$$Y = \beta_1 T + \beta_2 NO_3^- \cdot N + \beta_3 v + \text{Intercept} \qquad \text{Equation 3-1}$$

$$Y = \beta_{I1} T * NO_3^- \cdot N + \beta_{I2} T * v + \beta_{I3} NO_3^- \cdot N * v + \text{Intercept} \qquad \text{Equation 3-2}$$

Table 3.4 Parameter estimates for multiple linear regression (β_1, β_2, β_3) and stepwise multiple linear regression including interactions (β_{I1}, β_{I2}, β_{I3}). All values reported are significant to $p<0.05$

Y	Intercept	β_1	β_2	β_3	R^2
NO_3^--N	1.59	0	0.74	0	0.54
Y	Intercept	β_{I1}	β_{I2}	β_{I3}	R^2
log(N_2O-N)	-0.27	0	0	0.16	0.11

From the linear regressions we find that in the field NO_3^- is dominantly controlled by the NO_3^- concentrations at 70 cm. Greater N_2O concentrations at all depths were determined by an interaction of increased NO_3^- concentrations at 70 cm and pore water velocity.

3.2 Results - Column Experiment

3.2.1 Column Core Characteristics

Hydraulic conductivity of the collected cores was found using the falling head method. The hydraulic conductivity of the A column was 1.21 x 10^{-3} cm s^{-1} and for the B column, it was 1.41 x 10^{-3} cm s^{-1} which is known to be in the general range of a fine or silty sand (Fetter, 2001) and within the range of previously measured hydraulic conductivities for sediments at CMC and in the local area (Hubbard *et al.*, 2001; Gu, 2007; Flewelling, 2009).

Breakthrough curves were determined for each column at each set pore water velocity using Cl^- as the conservative tracer. In all columns and at all pore water velocities Cl^- concentrations plateaued around 2 pore volumes (Figure 3.25). Breakthrough curves for pore water velocities of 0.5 to 2.5 cm h^{-1} were all very similar in shape. The breakthrough curve for the pore water velocity of 4.5 cm h^{-1} took on a different shape and appeared to be less dominated

by dispersion. The dispersion/diffusion coefficient was found for each breakthrough curve and the Peclet number was calculated. The Peclet number is the dimensionless ratio of the advective to the diffusive transport rate within sediment. If the Peclet number is greater than 1 then advection dominates the system. In all cases in this study the Peclet number was found to be greater than 10. Therefore all columns were assumed to be advection dominated and dispersion/diffusion was not considered in calculations of denitrification rates.

Total organic carbon (TOC) content was measured at each sampling port for both columns (Figure 3.26). Average TOC values for column A and B were 2.11% +/-1.8% and 1.17% +/-1.07%, respectively. The distribution of TOC with depth was different between the columns; however, the difference was not significant (paired t-test, p=0.27). In column A, the largest percentage TOC, 6.6% was found at 50 cm depth, however from 20 to 0 cm depth there was a consistent amount of TOC ranging from 1.4% to 3.4%. In column B the largest percent TOC was found at 25 cm depth at 3.9% and was flanked on either side at 20 and 30 cm with values from 1.4% to 2.4% TOC. Upon inspection of the sediment in each column, there were notably large organic fragments (>1 cm) found at different locations, thus these measurements might not fully represent the heterogeneity of TOC throughout the whole of each column.

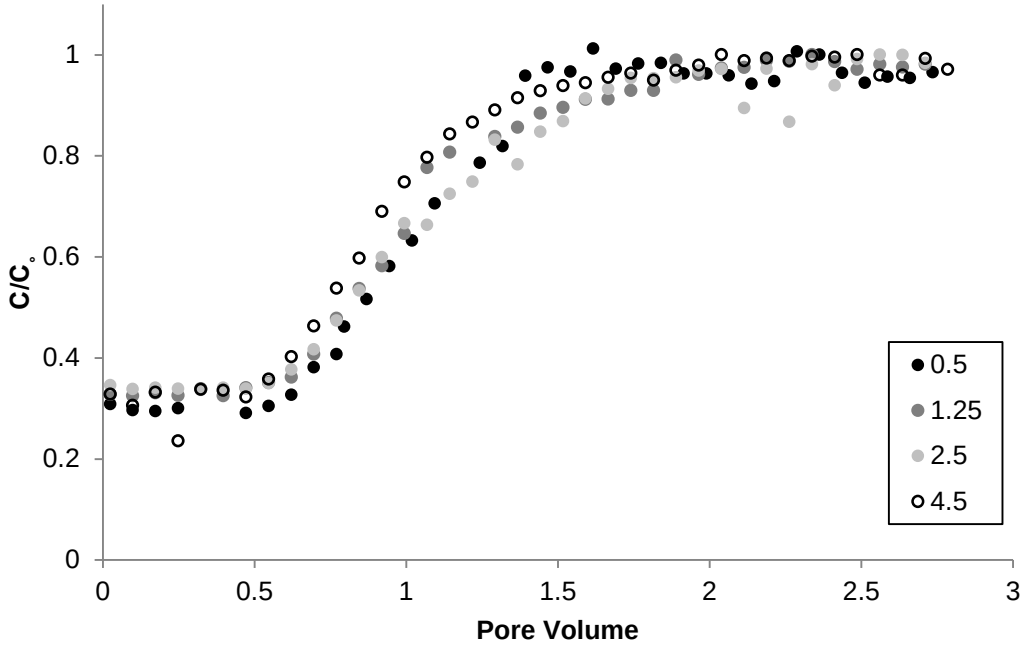

Figure 3.25 Cl^- breakthrough curves for 4 pore water velocities in cm h^{-1}.

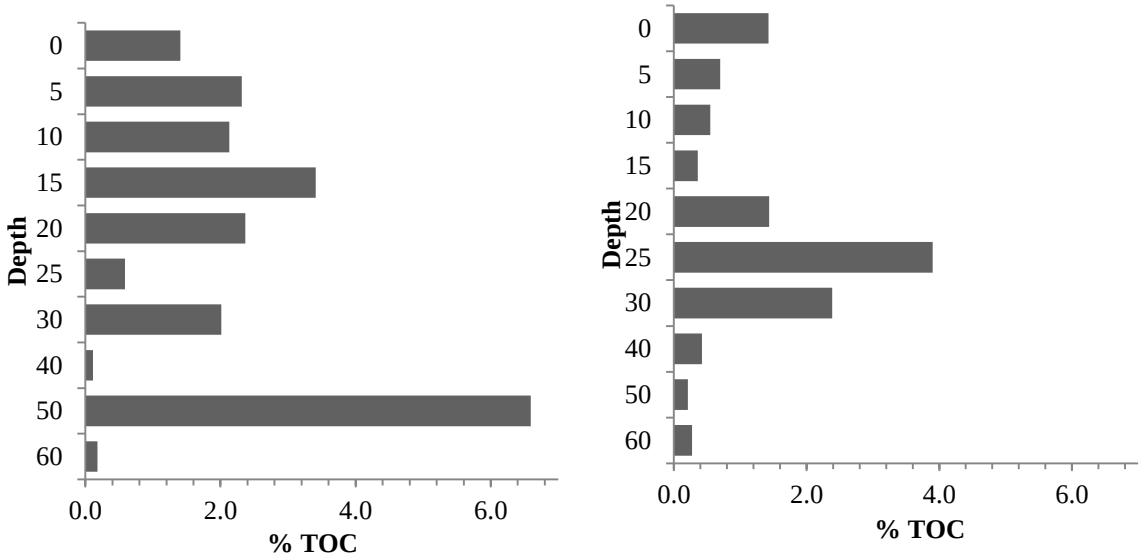

Figure 3.26 Total Organic Carbon (TOC) for column A (left) and column B (right).

N_2O and NO_3^- and other anions were measured at each depth port for all 36 experimental scenarios for both column A and B. Results of N_2O and NO_3^- are displayed in Figure 3.27 and Figure 3.28, respectively.

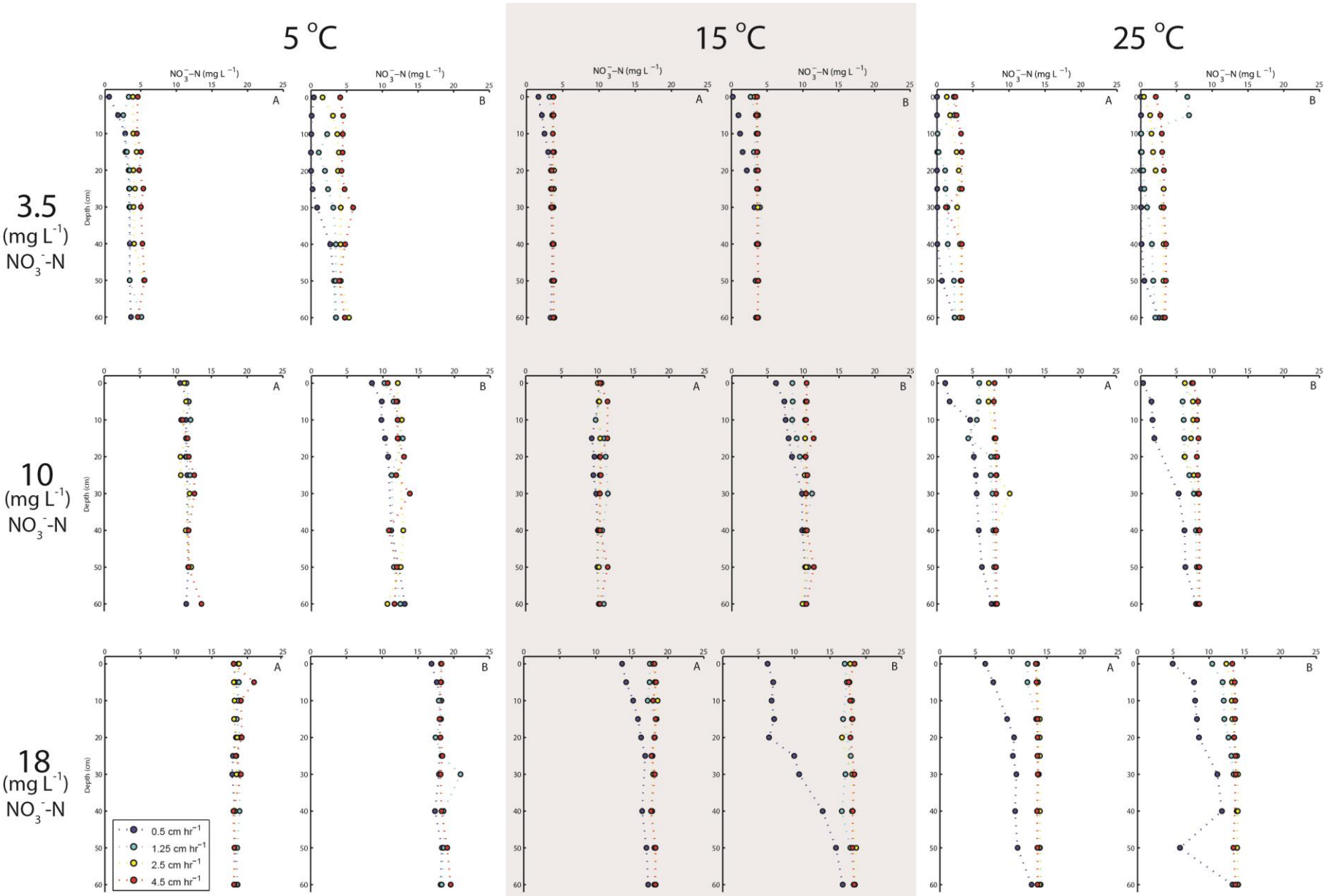

Figure 3.27 NO_3^--N at depth for all temperatures (horizontal), initial NO_3^- concentrations(vertical), and pore water velocity (profiles within graphs)

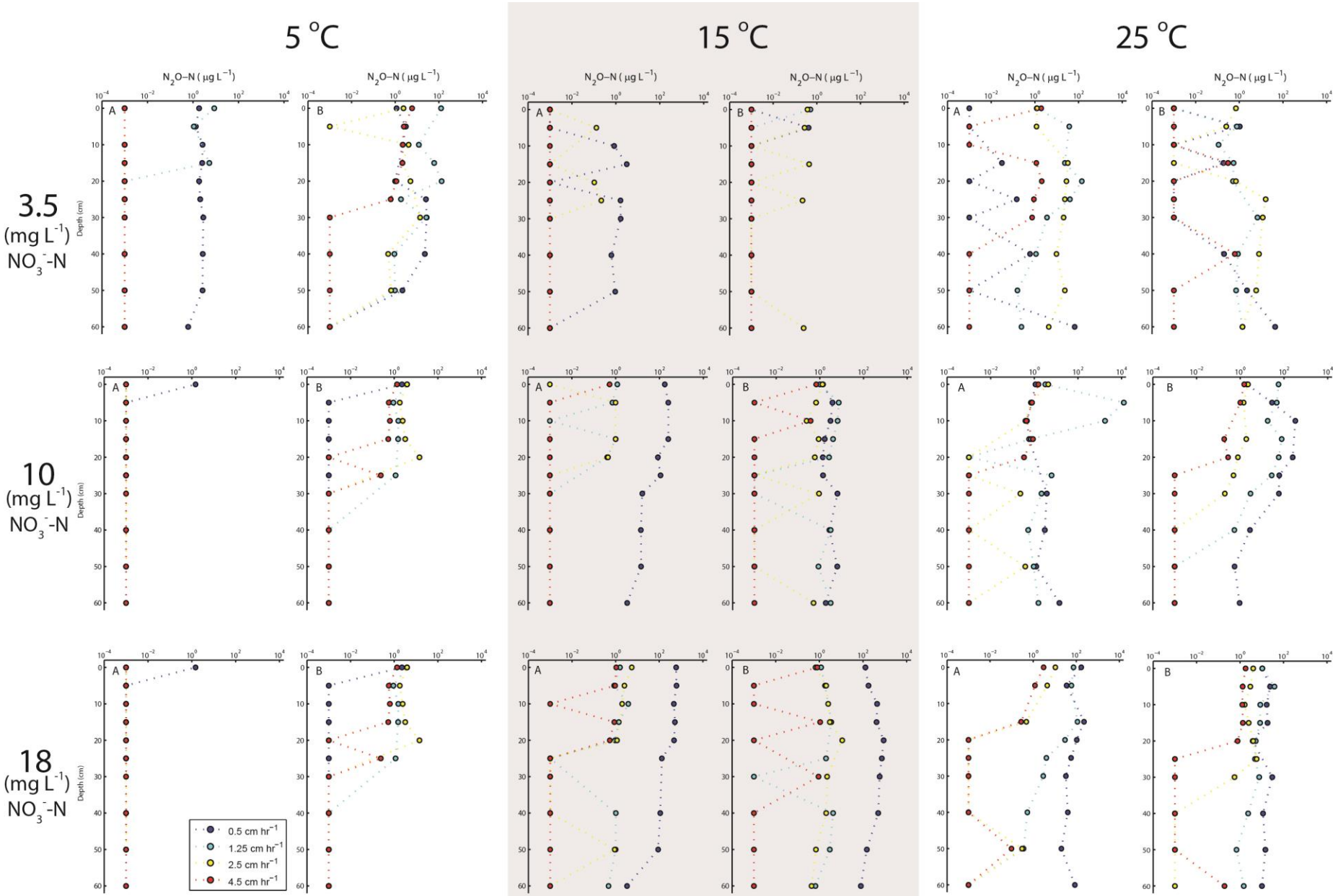

Figure 3.28 N_2O-N at depth for all temperatures (horizontal), initial NO_3^- concentrations(vertical), and pore water velocity (profiles within graphs)

3.2.2 Effect of Temperature

Temperature was controlled at 5°C, 15°C, and 25°C for these experiments. The results reported in the following paragraphs are representative of both columns, all initial NO_3^- concentrations, and all pore water velocities unless otherwise noted.

Temperature did not have a significant impact on the concentration of NO_3^- in the columns; at the top of the column (0 cm) NO_3^- concentration was not significantly different between 5°C and 25°C in pairwise comparison, ($p=0.029$, $\alpha=0.017$) (Figure 3.29). Also there was not, a relationship between temperature and NO_3^- flux ($p=0.361$). The denitrification rate at 25°C was significantly larger than at 15°C ($p=0.003$, $\alpha=0.017$). However, the denitrification rates at 5°C were similar to those obtained at 15°C, and included a single outlier high value of 3.71 mg N L^{-1} day^{-1}. Because denitrification rates were determined from NO_3^- removed there was a significant increase in percent of NO_3^- removed from the column from 15°C to 25°C ($p<0.001$, $\alpha=0.017$) corresponding to the increase in denitrification rates over the same temperature increase (Figure 3.29).

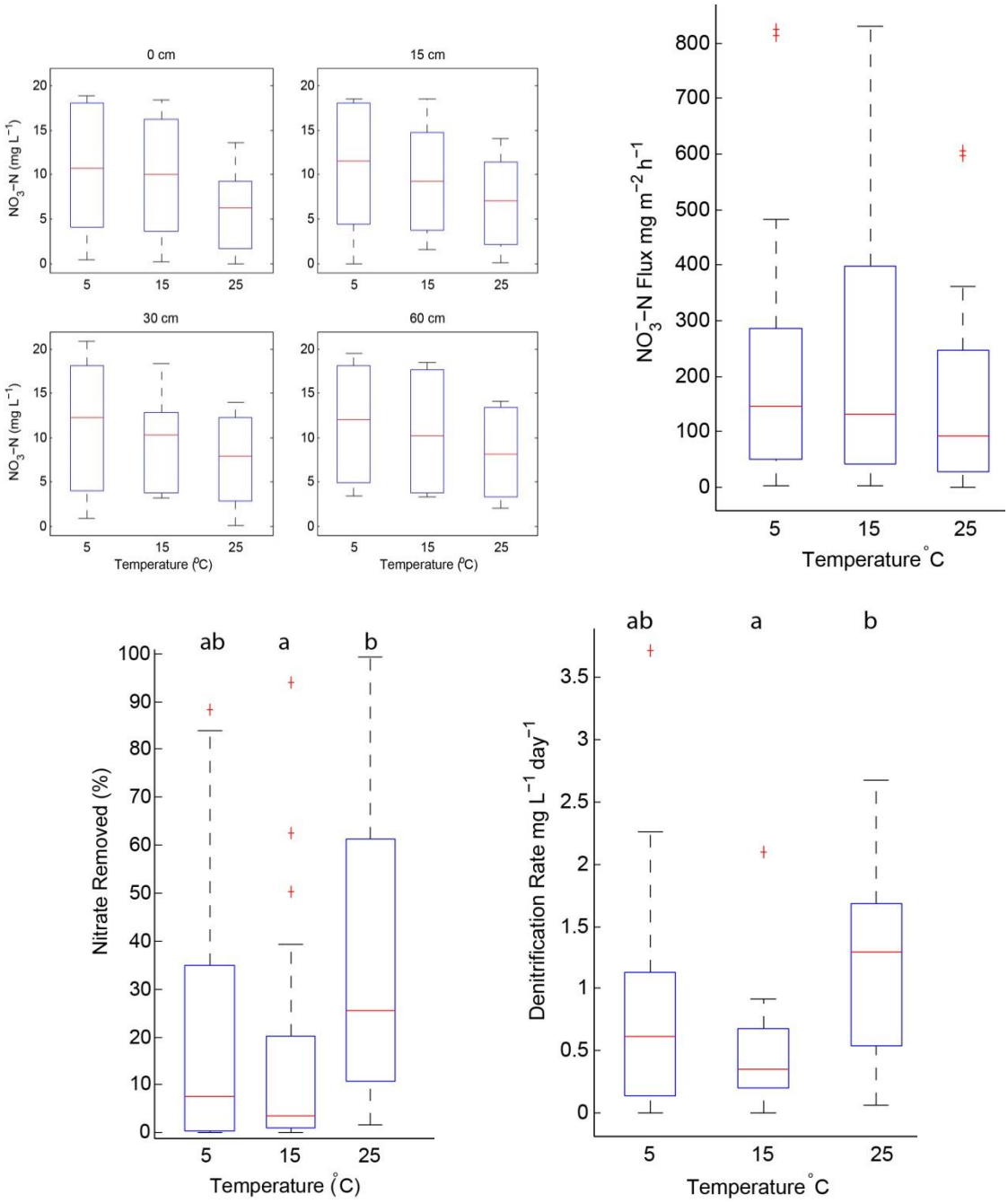

Figure 3.29 Nitrate concentration (upper left), nitrate flux (upper right), percent nitrate removed (lower left), and denitrification rate (lower right) for 3 temperatures. Letters above the graphs indicate a significant difference (α=0.017) for 3 pairwise tests.

At each depth, mean NO_3^- concentrations decreased with decreasing depth and increasing temperature (Figure 3.30). At 5°C and 25°C the highest mean denitrification rates were observed in the last interval of sediment (5 to 0 cm) at 9.93 and 6.00 mg NO_3^--N L^{-1} day^{-1}

respectively. The highest mean denitrification rate at 15°C occurred at 15-10 cm at 4.52 mg NO_3^--N L^{-1} day^{-1}.

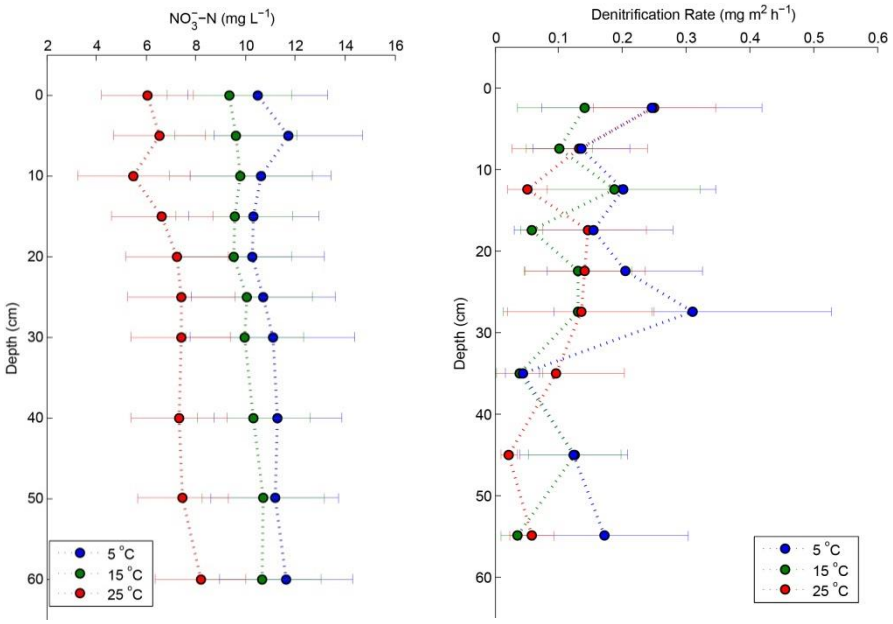

Figure 3.30 Depth profile of mean NO_3^--N concentration and denitrification rate at 3 temperatures. Error bars represent 95% confidence intervals.

Increasing temperature caused a significant increase in N_2O concentrations at 30 and 60 cm depth from 5°C to 25°C ($p<0.017$) (Figure 3.31). However, at 15 and 0 cm depths we did not observe a significant difference at different temperatures due to an overall increase in N_2O at all three temperatures. In addition, we observed an increase in variability in N_2O concentrations with increasing temperatures. N_2O flux increased with increasing temperature from a mean of 101.58 µg m^{-2} h^{-1} at 5°C to 157.31 µg m^{-2} h^{-1} at 25°C (Figure 3.32). Difference in N_2O flux between 5°C and 15°C was not significant ($p=0.34$). The N_2O yield, defined as the amount of N_2O-N produced expressed as a percentage of the NO_3^--N removed, rose from a median of 0.09% at 5°C to 0.23% at 25°C. However, there was no significant difference between N_2O yields at different temperatures.

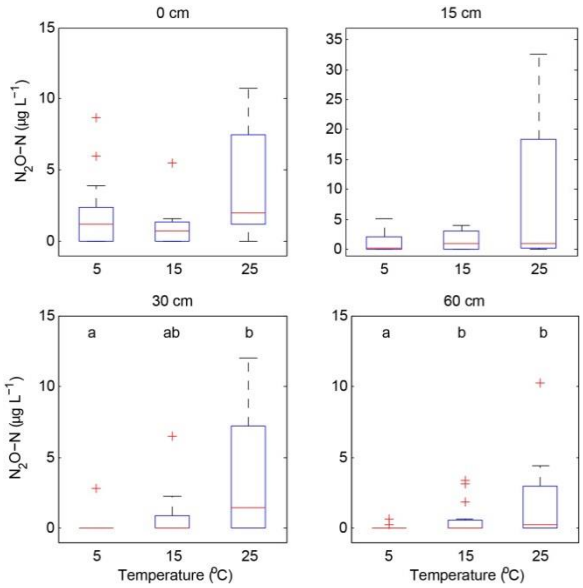

Figure 3.31 N_2O-N concentration for three temperatures at four depths. Letters above boxes represent statistically different groups (α=0.017).

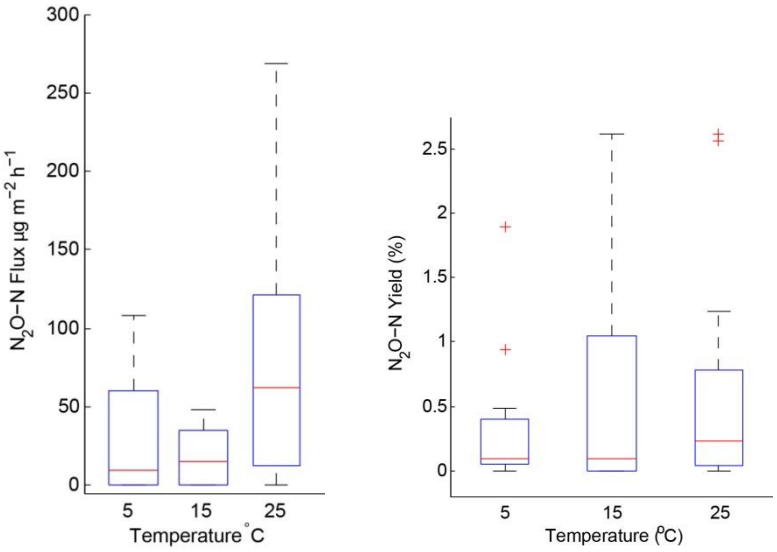

Figure 3.32 N_2O flux and N_2O yield (N_2O-N produced / NO_3^--N reduced expressed as a percentage) for 3 temperatures.

Patterns of N_2O concentrations at depth were different for each temperature (Figure 3.33). N_2O concentrations at 5°C began at values close to 0 µg N L^{-1} and then ramped up to a peak mean of 7.22 µg N L^{-1} at 20cm. There was a small decrease in concentration following the peak at 20 cm, however, there was a final peak in N_2O concentration at 0 cm. N_2O concentrations at

15°C followed a similar arch in concentration with a mean peak of 63.69 µg N L^{-1} at 20 cm. N_2O concentrations at 25°C begin at depth 60 cm with a peak in concentration. N_2O concentration increased along the flow path to a mean peak concentration located at 5 cm of a mean of 535.49 µg N L^{-1}.

Change in N_2O concentrations along the flow path illuminates regions of heightened N_2O production and N_2O removal (Figure 3.34). At 5°C minimal N_2O production occurs before 30 cm depth and the majority of N_2O production occurs in the 5 to 0 cm depth interval. At 15°C, there is consistent N_2O production from 60 to 15 cm followed by balanced production and removal from 15 to 0 cm. At 25°C, there is a shift and N_2O production is heightened at all depths especially at the 25 to 20 cm depth interval. The zone of N_2O removal is mainly found at 15 to 10 cm depth. During scenarios at 5°C and 25°C there was overall N_2O production in the last 5 cm of sediment which means that in these cases there would be no other chances for N_2O removal before effluxing into surface water.

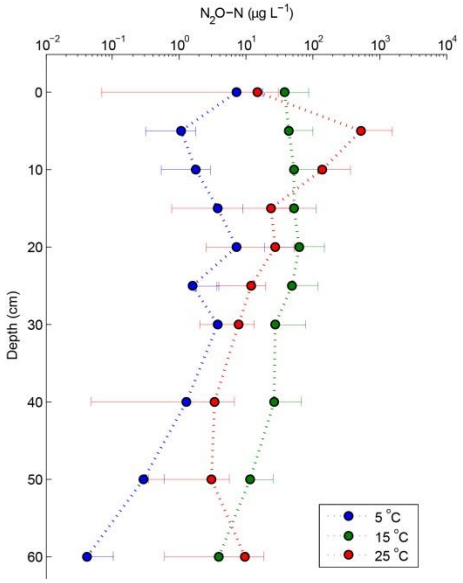

Figure 3.33 Depth profiles of mean N_2O-N (left) for three temperatures. Error bars represent 95% confidence intervals

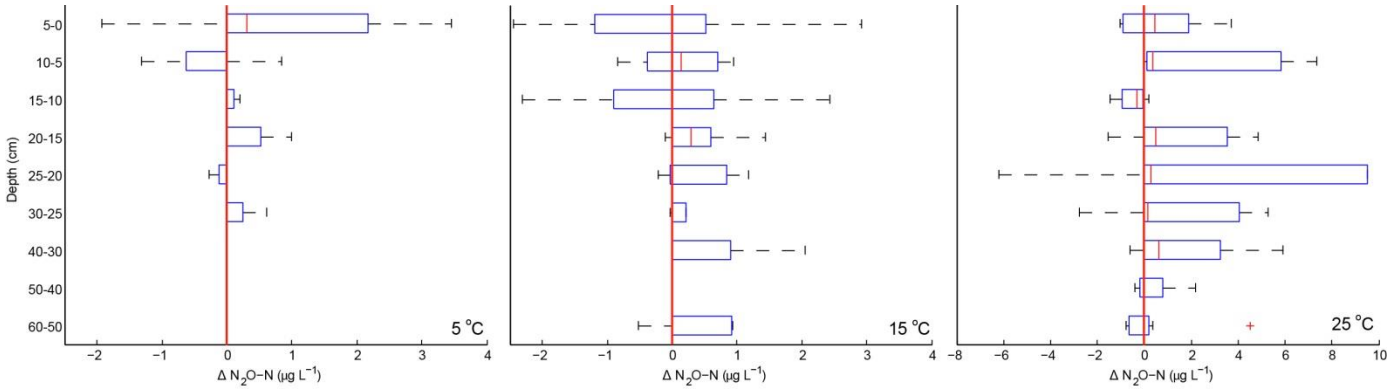

Figure 3.34 Change in N_2O with depth for 5°C (left), 15°C (center), and 25°C (right). Note different scales along the x-axis. The vertical red line indicates zero change.

Temperature had a significant effect on DO concentrations in both columns. There was a decreasing trend of DO concentrations with increasing temperature ($p<0.001$, $\alpha=0.017$). As shown in Figure 3.35, DO concentrations ranged between 2 and 9 mg L^{-1} which is above the known limit for denitrification to occur (Firestone *et al.*, 1979), however, we have observed NO_3^- removal (denitrification) occurring within the columns. The error in DO measurements lies in the methodology which consistently added on average 2.57 mg L^{-1} to the measurements. All discussion following will exclude DO data. The removal of NO_3^- and the accumulation of N_2O in the columns confirm denitrification occurred during the experimental scenarios.

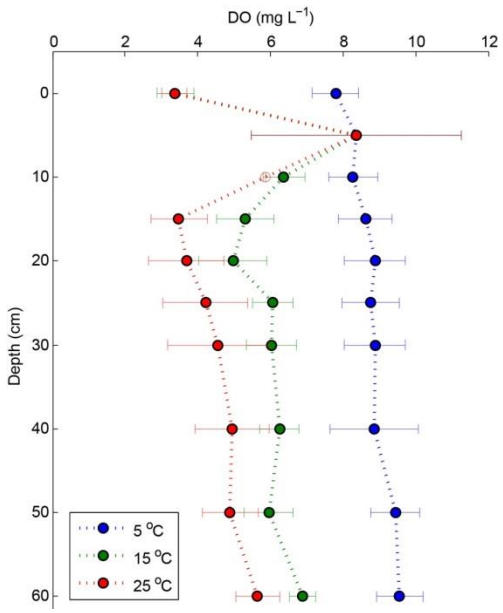

Figure 3.35 DO concentration at all sample depths for 3 temperatures

3.2.3 Effect of Initial NO_3^- Concentration

Initial NO_3^- concentration had a significant impact on the concentration of NO_3^- throughout both columns ($p<0.001$, $\alpha=0.017$). As would be expected, increasing initial NO_3^- concentrations resulted in increasing NO_3^- within the columns (Figure 3.36). Increasing initial NO_3^- concentrations accounted for 81.2% of the variance associated with NO_3^- concentrations within the columns. Increasing initial NO_3^- concentration increased the flux of NO_3^- between 3.5 and 18 mg N L^{-1} initial concentration ($p<0.001$, $\alpha=0.017$) and accounted for 28.3% of the variance of the NO_3^- flux ($p<0.001$). In addition, increasing initial NO_3^- concentration reduced the mean percent of NO_3^- removed from 43% at 3.5 mg N L^{-1} to 13% at 18 mg N L^{-1} ($p=0.006$, $\alpha=0.017$). There was no significant difference in denitrification rate for each initial NO_3^- concentration ($p=0.94$).

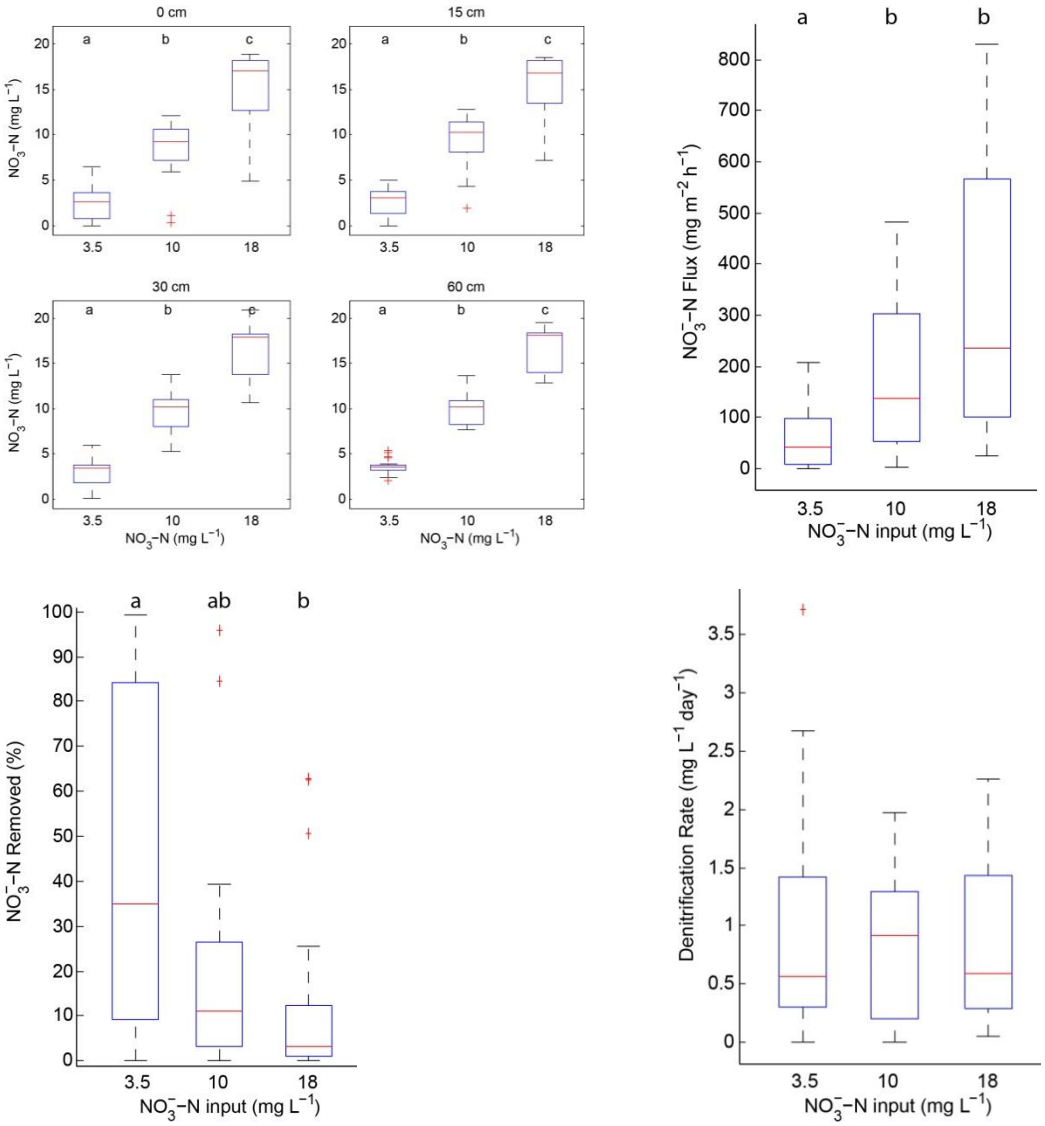

Figure 3.36 NO_3^--N concentration, NO_3^- flux, nitrate removal percentage, and denitrification rate for 3 initial NO_3^--N concentrations. Letters represent statistically significant difference between groups (α=0.017).

Denitrification rates were variable at each depth and initial NO_3^- concentration. There was not a difference in denitrification rates for each of the three initial NO_3^- concentrations (Figure 3.36). At most depths the largest mean denitrification rates were observed when the initial NO_3^- concentration was 10 mg N L^{-1} (Figure 3.37). Peaks in denitrification rates were detected from 5 to 0 cm for both 3.5 and 18 mg N L^{-1} initial NO_3^- concentration. The peak mean

denitrification rate when the initial NO_3^- concentration was 10 mg N L^{-1} was located at the beginning of the flow path from 30 to 25 cm.

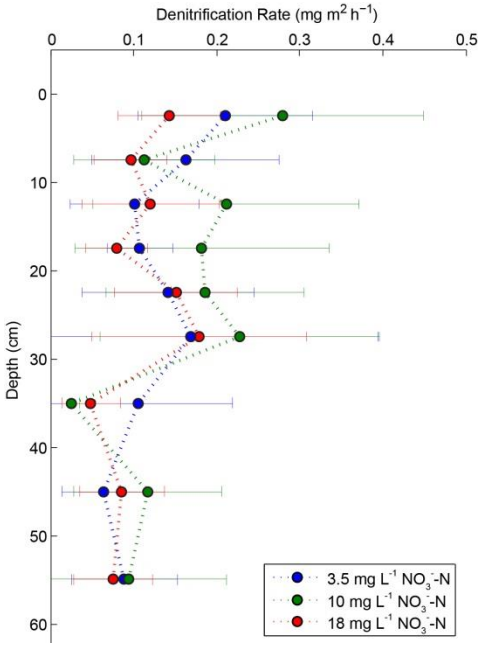

Figure 3.37 Mean denitrification rate for 3 initial NO_3^--N concentrations. Error bars represent 95% confidence intervals.

Increasing initial concentrations of NO_3^- resulted in increased concentrations of N_2O between 3.5 mg N L^{-1} and 18 mg N L^{-1} at the top of the columns ($p<0.001$, $\alpha=0.017$), but was not significantly different at 15, 30, or 60 cm depth (Figure 3.38). In addition, there was an increase in N_2O flux with increased initial concentrations of NO_3^- between 3.5 and 18 mg N L^{-1} ($p<0.001$, $\alpha=0.017$) (Figure 3.39). The mean N_2O flux increased from 4.93 µg m^{-2} h^{-1} at 3.5 mg N L^{-1} to 39.29 µg m^{-2} h^{-1} at 18 mg N L^{-1}. There was a significant increase in mean N_2O yield with increasing initial NO_3^- concentration; 0.03% at 3.5 mg N L^{-1} to 0.44% at 18 mg N L^{-1} ($p=0.013$, $\alpha=0.017$).

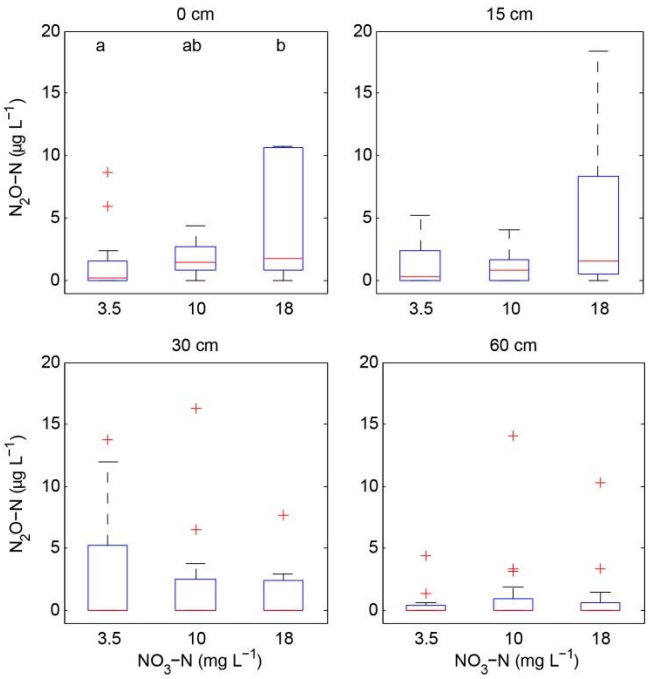

Figure 3.38 N_2O-N concentration at three initial NO_3^--N concentrations at 4 depths. Letters above the boxes indicate statistically different groups (α=0.017).

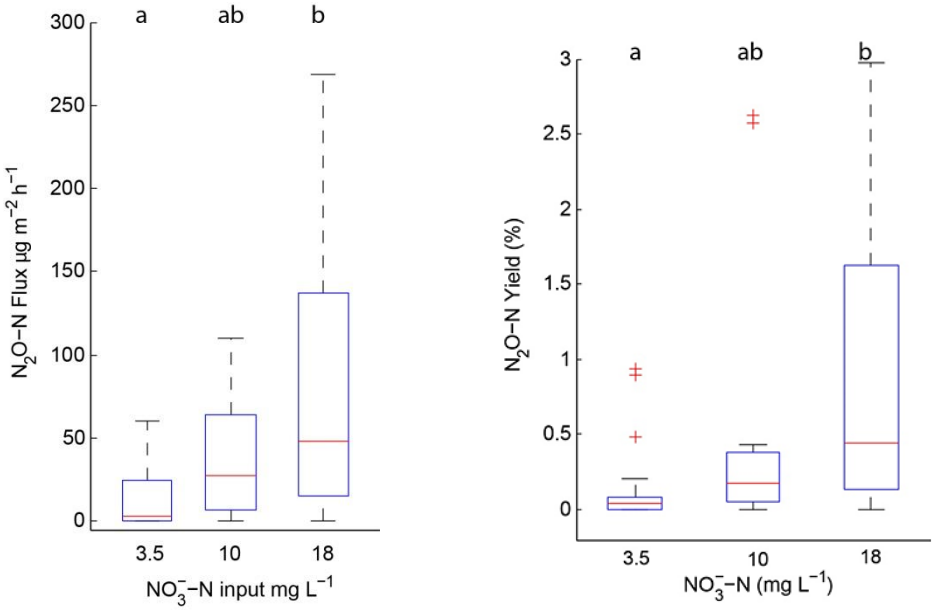

Figure 3.39 N_2O-N Flux, and N_2O yield for three input NO_3^--N concentrations. Letters represent statistically significant different groups (α=0.017).

Mean N_2O concentrations at depth created different patterns along the flow path for each initial NO_3^- concentration (Figure 3.40). There were three peaks in mean N_2O concentrations at 60 cm, 20 cm, and 0 cm for the initial NO_3^- of 3.5 mg N L^{-1}. For the initial NO_3^- concentration of 10 mg N L^{-1} the mean concentration of N_2O rose from close to 0 to a peak of 537.96 µg N L^{-1} at 5 cm, however the mean concentration was reduced to 11.05 µg N L^{-1} at 0 cm. Similarly, at the initial NO_3^- concentration of 18 N mg N L^{-1}, mean N_2O concentrations increased from 60 cm to a peak of 69.43 µg N L^{-1} at 20 cm and then decreased to 44.53 µg N L^{-1} at 0 cm.

For all initial NO_3 concentrations there were zones of N_2O production from 60 to 25 cm shown by changes of N_2O at depth intervals in Figure 3.41. Removal of N_2O began to become more significant from 25 to 0 cm, however it was most apparent at 15 to 10 cm and 5 to 0 cm.

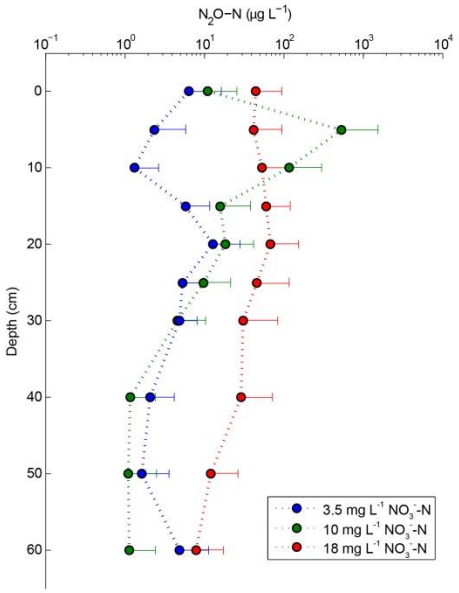

Figure 3.40 Mean N_2O-N concentrations at depth for three initial NO_3^- concentrations. Error bars represent 95% confidence intervals.

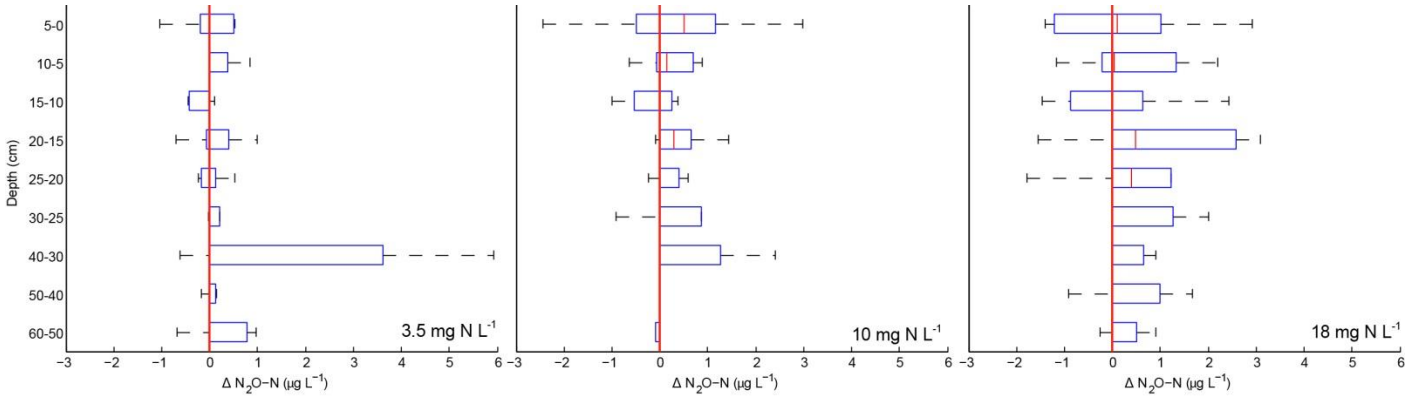

Figure 3.41 Change in N_2O for sampled depth intervals for 3.5 (left), 10 (center), and 18 (right), mg N L^{-1} initial NO_3^--N concentrations. The vertical red line indicates zero change.

3.2.4 Effects of Pore Water Velocity

Pore water velocity had a moderate effect on NO_3^- concentrations in the columns. NO_3^- values at all pore water velocities were not significantly different at the top of the column ($p=0.113$) (Figure 3.42). The percentage of NO_3^- removal was significantly higher at a pore water velocity of 0.5 cm h^{-1} than at 4.5 cm h^{-1} with means of 54.65% and 8.28% respectively ($p<0.001$, $\alpha=0.009$). There was not a linear trend in decreasing percentage of NO_3^- removed with increasing pore water velocity. The mean percentage of NO_3^- removal at 2.5 cm h^{-1} was 23.70% which was higher than the mean at 1.25 and 4.5 cm h^{-1}, but these relationships were not significantly different.

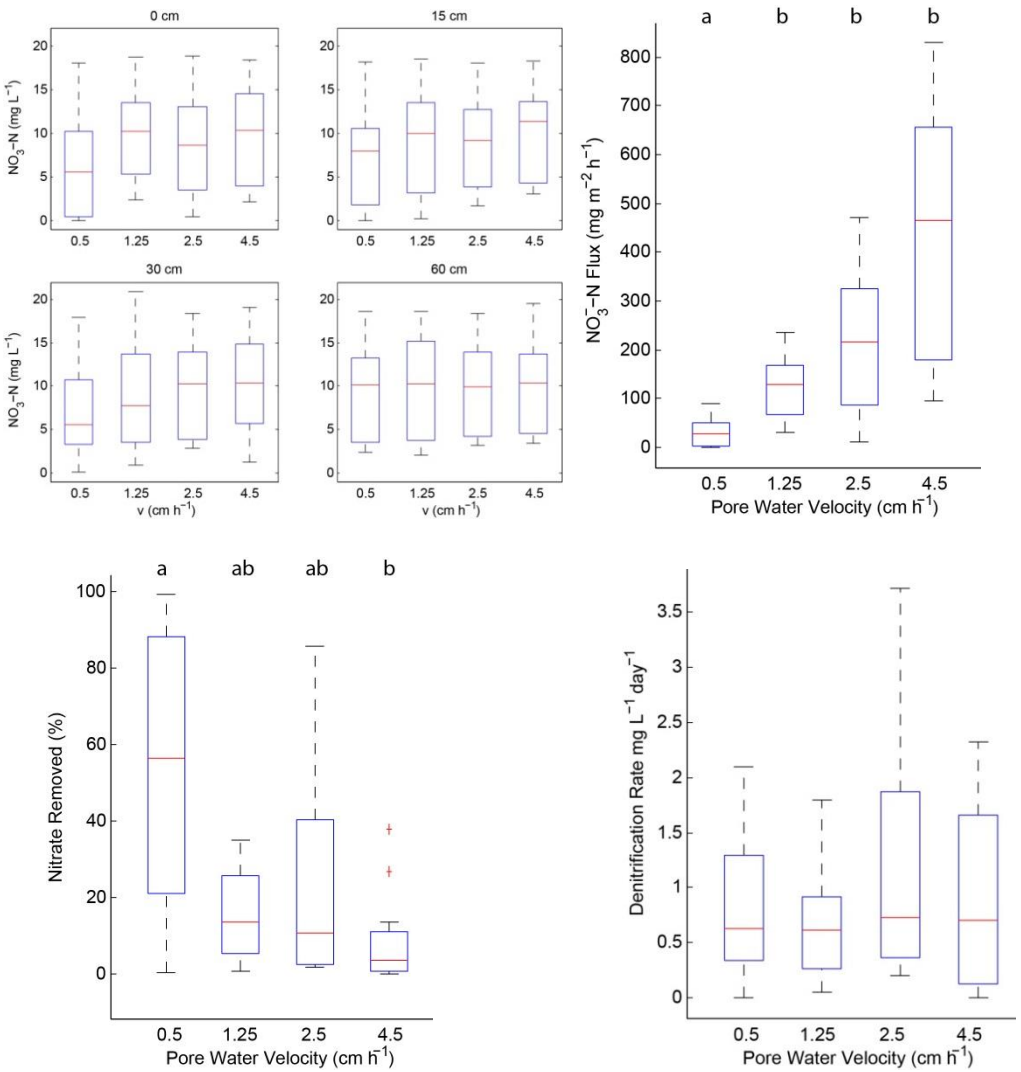

Figure 3.42 NO_3^--N concentration at four depths, NO_3^--N flux, NO_3^- removal percentage, and denitrification rate for 4 pore water velocities. Letters above the graphs represent statistically significant different groups (α=0.009).

Pore water velocity had a significant effect on the concentration of N_2O in the columns at 15, 30, and 60 cm depth, but not at the top of the column (0 cm) (Figure 3.43). We observed accumulation of N_2O at 60 cm depth for pore water velocities 0.5 and 1.25 cm h^{-1}. There was also a marked decrease in variance with increased pore water velocity. In contrast, there was a general trend of increased median N_2O flux with increasing pore water velocity (p=0.01, α=0.009) (Figure 3.44). The trend in means and medians for N_2O flux at each pore water velocity were the inverse of each other. There was a general trend of decreasing mean N_2O flux with

increasing pore water velocity from a mean of 302.86 µg m^{-2} h^{-1} at 0.5 cm h^{-1} to 53.44 µg m^{-2} h^{-1} at 4.5 cm h^{-1}, converse to the trends in medians shown in Figure 3.44. There was not a significant difference in N_2O yield with increasing pore water velocity. The overall total mean value of N_2O yield for all scenarios was 2.51% +/- 1.74% standard error of the mean.

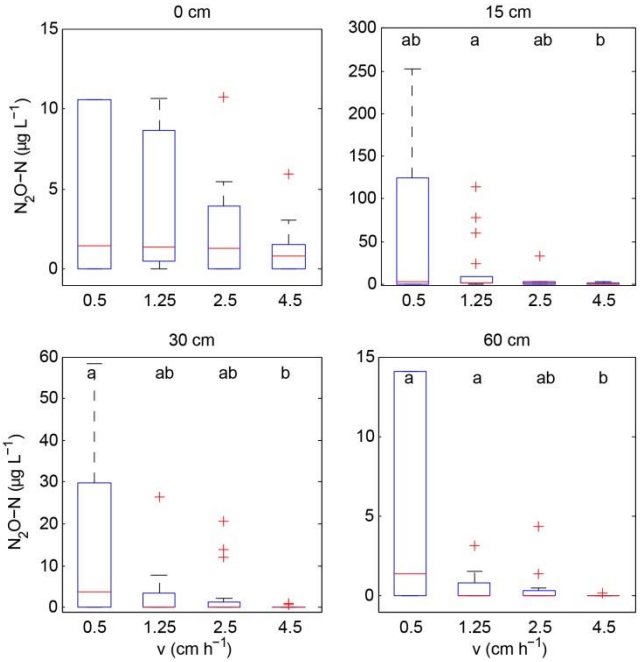

Figure 3.43 N_2O-N at 4 depths for 4 pore water velocities. Letters above boxes indicate statistically significant groups (α=0.009). Note different scales on the y-axis for each graph.

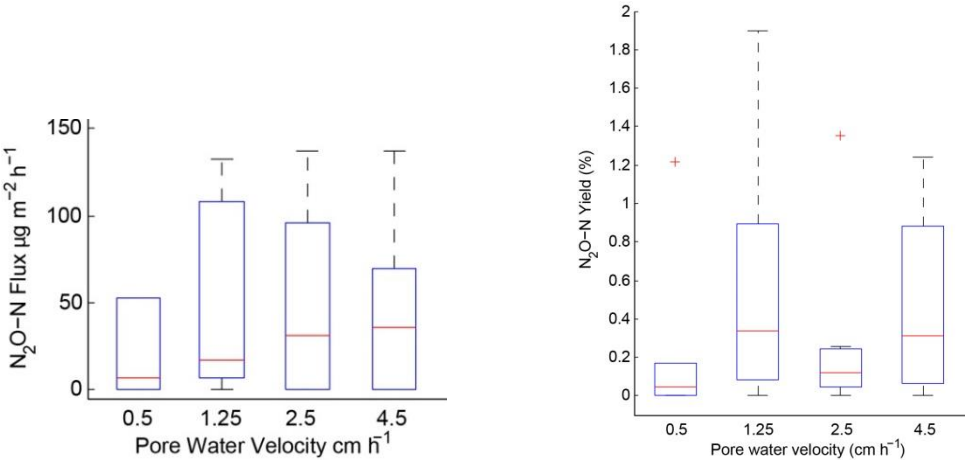

Figure 3.44 N_2O-N flux, and N_2O yield for 4 pore water velocities.

There were distinguishable patterns in mean N_2O concentration with depth at all four pore water velocities (Figure 3.45). The mean N_2O concentrations at 0.5 cm h^{-1} gradually rose to a peak at 20 cm and then decreased to the outlet. Mean N_2O concentrations for 1.25 cm h^{-1} gradually increased and peaked at 5 cm and then decreased at the outlet. The peak mean N_2O concentration at 5 cm was 750 µg N L^{-1} and was the highest for all 4 pore water velocities and depths. This value was much larger than most other mean N_2O concentrations and represents a skewing by one sample that measured 12.5 mg N L^{-1} at a temperature of 25°C and initial NO_3^- concentration of 15 mg N L^{-1}. N_2O concentrations at 2.5 cm h^{-1} peaked at 20 cm depth and again at 0 cm depth. N_2O concentrations at 4.5 cm h^{-1} were the lowest of all pore water velocities and peak mean concentration occurred at the outlet of the columns.

Pore water velocity had a significant impact on production and removal of N_2O at depth within the columns (Figure 3.46). At 4.5 cm h^{-1} there was not any significant increases in N_2O until 30 cm depth and production dominated the columns during this flow regime. At 2.5 cm h^{-1} there was noticeable production of N_2O up to 25 cm where increased N_2O removal began to occur up to 10 cm. At 0.5 and 1.25 cm h^{-1} there was dominant production within the columns especially at the depth interval of 25-20 cm. At the faster pore water velocities of 2.5 and 4.5 cm h^{-1} the last interval of 5 to 0 cm was dominated by N_2O production, whereas at 0.5 cm h^{-1} it was dominated by N_2O removal.

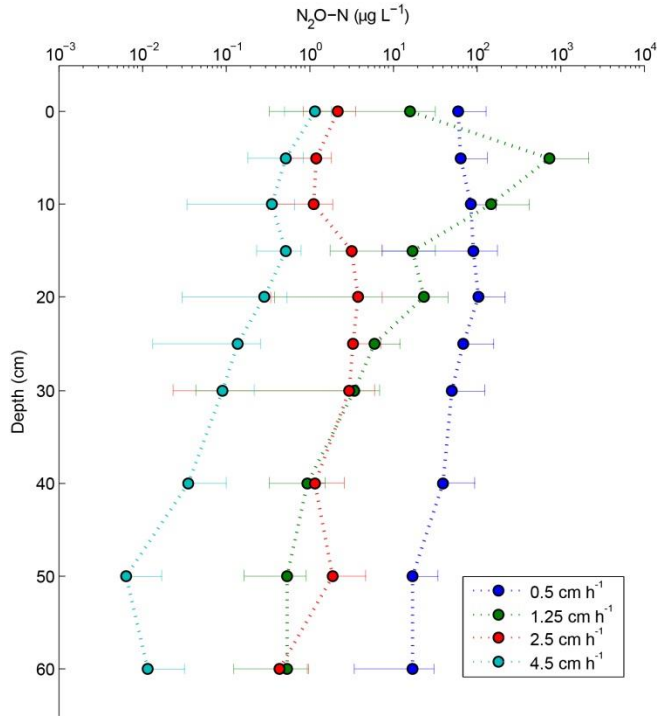

Figure 3.45 Mean N_2O-N concentration at depth for 4 pore water velocities.

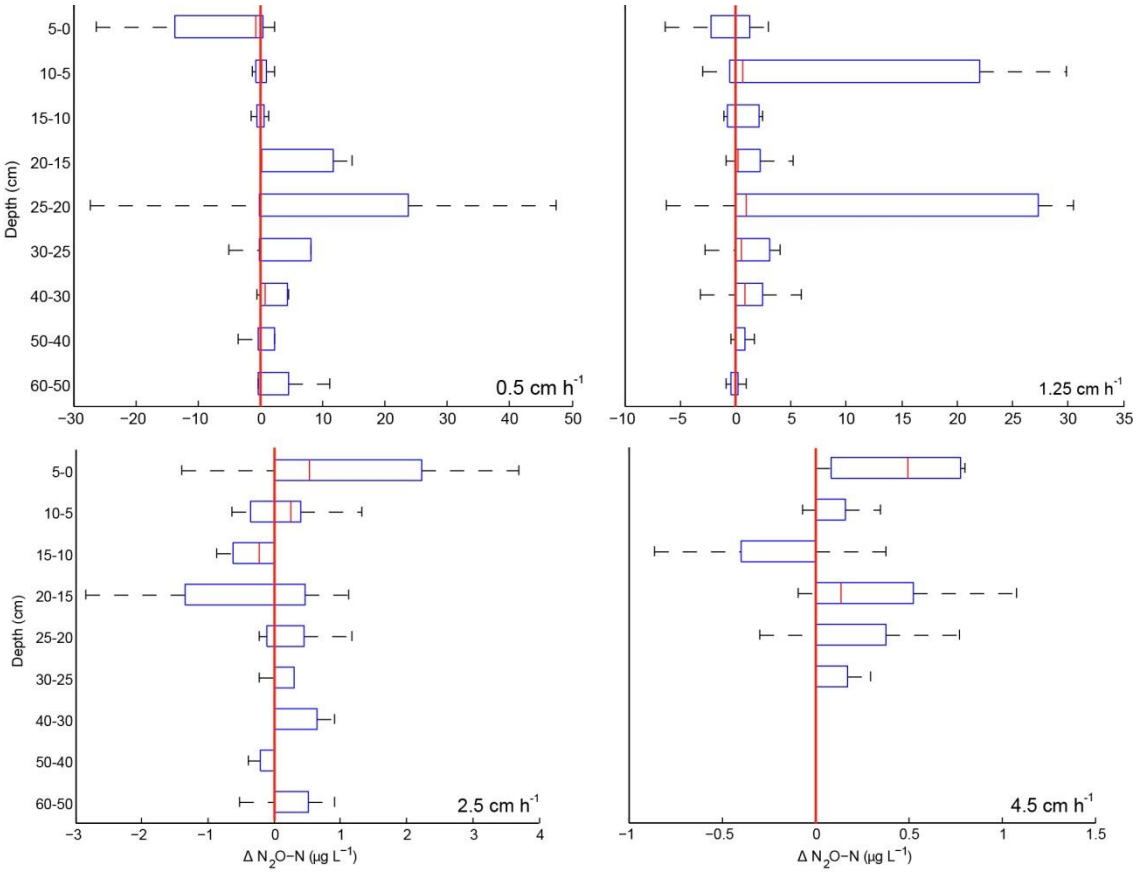

Figure 3.46 Change in N_2O at depth intervals for 4 pore water velocity values. The red line indicates zero change. Note different scales of the x-axis for each graph.

3.2.5 Interactions of Temperature, Initial NO_3^- Concentrations, and Pore Water Velocity

Due to the fact that most distributions in this study failed the assumptions necessary to conduct a parametric ANOVA (normality and homogeneity of variances), non-parametric tests were used for comparisons of groups of data. The experimental design of this research was performed in a factorial design. However, there are not any forms of non-parametric factorial ANOVAs available. Despite this, factorial ANOVA's were performed on the data in order to identify potentially important interactions amongst control variables for NO_3^- flux (Table 3.5) and N_2O flux (Table 3.6). Interactions that were found to be significant in a factorial ANOVA and linear regression analysis are reported below. The following results are not proven to be statistically significant (unless stated so), however they do illuminate important trends in the behavior of the data.

Table 3.5 ANOVA table for NO_3^--N flux for temperature (T), input NO_3^- (No), and pore water velocity (v)

Source	Sum. Sq	D.F.	Mean Sq.	F	Prop>F
T	2.25	2	1.12	33.19	<0.001
No	11.60	2	5.80	171.29	<0.001
v	24.92	3	8.31	245.21	<0.001
T×No	0.27	4	0.07	2	0.1175
T×v	1.63	6	0.27	8.03	<0.001
No×v	2.17	6	0.36	10.67	<0.001
T×No×v	0.68	12	0.06	1.67	<0.001
Error	1.12	33	0.03		
Total	45.23	68			

Table 3.6 ANOVA table for N_2O-N flux (log transformed) for temperature (T), input NO_3^- (No), and pore water velocity (v)

Source	Sum. Sq	D.F.	Mean Sq.	F	Prop>F
T	9.93	2	4.97	2.54	0.0935
No	26.62	2	13.31	6.8	0.0032
v	2.26	3	0.75	0.38	0.7645
T×No	45.37	4	11.34	4.58	0.0011
T×v	10.98	6	1.83	0.93	0.4826
No×v	13.55	6	2.26	1.15	0.3526
T×No×v	19.77	12	1.65	0.84	0.6091
Error	68.49	35	1.96		
Total	195.97	70			

Two forms of linear regressions were used in this analysis. A simple multiple linear regression was used to identify the overarching controls of each variable on the resultant dependent variable and a stepwise multiple linear regression was used to investigate interactions of independent variables on the resultant dependent variable. Independent variables were temperature, NO_3^-, and pore water velocity for NO_3^- and N_2O concentrations within the column. Pore water velocity was removed as an independent variable in the models of NO_3^- and N_2O flux. All the estimated coefficients reported are significant to the $p<0.001$ level and are defined by the following equations:

$$Y = \beta_1 T + \beta_2 NO_3^- \cdot N + \beta_3 v + \text{Intercept} \qquad \text{Equation 3-3}$$

$$Y = \beta_{I1} T * NO_3^- \cdot N + \beta_{I2} T * v + \beta_{I3} NO_3^- \cdot N * v + \text{Intercept} \qquad \text{Equation 3-4}$$

Table 3.7 Parameter estimates for multiple linear regression (β_1, β_2, β_3) and stepwise multiple linear regression including interactions (β_{I1}, β_{I2}, β_{I3}). All values reported are significant to $p<0.001$

Y	Intercept	β_1	β_2	β_3	R^2	Intercept	β_{I1}	β_{I2}	β_{I3}	R^2
NO_3^--N	1.64	-0.20	0.65	0.53	0.91	0.02	-0.01	0.02		0.93
NO_3^--N Flux	-10.33		14.09	NA	0.28			NA	NA	
log(N_2O-N)	-1.60	0.07	0.03	-0.45	0.24	-1.53	0.01	-0.02	-0.02	0.28
log(N_2O-N Flux)	-0.36		0.11	NA	0.14	1.07	0.01	NA	NA	0.31

Concentrations of NO_3^- throughout the columns were dominantly determined by initial NO_3^- concentration followed by pore water velocity each of which had a positive effect on concentration. At low temperatures initial NO_3^- concentrations had a larger effect on overall NO_3^- concentrations. With increasing temperature, initial NO_3^- concentrations had less of an effect on the overall NO_3^- concentrations. Despite increasing NO_3^- concentrations, increasing temperature resulted in the overall NO_3^- concentrations decreasing for each NO_3^- input value. This effect is shown in Figure 3.47 and in the negative coefficient of the interaction term within the interaction regression model. The interaction between increasing temperature and pore water velocity, resulted in different patterns of mean NO_3^- concentrations at each temperature (Figure 3.47). At the lowest temperature there was variability in the NO_3^- concentration, however, at 15°C and 25°C there was an increasing trend of NO_3^- concentrations with increasing pore water velocity.

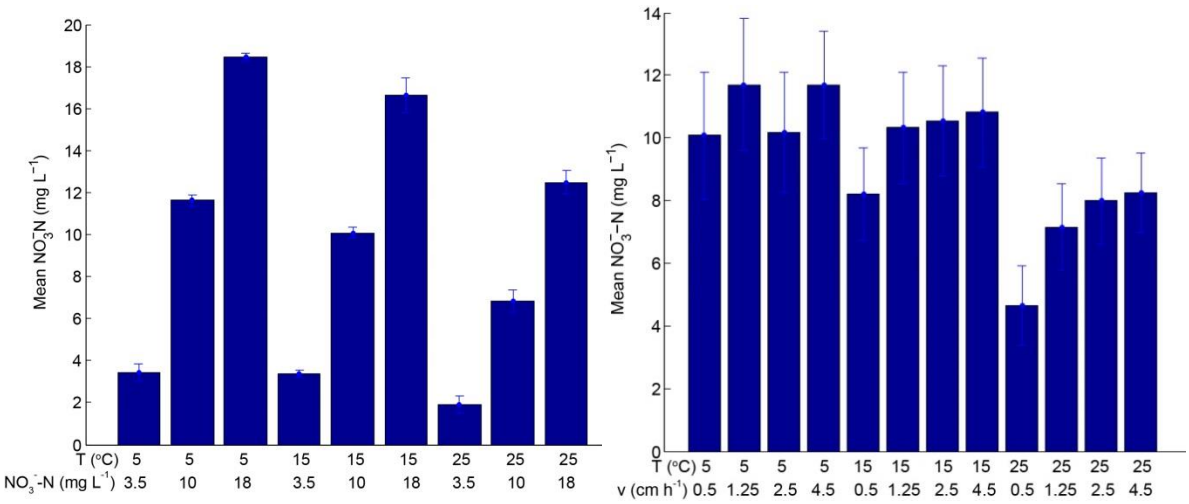

Figure 3.47 Mean NO_3^--N concentrations for interactions of T×N_o (left) and N_o×v (right).

Initial NO_3^- concentration had less of an effect on NO_3^- flux at higher temperatures than at lower temperatures (Figure 3.48). Also, increasing temperature resulted in the largest change in NO_3^- flux at the intermediate initial NO_3^- concentration of 10 mg N L^{-1}. Similarly, increasing pore water velocity had a decreasing effect on NO_3^- flux with increasing temperature. However, at the pore water velocity of 2.5 cm h^{-1} there was a maximum mean flux at 15°C, while at all other pore water velocities NO_3^- flux decreased with increasing temperature. Overall, increased pore water velocity or initial nitrate concentration interacting with increased temperature resulted in decreased values of NO_3^- flux. Pore water velocity had an additive effect on values NO_3^- flux with increasing initial NO_3^- values. NO_3^- flux was maximized with both increasing pore water velocity and initial NO_3^- concentration.

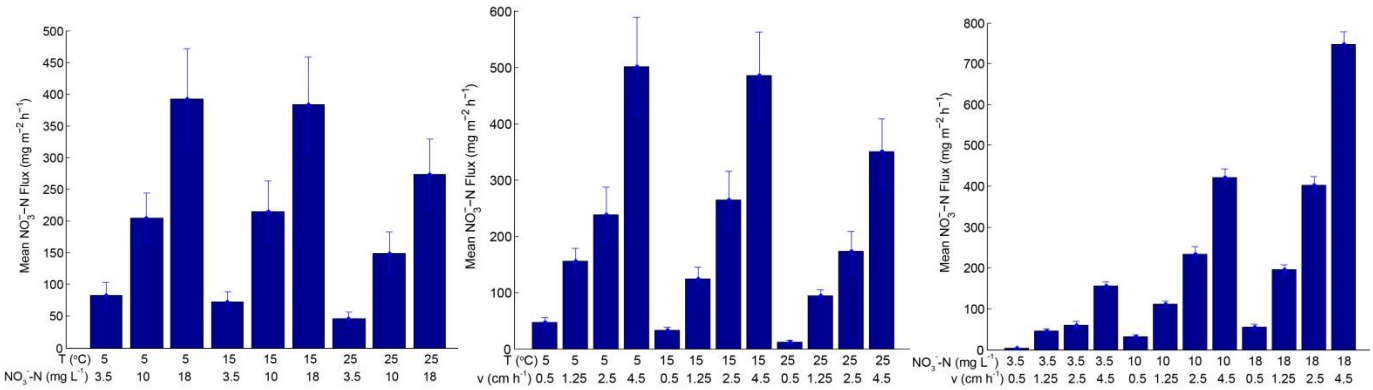

Figure 3.48 Mean NO_3^--N flux as the result of interactions of T×N_o (left), T×v (center), N_o×v (right)

There was a distinct interaction effect of temperature and initial NO_3^- concentration on the concentration of N_2O in the columns (Figure 3.49). At 5°C, increasing the initial concentration of NO_3^- resulted in decreasing N_2O concentrations. However, at 15°C, the reverse is true, where increasing NO_3^- concentration resulted in increasing N_2O concentrations. The pattern at 25°C is more complex with the peak N_2O concentration occurring at 10 mg N L^{-1} NO_3^-. Overall, the interaction of increasing temperature and initial NO_3^- concentration resulted in an increase in the concentration of N_2O. The interaction of temperature and pore water velocity and initial NO_3^- concentration and pore water velocity both resulted in an overall decrease in N_2O concentration. These interactions are fairly complicated and do not follow a distinct pattern. These complexities are possibly the cause of the weakness in the regression model predicting N_2O concentrations.

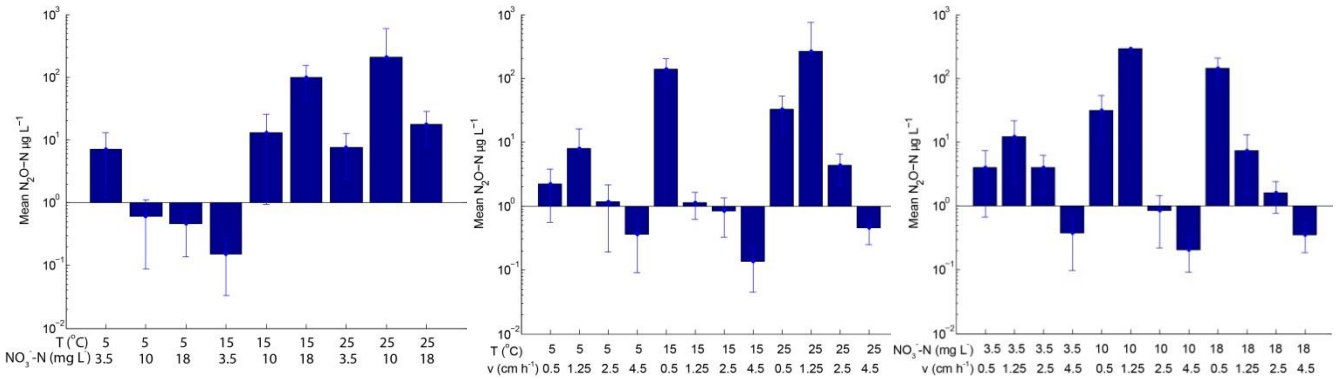

Figure 3.49 Mean N_2O-N concentration as the result of interactions of T×N_o (left), T×v (center), N_o×v (right)

N_2O flux was defined by the interaction of temperature and initial NO_3^- concentration, where increasing temperature and NO_3^- concentration resulted in increased N_2O flux in a regression model (R^2=0.31,p<0.001). However, the individual coefficient stepwise model determined that initial NO_3^- concentration was the most significant predictor of the N_2O flux. The regression model predicted 14.2% of the variance in N_2O flux (p<0.001).

While a regression analysis of the control variables and interactions for N_2O yield did not result in a significant model, the interaction of temperature and initial concentration of NO_3^- is of interest. At 5°C the increase in initial NO_3^- concentration resulted in a decrease in the N_2O yield (Figure 3.50). Conversely at 15°C an increase in the initial NO_3^- concentration resulted in an increase in N_2O yield. At 25°C the peak N_2O yield occurs at 10 mg N L^{-1}. At each temperature there is a completely different trend in response of the mean N_2O yield to increasing NO_3^- concentrations. The largest mean N_2O yields within the colums were observed at 25°C for initial NO_3^- concentrations of 10 mg N L^{-1} at 11.9%. Of significance are the errors associated with each mean, indicating a high variability in N_2O yield in most experimental scenarios.

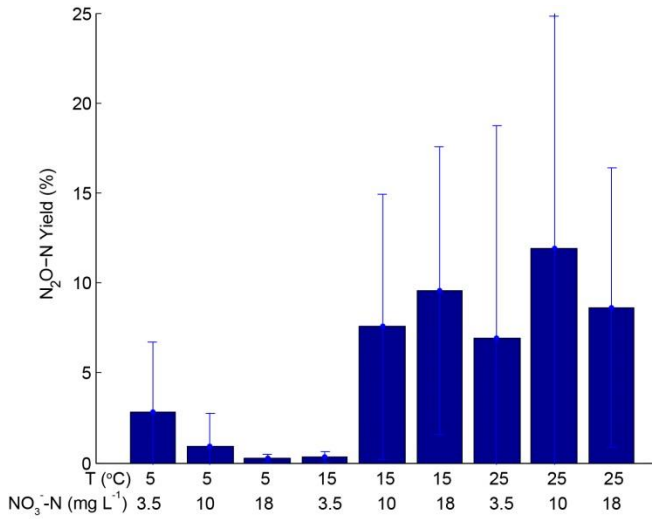

Figure 3.50 Mean N_2O yield within the columns for the interaction of $T \times N_o$

3.2.6 Column model of NO_3^- and N_2O model

The concentration of NO_3^- and N_2O was estimated using a model described in section 2.2.5. While the use of multiple linear regressions allows us to begin to quantify the relative contributions of each environmental parameter to NO_3^- and N_2O concentration, the model used here demonstrates more accurately the exponential and power relationships of temperature and N_2O yield, respectively. Modeled concentrations of NO_3^- at the outlet as a function of residence time for different temperatures and initial NO_3^- concentrations demonstrates how longer residence times allow for more NO_3^- to be removed via denitrification (Figure 3.51). The longest residence times effectively demonstrate a column condition of low to minimal flow mimicking a near closed environment where all N is transformed to N_2. In response to the longer residence times N_2O is also ultimately removed in the "closed" environment. The model predicts that concentrations of N_2O would fall to 0 at longer residence times above 300 hours. At residence times around 70 to 85 hours N_2O concentrations reach their peak at the outlet. In the model concentrations of N_2O reach their peak with a shorter residence time at 25 ^oC (70 hours) and a

longer residence time at 5 ^{o}C (85 hours). The model shows the impact of NO_3^- concentration on the amount of N_2O that is emitted from the column. It shows an increase in maximum N_2O concentration of 800% from 5 mg N L^{-1} to 15 mg N L^{-1} and 265% increase from 15 to 25 mg N L^{-1}.

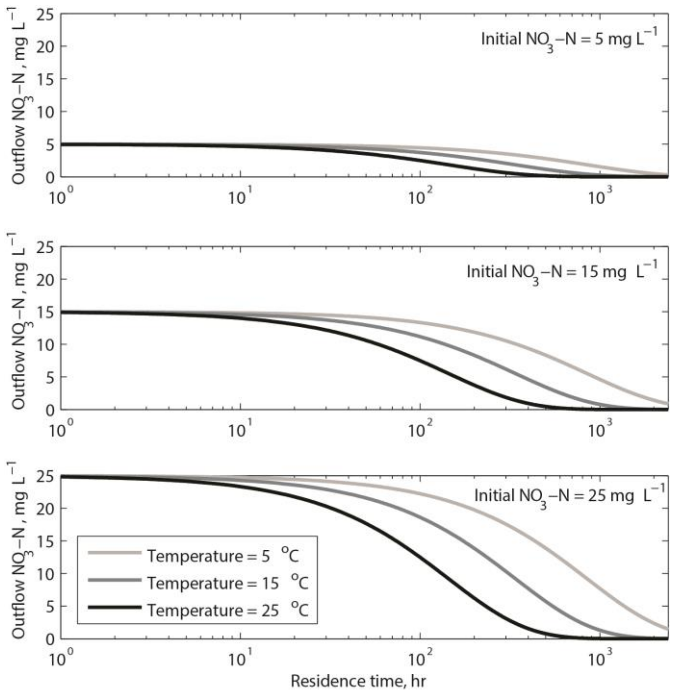

Figure 3.51 Simulated concentrations of NO_3^- at the outlet of the column over increasing residence time within the column for 3 temperatures and initial NO_3^- concentrations.

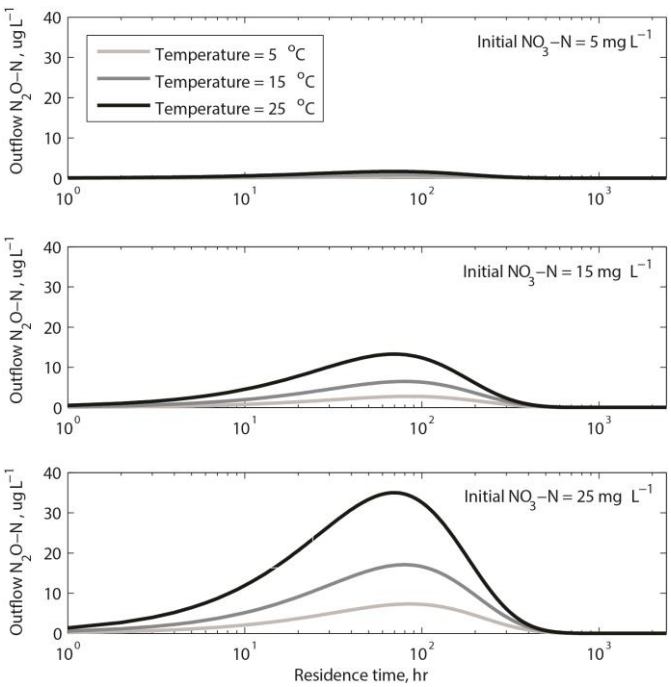

Figure 3.52 Simulated concentrations of N_2O at the outlet of the column over increasing residence time within the column for 3 temperatures and initial NO_3^- concentrations.

NO_3^- flux was simulated for a range of temperatures and initial NO_3^- concentrations. The simulated results show the large increase in NO_3^- flux with the combination of increased NO_3^- concentration similar to the results shown in Figure 3.48. In the model of NO_3^- flux, temperature has relatively minimal effect on flux at higher pore water velocities compared to at lower pore water velocities. Counter to the large effect temperature can have on the NO_3^- concentration at the outlet as shown in Figure 3.51, it overall has less of an effect on the NO_3^- flux compared to initial NO_3^- concentration and pore water velocity.

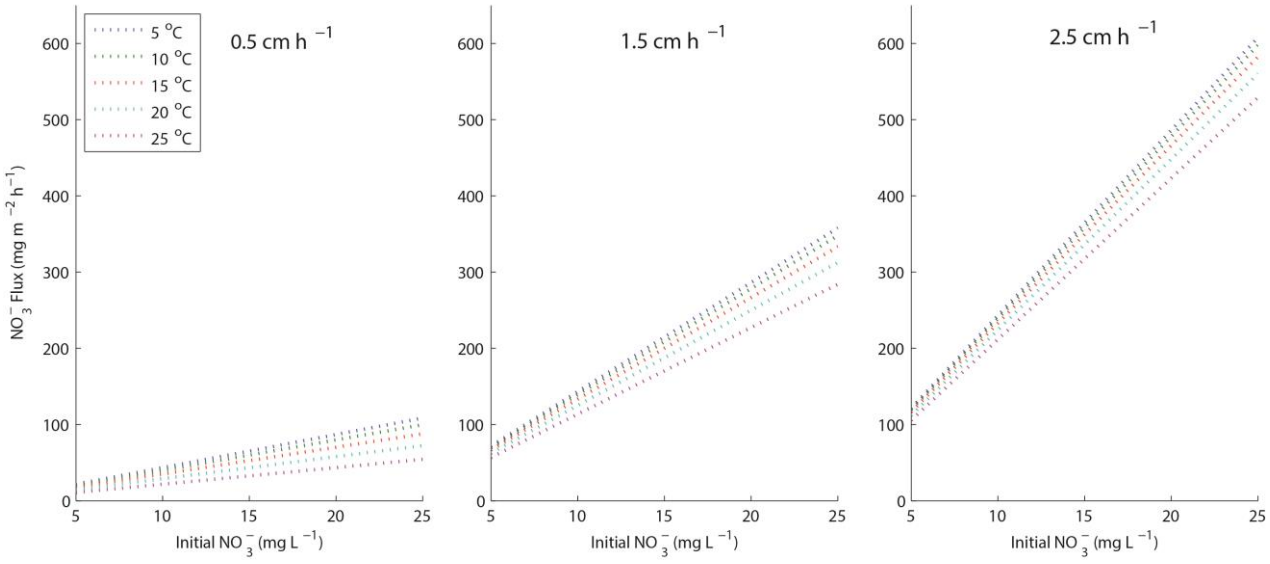

Figure 3.53 Simulated NO_3^- flux for increasing initial NO_3^- concentrations at 5 temperatures and 3 pore water velocities.

Simulated N_2O flux with increasing temperature shows minimal effect of pore water velocity at low initial concentrations of NO_3^- (Figure 3.54). However, as both temperature and initial NO_3^- concentration increase pore water velocity is shown to have an increasing effect on the overall flux of N_2O from the columns. At longer residence times (slower pore water velocities) and higher temperatures we observe a flattening out of the N_2O flux which is indicative of a steady state balance of N_2O production and removal within the column.

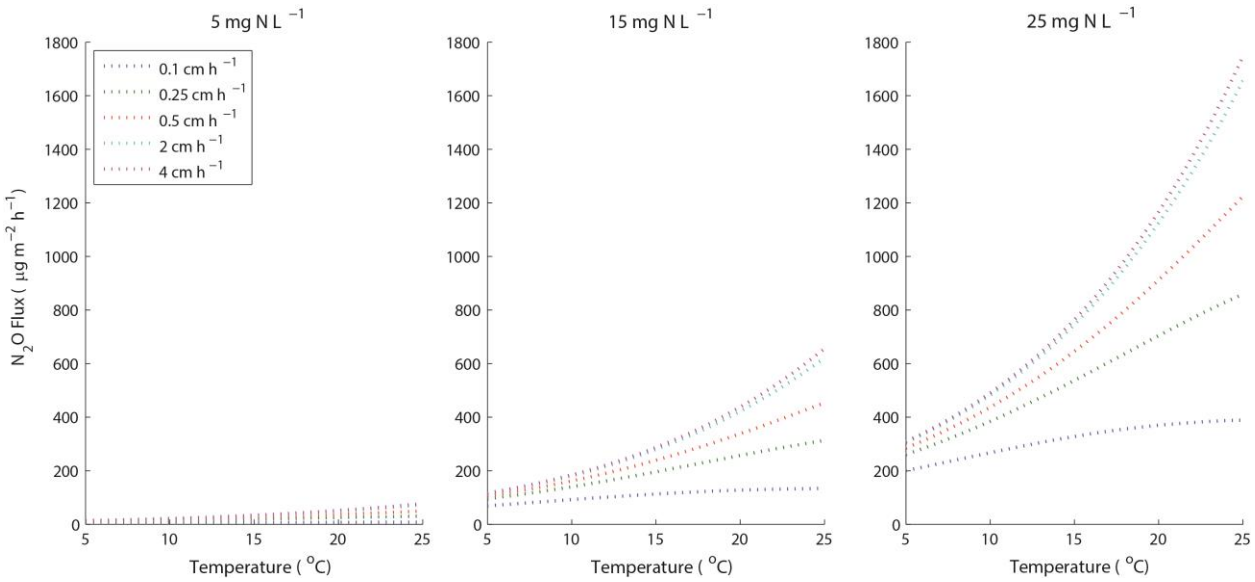

Figure 3.54 Simulated N_2O flux for increasing temperature at 5 pore water velocities and 3 initial NO_3^- concentrations.

4 Discussion

4.1 Discussion Column Study

Nitrous oxide production and removal were observed along a 1-D flow path in sediment columns subjected to a factorial experimental design of different temperatures, initial NO_3^- concentrations, and pore water velocities. Nitrate behaved in the columns as would be expected based on fundamental understanding of denitrification in sediment in response to changing environmental parameters. From this established understanding we can base our interpretations of N_2O production and removal in regards to the same environmental changes. The overall flux of N_2O from the columns was dependent mainly on the input NO_3^- concentration and to a minor extent temperature. Increasing input NO_3^- and temperature both resulted in increasing N_2O flux and N_2O yield. Pore water velocity did not have a significant impact on N_2O fluxes due to a balance of transport rate and reaction time. Overall, the results suggest that projected increases in NO_3^- in the environment and rising stream water temperatures may result in increases in N_2O fluxes as water discharges from streambed sediments where denitrification is occurring.

Two sediment columns were used for this research in order to replicate the *in situ* conditions of the stream bed sediment at the groundwater stream water interface. The sediment columns were collected from Cobb Mill Creek in a fashion that preserved their natural structure. Through maintaining the natural structure of the sediment, we were able to retain the sediment stratigraphy with minimal disturbance and compaction. Maintaining the sediment structure in turn helped to simulate *in situ* hydrologic characteristics of advection and dispersion. In addition, we maintained the resident microbial community and distribution of organic carbon,

thus aiding in replication of the natural biogeochemical gradients in the streambed sediment (Marxsen & Fiebig, 1993; Sheibley *et al.*, 2003; Gu *et al.*, 2007). Doing so was important for us to capture how a natural microbial community produces and removes nitrous oxide through denitrification under a variety of environmental scenarios. Unlike many past studies on N_2O production from denitrification, that were performed in a closed flask environment, the column experiment allows for us to replicate an open system where N_2O is advected along a natural flow path as it would beneath a gaining stream. Thus the processes of formation and removal of N_2O in a dynamic system can be represented.

This research was performed under the assumption of 1-D flow from the bottom of the sediment column to the top, simulating a stream under gaining conditions. While it is, understood that *in situ* hydrologic conditions rarely operate under a simplified flow model, gaining conditions have been identified at Cobb Mill Creek (Gu, 2007; Flewelling, 2009). We used a 1-D flow simulation in order to simplify the controlled environment so that we could focus on the changes in N_2O due to changes in the physicochemical controls of the experiment.

Many studies have previously investigated the fate of NO_3^- in sediment cores and in aquatic environments under a variety of conditions (Willems *et al.*, 1997; Piña-Ochoa & Álvarez-Cobelas, 2006; Seitzinger *et al.*, 2006; Gu *et al.*, 2007). These studies have established a well-documented baseline for how NO_3^- behaves under varying temperature, NO_3^- concentration, and pore water velocities. We are able to compare our results to previous studies in order to confirm that the microbial populations in the columns are operating in a normal and expected fashion in regards to denitrification providing a base understanding for our interpretation of how N_2O behaved in the columns.

Increasing temperatures resulted in lower overall NO_3^- concentrations throughout the columns and in NO_3^- flux. Increasing temperature heightens biological reactions and is commonly measured by the value of Q_{10} where a temperature step of 10°C results in an increase of the measured rate. The Q_{10} value for the denitrification rate in these columns was, on average, 2.55 for 15°C to 25°C. Most Q_{10} values fall between 1.8 and 6 for denitrification (Malhi *et al.*, 1990; Ambus, 1993; Willems *et al.*, 1997), Per Ambus [1993] found very similar Q_{10} values in saturated riparian soil of 2.53 and 2.71 for temperature steps 12°C to 22°C and 2°C to 12°C respectively. While denitrification rates increased as expected from 15°C to 25°C there was not a significant change in denitrification rates from 5°C to 15°C. The percentage of NO_3^- removed at 5°C was surprisingly high with some values reaching up to 88 % removal. The response of the sediment communities to the low temperature is confounding and contrary to established understanding of how increasing temperature accelerates denitrification rates (Dawson & Murphy, 1972; Willems *et al.*, 1997).

The divergent behavior of the denitrification rate at 5 °C can be explained based on carbon depletion or outlying data points. Tiedje [1988] found that carbon and oxygen were the most important factors for determining denitrification rate. The carbon supply is possibly responsible for the increased denitrification activity at 5°C. Peaks in denitrification rate at 5°C coincided with areas of concentrated carbon content within the columns at 60 to 50 and 30 to 20 cm. The mean carbon content, measured after the experiment, was 1.64%, which is above the amount of carbon limitation suggested by previous studies (Gu, 2007). However, the original carbon content of the sediment columns was unknown. Gu [2007] operated columns under similar conditions and determined that the maximum rate of carbon depletion for one month would result in about 30% loss of the organic material. The columns were run through all

experimental scenarios starting from 5°C to 15°C to 25°C over 10 months. It is possible that despite operating at sub-optimal temperature, enough carbon was lost between the experiments run at 5°C and 15°C that it negatively impacted the denitrification rates observed during 15°C experimental scenarios. The other possible factor is the two high values observed at 5°C (Figure 3.29). If those points are accepted as anomalous outliers and are disregarded, the mean denitrification rates fall within a range of 0.5 to 6 mg N L^{-1} day^{-1}. In addition, mean NO_3^- fluxes and the overall concentrations of NO_3^- followed expected trends in response to increasing temperatures suggesting the two high values for denitrification rate were, indeed, unexplained anomalies. The columns, therefore, did remove more NO_3^- with increasing temperature, and, as a result, less NO_3^- exited from the top of the columns as temperature increased due to enhanced denitrification activity.

Increasing initial NO_3^- concentrations elicited expected responses within the columns. The increase of initial NO_3^- concentrations into the columns resulted in an overall increase in NO_3^- concentrations at all depths. As a result of increasing initial NO_3^- concentrations, the percentage of NO_3^- removed from the columns decreased which, in turn, resulted in increased NO_3^- fluxes from the columns. The percent NO_3^- removed at 3.5 mg N L^{-1} had a large range of up to 99% however, the percentage dropped by over half at 10 mg N L^{-1} and then half again at 18 mg N L^{-1}. In previous studies, a correlation between NO_3^- concentration and denitrification rates was not found (Smith *et al.*, 1978; Murray *et al.*, 1989). In the present study, there was not a significant difference in denitrification rate with increasing NO_3^- concentration. The average amount of NO_3^- removed for each input NO_3^- concentration ranged from 1.55 to 2.17 mg N L^{-1} which is less than the smallest NO_3^- concentration of 3.5 mg N L^{-1}. Therefore, the NO_3^-

concentrations applied in this experiment were all above the rate-limiting concentration for denitrification in this system.

Pore water velocity had a significant impact on the ability of the resident microbial populations to remove NO_3^- from the water passing through the columns. At the lowest pore water velocity, 0.5 cm h^{-1}, up to 99% of the NO_3^- was removed within the column. At higher pore water velocities, less NO_3^- was removed and ultimately at 4.5 cm h^{-1} only a maximum of 38% was removed when the initial NO_3^- concentration was 3.5 mg N L^{-1}. The pore water velocity of 0.5 cm h^{-1} was not sufficiently slow as to allow full denitrification of all input NO_3^- concentrations, slower pump rates would have been needed to achieve 100% removal for all input NO_3^- scenarios. Previous work has shown that denitrification is kinetically controlled when pore water velocity alters the capacity of denitrifiers in a sediment core to remove NO_3^- (Willems *et al.*, 1997; Gu *et al.*, 2007). Slower pore water velocities increase the residence time of both DO and NO_3^- therefore allowing the resident microbial communities more time to consume their optimal electron acceptor. DO is consumed first along the flow path which then creates an anoxic environment prime for denitrification. With increasing pore water velocity, the residence time is reduced and less DO is consumed, making the environment more oxic and less optimal for denitrification to occur. Gu [2007] found with similar sediment columns from CMC, that increased flow rates caused the oxic zone in the columns to expand upward and the denitrification zone to be limited to shallower depths. As the oxic zone in the columns was pushed to shallower depths, less time and space were available for denitrification to occur and NO_3^- fluxes increased. The present results agree with the findings of Gu [2007], thus, we can conclude that the removal of nitrate in these columns was the result of kinetically controlled denitrification.

Interactions among the control variables of temperature, input NO_3^- concentration, and pore water velocity had strong effects on the overall flux of NO_3^- from the columns. Interactions represent combined effects that can reinforce one another (i.e., both have an effect in a similar direction) or that can dampen one another (the effects have different directions; one might cause an increase in the phenomenon being examined while the other causes a decrease). The interaction between increasing NO_3^- concentration and temperature resulted in reducing NO_3^- fluxes. The same was true for increasing pore water velocity and temperature. In both these cases the total additive effect is the decrease of NO_3^- flux, however, temperature has less control over the flux than either NO_3^- concentration or pore water velocity. Together, NO_3^- concentration and pore water velocity work together to enhance overall NO_3^- flux from the sediment in the columns. Optimal conditions for minimizing NO_3^- flux were the lowest pore water velocity and NO_3^- concentration while maximum NO_3^- flux was observed at the highest levels of NO_3^- concentration and pore water velocity, 18 mg N L^{-1} and 4.5 cm h^{-1}. Willems [1997] performed a multiple regression analysis on NO_3^- effluent as the result of flow, influent NO_3^-, and temperature on four different soil horizons. Influent NO_3^- and flow were found to have the largest impact on effluent NO_3^- concentrations in all cases. The present results are consistent with those of Willems establishing that temperature has less of an impact on effluent NO_3^- concentrations than do either influent NO_3^- or flow rate.

Overall, the response of NO_3^- concentration within and flux from the columns in response to changes in temperature, NO_3^- concentration, and flow correspond to the expected results as established by previous investigating similar scenarios (Willems *et al.*, 1997; Gu, 2007). The ability of resident microbial communities within the sediment columns to remove NO_3^- is dependent on the decrease of flow and the increase of temperature. As a result, increasing NO_3^-

fluxes occur from the columns when flow and NO_3^- concentration are increased and temperature is decreased. These results establish a fundamental understanding of denitrification in order for us to base our interpretation of how N_2O behaves in the columns as a result of the changing environmental parameters. There are only a few studies that have studied how N_2O production or flux responds to environmental variables (Nommik, 1956; Weier *et al.*, 1993; Hedin *et al.*, 1998; Holtan-Hartwig *et al.*, 2002; Hefting *et al.*, 2003), and none were found that investigated the natural evolution of N_2O along a flow path. Using our understanding of how denitrification occurs within these columns we can begin to better understand the full denitrification sequence in more detail by including N_2O into our analysis.

In this study, production of N_2O was dependent on temperature. Concomitantly, along with increasing denitrification, upon increasing the temperature, there was a significant increase in N_2O produced within the columns at depth. In a closed system, the accumulation of N_2O may not be observed or may be ephemeral because NO_3^- supply would diminish as denitrification proceeds with time, and all accumulated N_2O is reduced to N_2 as the denitrification reaction sequence proceeded to completion. In open systems where NO_3^- is not limiting, temperature is often found to enhance N_2O production (Smith, 1997). Many previous studies have reported Q_{10} values for N_2O production from soils and sediments ranging from 1.5 up to 23 [*Maag and Vinther*, 1996; *Smith*, 1997 (and references therein)] confirming that temperature can play a significant role on the fluxes of N_2O from a soil or sediment.

Increasing temperature is crucial to speeding up microbial processes such as respiration which results in an increase in the anaerobic volume of the sediment (Firestone *et al.*, 1979; Tiedje, 1988). At 5°C there was minimal N_2O production below the 30 cm depth. At low temperatures, it takes a longer distance along the reaction flow path for the development of

conditions optimal for denitrification and N_2O production. At 25°C, N_2O production began at 50 cm depth, indicating an increase in microbial activity and optimal denitrification conditions at a deeper in the sediment (at an earlier point along the flow path).

Warmer temperatures not only increase N_2O production, but they increase N_2O yield as well. N_2O yield is used here a surrogate for the commonly used N_2O/N_2 ratio. Instead of investigating the ratio of the end products N_2O and N_2 we look at the ratio of N_2O to the total amount of NO_3^- lost. Ultimately, the N_2O yield is the percentage of N_2O to all gaseous end products if we assume all lost NO_3^- results in a gaseous end product. In this case, N_2O yield would always be smaller than the equivalent N_2O/N_2 ratio. The use of N_2O yield has been the preference of the LINX II experiment which investigated N_2O emissions from 72 streams comprising different land use practices across the United States (Beaulieu *et al.*, 2011). N_2O yield is beneficial for calculating the percentage of NO_3^- that is not fully reduced to N_2. In other words it can be the measure of denitrification inefficiency where high N_2O yields mean that denitrification is less efficient in the environment of study versus an environment with low N_2O yields denitrification would be more efficient at reducing NO_3^- all the way to N_2

From the foundational work of Nommik to more recent studies it has been shown that the N_2O/N_2 ratio goes down with increasing temperature (Nommik, 1956; Maag & Vinther, 1996; Holtan-Hartwig *et al.*, 2002; Silvennoinen *et al.*, 2008b). However, the present study reports the exact opposite outcome. In the present work, increasing temperature resulted in direct and indirect effects on increasing denitrification and concomitantly N_2O efflux. This is a function of the system being an open advective environment and not NO_3^- limited. When there is a constant supply of NO_3^- advecting through sediment, denitrifiers will opt to consume NO_3^- until the supply diminishes and it becomes energetically advantageous to maximize transcription of nosZ,

the nitrous-oxide-reductase gene (Molstad *et al.*, 2007; Bergaust *et al.*, 2011). Until this point comes, N_2O continues to be produced, accumulated, and advected out of the sediment regardless of temperature. If the sediment is rarely NO_3^- limited, the increase in denitrification caused by an increase in temperature would, in turn, increase N_2O production. At increased temperatures, without the limitation of NO_3^-, the proportion of incomplete denitrification increases relative to complete denitrification, resulting in an increase in the N_2O yield.

A key difference between the present study and earlier studies that have shown that the ratio of N_2O/N_2 goes down with increasing temperature is that they were done in a closed system and or one that was NO_3^- limited (Nommik, 1956; Maag & Vinther, 1996; Holtan-Hartwig *et al.*, 2002; Silvennoinen *et al.*, 2008b). In these cases, inherently, if the temperature increases, metabolic processes are enhanced, and therefore, NO_3^- limitation is induced as more NO_3^- is consumed. With less NO_3^- available at higher temperatures it becomes necessary for denitrifiers to maximize expression of nosZ and thereby bring denitrification to full completion. Thus, in these nitrate limited systems you see smaller N_2O/N_2 ratios at higher temperatures. Hefting et al. [2006] found conflicting results when examining environmental controls on the N_2O/N_2 ratio *in situ* in a riparian zone. They found low N_2O emissions from a riparian transect in the summer due to low NO_3^- concentrations and high denitrification rates. However, on a different transect in the summer, they found high N_2O emissions associated with high NO_3^- concentrations and low denitrification rates. Weak relationships between environmental parameters and the N_2O/N_2 ratio *in situ* make it difficult to use the ratio as a predictor of denitrification efficiency in a natural environment (Groffman *et al.*, 2002; Hefting *et al.*, 2006). When measurements can be made along a hydrological reaction flow path, N_2O yield provides a better picture of denitrification efficiency of a system by quantifying how much N_2O is produced as a result of

NO_3^- lost [*Beaulieu et al.*, 2007; *Clough et al.*, 2006]. Unlike Beaulieu and others [2007], who only quantified N_2O yields from water column and hyporheic processes, the present study has calculated N_2O yields along groundwater flow paths prior to the groundwater-surface water interface. These values allow us to quantify how efficiently the sediment beneath the stream is able to bring denitrification to full completion which provides a much more holistic picture of N_2O emissions from riparian zones than single N_2/N_2O ratio snapshots.

This study has found that increasing NO_3^- concentrations result in increasing concentrations of N_2O at all depths, increasing N_2O fluxes, and increasing N_2O yield. The results of the sediment-column experiment are in agreement with earlier studies that have established the presence of an inhibitory effect of NO_3^- on the reduction of N_2O to N_2 (Blackmer & Bremner, 1978). This effect has been seen not only in closed-system laboratory investigations, but has been confirmed in soils and hyporheic sediments where they have shown a positive correlation between NO_3^- and N_2O concentrations and N_2O yields (Blackmer & Bremner, 1978; Weier *et al.*, 1993; Hedin *et al.*, 1998; Silvennoinen *et al.*, 2008a; Beaulieu *et al.*, 2011). Within the columns, there was not a difference in the amount of NO_3^- removed resulting from each initial NO_3^- concentration; however, there was significantly more N_2O produced, which suggests that the inhibitory effect of NO_3^- on the reduction of N_2O to N_2 was at play. When NO_3^- becomes unlimited in an environment where denitrification is occurring, N_2O is often preferred as the reaction end product and the N_2O concentration builds up resulting in increased N_2O yields (Firestone *et al.*, 1979; Hutchinson & Davidson, 1993). Values of N_2O yields for eutrophic aquatic ecosystems have been reported in the range of 0.05 to 5% however values have been observed up to 80% in some extreme cases (García-Ruiz, 1998; Beaulieu *et al.*,

2011). In this study the mean N_2O yield value for all experimental scenarios was found to be 2.19% with extreme instances up to 66.4%.

The rate at which the NO_3^- was delivered to the columns had a significant impact on the amount of NO_3^- denitrified within the columns and the concomitant production of N_2O. Ultimately the amount of N_2O emitted by the columns is the net balance between N_2O produced and N_2O removed along the reaction flow path. As shown previously, denitrification in the experimental columns was kinetically controlled, and the balance of the production and removal of N_2O was kinetically controlled as well. Overall, at slower pore water velocities more reaction time is allowed for denitrification and N_2O production to occur. At 0.5 cm h^{-1} there was significantly more N_2O at all depths of the columns than at 2.5 and 4.5 cm h^{-1}. However, no significant relationship between pore water velocity and N_2O flux was found. This is the result of the balance of N_2O production and consumption along the flow path due to residence time. At 0.5 cm h^{-1} up to 50 µg N L^{-1} of N_2O accumulated at middle depths of the columns, however in the last 5 cm of the column, a large portion of that N_2O was removed. The slower pore water velocity increased the residence time of produced N_2O therefore increasing the opportunity for it to be removed. At fast pore water velocities, there was significantly less N_2O production overall. However, at the last 5-cm depth increment there was an increase in N_2O production, and that N_2O was then ultimately emitted from the columns escaping any chance of removal by microbes within the columns.

Overall, at slow pore water velocities, there is a large buildup of N_2O within the sediment, but the N_2O is reduced before it is slowly emitted from the sediments, whereas, at higher pore water velocities smaller amounts of N_2O are produced, but less of it is reduced, therefore more N_2O is quickly emitted. The rate at which the small or large concentrations of

these end products are emitted balances the overall amount of N_2O that is effluxed from the sediments. The results for the column experiments show that residence time is important in determining the balance of N_2O production and removal, which ultimately determines how much N_2O escapes the streambed sediments. The pore water velocities used in this research represent the range of pore water velocities within the natural range observed by previous investigations at CMC (Gu, 2007; Flewelling, 2009). By replicating the natural pore water velocities and a variety of NO_3^- concentrations a range of median N_2O fluxes from 7.19 to 35 µg N m^{-2} h^{-1} were observed (means were 53 to 503 µg N m^{-2} h^{-1}). In the LINX II work an average flux of 27.4 µg N m^{-2} h^{-1} from 72 streams could not be accounted for based on their measurements of water column NO_3^- processing. The fluxes that have been observed in this study identify that the missing component was most likely from groundwater components. This work has established that there are indeed are potentially significant N_2O fluxes occurring from streambed sediments of gaining streams without NO_3^- limitation.

The range of environmental conditions enacted on the sediment columns in this experiment were chosen in order to mimic the range of *in situ* conditions as well as predicted changes in temperature and NO_3^- load to aquifers (Böhlke & Denver, 1995; Kaushal *et al.*, 2010). The present findings suggest that the increase in NO_3^- loading to aquifers in agricultural catchments has negative implications on the increase of N_2O emissions from biologically active streambed sediments. Furthermore, these results are consistent with the concept that there is an inhibitory effect of NO_3^- on the reduction of N_2O to N_2 in eutrophic environments. An increase in NO_3^- in the aquatic environment does not mean that there will be a linear increase of N_2O, instead more rapid increases in N_2O emissions can be expected. Increases in temperature will

only amplify this effect as streambed sediments will become more biologically active and process more of the incoming NO_3^- resulting in even greater N_2O emissions.

The effects of temperature and NO_3^- concentration on N_2O flux are independent of the flow regime of the streambed. Denitrification and N_2O production are kinetically controlled processes, therefore, N_2O fluxes are a measure of the balance of production and removal allowed by the residence time of the water in the sediments. However, in sediments that are not NO_3^- limited, the flux of N_2O at the groundwater surface water interface should be similar for most pore water velocities. Slow pore water velocities allow for a greater buildup of N_2O resulting in large concentrations emitted at slow rates. In contrast, fast pore water velocities don't allow for as much denitrification to occur thus small concentrations are emitted at faster rates. The balance of rate and quantity seem to balance such that similar fluxes of N_2O from the columns are expected. Overall, while biologically active areas in a riparian zone or streambed are efficient at removing NO_3^- contamination, the increasing NO_3^- burden placed on these natural systems to remedy one problem only results in the causation of another, *viz.*, increased N_2O emissions.

4.2 Discussion: Field Study

For each of the four seasons in 2013, NO_3^- and N_2O were sampled in the streambed sediment beneath Cobb Mill Creek in order to understand better the fate of NO_3^- and N_2O along a natural flow path and to determine the environmental parameters controlling benthic N_2O effluxes to the overlying stream. Previous work has quantified N_2O emissions from riparian zones, streams, and rivers and has established that these environments are significant contributors to indirect fluxes of N_2O to the atmosphere (Cole & Caraco, 2001; Groffman *et al.*,

2002; Machefert & Dise, 2004; Well *et al.*, 2005; Silvennoinen *et al.*, 2008a; Beaulieu *et al.*, 2011). All previous stream studies have focused on hyporheic and water column processing of NO_3^-. However the study by Beaulieu et al. of 72 streams across the United States [2011] was unable to pinpoint the source of up to 70% of the N_2O found in stream water column, and the authors alluded to a significant groundwater input. Our experimental sediment column work has confirmed that, indeed, streambed sediments can be a location of denitrification and a significant source of N_2O effluxes to the water column and thence the atmosphere. The field-work portion of the present work aimed to quantify the *in-situ* benthic fluxes of N_2O as well as to characterize how it is produced and consumed at depth within natural sediments.

Within the shallow Columbia Aquifer on the Delmarva Peninsula, NO_3^- concentrations are often above the EPA safe drinking water limit of 10 mg N L^{-1}. Broad studies of the Delmarva Peninsula have found maximum values in agricultural wells from 22 to 37 mg N L^{-1} (Böhlke & Denver, 1995; Dillow & Greene, 1999; Debrewer *et al.*, 2007b). Closer to CMC, McFadden [2013] investigated NO_3^- concentrations in the streambed sediments of 4 streams on the ESVA and found maximum NO_3^- values of around 8 mg N L^{-1}. Galavotti [2004] surveyed NO_3^- concentrations at CMC beneath the riparian zone and the streambed. She found maximum NO_3^- concentrations of 12 mg N L^{-1} located 50 cm beneath the sediment surface which she concluded indicated a deeper groundwater flow path bypassing the riparian root zone. The present study obtained ranges of NO_3^- beneath the streambed from 4.5 to 11.2 mg N L^{-1} at 70 cm depth which matched the range observed by Galavotti in 2003 in CMC at similar depths.

There have been few investigations that have investigated the seasonal differences in the supply of NO_3^- to a streambed prior to the biologically active zone of shallow sediments. Most prior studies have investigated and confirmed seasonal differences in flux, which represents both

seasonally influenced groundwater and biological interactions (Foster *et al.*, 1989; Mulholland & Hill, 1997) or seasonal changes in denitrification in the hyporheic zone (Christensen & Sørensen, 1988). In this investigation we found that there was little difference in the deep (70 cm) groundwater supply of NO_3^- between seasons except during the fall. The NO_3^- concentrations in the fall, at 70 cm depth, were, on average, 6.3 mg N L^{-1} compared to 8.6 mg N L^{-1} for all other seasons. The fall sample was taken on October 27th and surface water temperatures were indicative of colder fall temperatures. However, at depth there is roughly a seasonal delay in the thermal signature, and deeper groundwater in the fall was found to reflect the thermal maximum observed in summer surface water. In the summer, evapotranspiration is high and biological activity and nutrient uptake are at their peak which deplete concentrations of NO_3^- in the groundwater (Foster *et al.*, 1989; Mulholland & Hill, 1997; Phillips *et al.*, 2003). In addition, evapotranspiration concentrates Cl^- which is not used by plants and is often used as a conservative tracer. The combination of evapotranspiration and biological uptake create a groundwater with characteristically lower NO_3^- and higher Cl^- concentrations.

Flewelling [2011] found that there was a higher Cl^- concentration associated with groundwater that had been influenced by riparian zone processes at CMC. They were able to discern two major flow paths based on Cl^- and NO_3^- concentrations, one deep path that bypasses the riparian zone and one shallow path that had noticeable biological influence from interaction with the riparian sediments. The deep groundwater samples collected in the fall had a much higher Cl^- to NO_3^- ratio than all the other seasons, an observation which is highly indicative of significant riparian influence. Groundwater flow paths can change seasonally as a result of changes in precipitation and evapotranspiration ultimately altering the chemical makeup of the groundwater at a sample point (Mulholland & Hill, 1997; Angier & McCarty, 2008). The

present study only had one sampling period for each season, a fact which severely limits any ability to discern smaller changes that might reveal a stronger seasonal signal in NO_3^- concentrations. However, while this study didn't observe any significant differences in NO_3^- from winter to summer, groundwater sampled in the fall is dominantly riparian influenced and the result of heightened biological processes in the summer and fall.

From the winter to the summer, groundwater at 70 cm had a lower Cl^- to NO_3^- ratio, and was therefore considered to be dominantly of a deeper groundwater origin. However, within each season there was a heterogeneous mix of groundwater flow path inputs indicated by the variation of NO_3^- and Cl^- concentrations. At one to three sample locations in the winter, spring, and summer samples, higher Cl^- to NO_3^- ratios were observed. These samples indicate groundwater inputs from shallow riparian-influenced flow paths. The location of bypass versus riparian influenced flow paths did not follow any patterns such as bypass flows focused in the center of the stream (Kennedy *et al.*, 2009). At CMC, Flewelling et al. [2009] also found a complicated distribution of Cl^- fluxes at the sediment surface which confirms the unpredictable heterogeneity of flow paths within the CMC riparian zone and streambed sediments. Many factors such sediment size distribution from different depositional events, macro pores, and organic debris can alter the conductivity of the sediments within a riparian zone thus creating complex groundwater flow paths that are difficult to discern and predict at the scale at which they occur.

Nitrate efflux from the streambed sediments was comparable to values seen at other agricultural streams (emissions to the atmosphere.

Table 4.1). CMC has a wide riparian buffer zone and thus may have a lower NO_3^- flux than many other agricultural streams due to the occurrence of more denitrification and biological uptake. There is a large difference in the amount of NO_3^- efflux observed in agricultural streams versus forested streams. Many agricultural streams experience a larger load of NO_3^- and are on average surrounded by less forested area which reduces the chances of biological uptake and denitrification. In the present study, increased NO_3^- concentrations increase the percentage of N_2O yield thus resulting in large N_2O effluxes. Streams and rivers proximal to agricultural areas that experience larger NO_3^- concentrations are also likely contributors of N_2O emissions to the atmosphere.

Table 4.1 Comparison of NO_3^- fluxes from streambed sediments in agricultural (Ag) and forested (F) streams.

Reference	Type	Mean NO_3^- Flux (mg N m^{-2} h^{-1})
Kennedy et al. [2009]	Ag	89.88
*Bohlke et al. [*2004]	Ag	11.09
Duff et al. [2008]	Ag	155.83
Duff et al. [2008]	Ag	6.42
Duff et al. [2008]	Ag	152.91
McMahon and Bohlke [1996]	Ag	119.64
McCutchan et al. [2003]	Ag	50.78
Staver and Brinsfield [1996]	Ag	92.21
Burns [1998]	F	14.59
Chesnut and McDowell [2000]	F	0.76
This study	F/Ag	42.50

Unlike the column experiments that were performed in the laboratory, N_2O was found above atmospheric equilibrium at the deepest measured depth of 70 cm (saturation is 0.26 µg N_2O-N L^{-1} at 18°C). Previous studies have observed aquifers with mean N_2O concentrations up to 89 µg N L^{-1} which indicates biological transformations of nitrogen occurring within the aquifers (Ronen *et al.*, 1988; Deurer *et al.*, 2008; Weymann *et al.*, 2008). Average values of N_2O

at 70 cm depth followed a seasonal pattern of a low at 0.38 µg N L^{-1} in the spring and a high in the fall of 3.40 µg N L^{-1}. In soils, production and emission of N_2O follows the soil temperature signal, where peaks in temperature coincide with peaks in N_2O (Holst *et al.*, 2008). At CMC the concentration of N_2O at 70 to 50 cm was correlated to the water temperature at 50 cm depth. While the one-season lag of the thermal signature is not clearly reflected in the NO_3^- concentrations at depth, concentrations of N_2O clearly display a lagged seasonal influence. Peak N_2O concentrations observed at depth in the fall are the result of a warm and biologically active summer season and the N_2O minimum in the spring coincides with a relatively inactive winter season and colder groundwater temperatures.

The excess N_2O found at the sampling depth of 70 cm was likely due to nitrification or denitrification occurring along the flow path prior to that point. Previous work at CMC has assumed minimal denitrification occurring at depths greater than 60cm. However, we found that the data reveal a significant negative correlation between N_2O and NO_3^- at 70 cm. At that depth of 70 cm, we observed that sample locations with less NO_3^- than the mean for that depth coincided with elevated concentrations of N_2O. The concomitant loss of NO_3^- and increase in N_2O indicates that at these locations, incoming groundwater was subjected to some prior denitrification and biological influence. While the dominant biologically active zone in streambed sediments has been shown to occur in the top 30 cm of sediments at CMC where there is a high concentration of organic matter (Galavotti, 2004; Gu, 2007), the presence of N_2O at 70-cm depth indicates that there is indeed the possibility of denitrification occurring in the aquifer at depths greater than that. Natural variability of carbon distribution in the sediments due to roots can create concentrated microsites of high microbial activity (Parkin, 1987; McClain *et al.*, 2003; Groffman *et al.*, 2009b). In these microsites, DO can drop significantly and denitrification can

occur despite the overall conditions of the aquifer being oxic, ultimately affecting the NO_3^- and N_2O concentrations in the aquifer. In addition, the excess of N_2O found in the deeper ground water could be due to nitrification. N_2O produced via nitrification in oxic groundwater and soil could have accumulated in the aquifer and followed groundwater flow paths to beneath the streambed. Due to the overall oxic conditions of the groundwater reduction of N_2O to N_2 would be minimal allowing for N_2O to persist within the aquifer for long durations. Without deeper groundwater samples we are unable to determine which process was dominantly responsible for the above atmospheric concentrations of N_2O in pore water samples taken at 70 cm depth.

The depth at which denitrification occurs along the flow path appeared to be dependent on the temperature of the groundwater. In the spring, groundwater temperatures were reflective of winter thermal conditions and corresponded to minimal changes of NO_3^- and N_2O concentrations at the deepest sample points. Denitrification in the streambed sediment in the spring was not significant until groundwater reached the carbon rich shallow sediments at 30-cm depth. Conversely, in the fall when the warmest groundwater temperatures reflected summer thermal conditions, large concentrations of N_2O accumulated at the deepest sample depth indicating denitrification occurring deeper than 70 cm. These results correspond well to our sediment column study in which we observed denitrification and N_2O accumulation at deeper sample points in the column at 25°C and at shallower points at 15°C.

In the shallow streambed sediments of CMC NO_3^- loss was observed from 50 cm to the surface with peak losses occurring between 20 cm and the surface. Galavotti (2004) performed denitrification potential assays on sediment columns from CMC and found that potential denitrification rates were greatest from 0 to 30 cm depth which corresponded to increased concentrations of organic matter (up to 5%) at those intervals. Sediment columns acquired in the

winter of 2013 contained similar organic matter profiles of organic matter content of up to 6.25% from 50 to 0 cm. The largest amount of denitrification was observed from 30 to 5 cm depth for all 4 seasons, however the magnitude of NO_3^- removal varied by season. Average NO_3^- removal of 35.5% was seen during all four seasons in 2013, however in the winter samples up to 94% of the incoming NO_3^- at 70 cm was removed by 5 cm depth.

Counter to the hypothesis that the highest nitrate removal would occur during the summer due to warmer surface water temperatures, the highest loss of NO_3^- occurred in the winter. This is likely due to two main environmental factors, organic carbon supply and groundwater temperature. The combination of fresh labile carbon input in the fall and the increased frequency of storm events in the winter would be optimal conditions to incorporate the fresh carbon into the surface layer of the sediment. Indeed, we observed a large loss of up to 8 mg N L^{-1} of NO_3^- from 5 to 10 cm depth in the winter. In addition, due to the gaining nature of CMC, groundwater temperature at 50-cm depth was found to average 16°C which was warmer than the groundwater in the spring and summer. The sediment column experiments showed that increased temperature results in an increase in denitrification and NO_3^- loss along flow paths. The seasonal delay effect of groundwater temperature brings warm fall water into the streambed sediment where the increased temperature in combination with the labile carbon inputs encourages more denitrification to occur in the winter.

In the fall, groundwater temperatures were also at a high, reflecting the seasonal delay of summer temperatures; however, significantly less NO_3^- was removed compared with winter. The fall samples revealed only 11.3% NO_3^- removal and they had minimal denitrification occurring in the top 30 cm of sediment. The fall sample was acquired just prior to leaf drop and reflects a year's worth of labile carbon depletion. Mulholland and Hill (1997) found in a 7 year-

long study of a first order stream, that there was a yearly minimum of DOC in the late summer just prior to leaf drop. It is possible that the lack of fresh labile carbon sources could be the main driver for why there is minimal denitrification activity observed in the fall despite the high groundwater temperatures. Without seasonal carbon measurements, however, the reason for the minimal denitrification activity that occurred in the fall sample cannot be fully identified.

In most sample profiles, for all seasons, N_2O was being removed along the flow path, resulting in net losses of N_2O. The stream bed sediments were effectively removing N_2O and completing the denitrification reaction in the last 70 cm of sediment removing 1 to 85% of the N_2O found at 70 cm. The concentrations of N_2O at 5 cm depth were on average lower than that at 70 cm as a result of N_2O removal. No significant difference was seen in the percent of N_2O removed for each season; therefore N_2O values at 5-cm depth reflected the seasonal trend of inflowing concentrations of N_2O at 70 cm depth. Concentrations of N_2O at 5 cm were higher in the winter and fall reflecting the seasonal lag of high biological activity in the summer and fall and concentrations of N_2O were lower in the spring reflecting the minimal activity of the winter.

There was a zonation of reaction steps of N_2O production and removal in the sediment profiles along a vertical flow path for all seasons. Removal of N_2O was concentrated in two areas along the profiles at 70 to 30 cm and 5 to 10 cm depth. The areas of preferential N_2O removal precede and follow the areas of greatest denitrification and N_2O production. At the deepest sample points we found an increase in preferential removal of inflowing N_2O over that of NO_3^-. However, as the groundwater entered the carbon rich depths of 30 to 5 cm, denitrification increased and N_2O was produced more rapidly than it was reduced. N_2O accumulated over 30 to 5cm depth as NO_3^- removal was the dominate process occurring. The increase in N_2O concentration and decrease in NO_3^- over the denitrification zone of 30 to 5 cm

was followed by another zone of increased preferential removal of N_2O in the last 5 cm of the sample profile. These results are in agreement with the sediment column experiments. In the column experiments we were only able to observe a small portion of the deepest N_2O removal zone at 25°C due to a small build-up of N_2O at the deepest sample point, otherwise the AGW was at atmospheric equilibrium of N_2O. For all temperature scenarios the zone of increased NO_3^- removal and N_2O production was in the middle of the columns followed immediately by a zone of N_2O removal. Due to the advective nature of these systems we are observing the reaction steps of denitrification along the flow path instead of occurring over time in stagnant conditions. Bergaust et al. [2011] demonstrated the timing of the peak in nosZ transcription coincided with the depletion of NO_3^- and increase of N_2O over reaction time. The zonation of reaction processes is a result of this cellular control of denitrification over distance in the column instead of time.

The balance of gain and loss of N_2O along the flow path for all seasons most commonly resulted in a net removal of N_2O. This observation has positive implications for the measure of efficiency of the microbial communities within the streambed sediments to bring denitrification to full completion (producing only N_2). If riparian zones and the streambed sediments are viewed as a natural buffer to removing NO_3^- from contaminated aquifers they would be most advantageous if they were able to remove NO_3^- with no other costs to the environment (i.e. no GHG emissions) (Weller *et al.*, 1994; Hill, 1996; Willems *et al.*, 1997). The microbial communities within the streambed sediments at CMC have shown to effectively reduce the concentrations of both NO_3^- and N_2O along a vertical flow path in streambed sediments reducing both unwanted pollutants.

Despite an average net loss of N_2O along the flow paths for all seasons, there were still locations in the sample area where net gains of N_2O occurred and ultimately contributed to benthic N_2O fluxes. Fluxes of N_2O were heterogeneous across the sample area, and were correlated with areas of low NO_3^- fluxes, indicating areas of high denitrification activity. Areas of high denitrification have been identified as often crucial to overall nitrogen balance of a study area (McClain *et al.*, 2003; Groffman *et al.*, 2009b). Areas of concentrated denitrification at the streambed surface produce large amounts of N_2O with minimal reaction time for N_2O removal. These locations are significant contributors to the overall flux of N_2O from the streambed sediments. In the winter, one sample location was responsible for 97% of the N_2O emitted of all the samples. In the spring to the fall, the impact of these concentrated areas was around 37% of the N_2O efflux to surface water. Previous studies have shown that these areas of high denitrification are controlled dominantly by available carbon and oxygen concentrations which can be highly variable in a natural aquatic environment and difficult to capture with a limited number of samples (Groffman *et al.*, 2009b). This study was able to capture a few of these highly active locations and observed N_2O effluxes ranging over 5 orders of magnitude, demonstrating that there is wide heterogeneity in N_2O and that prediction of N_2O efflux may be a difficult task for GHG emission models.

The annual mean N_2O efflux from the streambed sediment was 119 μg N m^{-2} h^{-1} similar to the mean of 154 μg N m^{-2} h^{-1} for all experimental scenarios in the sediment column study. These values are comparable to agricultural and urban canals in Mexico and from the agricultural LII river in New Zealand at 165 and 171 μg N m^{-2} h^{-1} respectively (Harrison & Matson, 2003; Clough *et al.*, 2006); however, in these studies N_2O effluxes could be the result of both nitrification and denitrification, as these studies were focused on water column and hyporheic

processes. The values from the present study represent N_2O effluxes from the groundwater to the surface water. CMC is characterized by minimal hyporheic exchange and oxic surface water would likely preclude further removal of N_2O, therefore we can assume that N_2O efflux values are well representative of the values measured in the surface water. Comparisons of N_2O efflux from soils and waterways show that there are large variations in both environments and that they can have comparable N_2O effluxes (Table 4.2). Previous measurements of N_2O flux from soils within 50 meters of CMC proved to be below detectable limits (<29.9 μg N m^{-2} h^{-1}), however, a couple samples closest to the creek detected fluxes around 158.4 μg N m^{-2} h^{-1} (Funk, 2011) indicating the potential for significant fluxes to be occurring at the nearby soils as well.

Table 4.2 Comparison of N_2O emission rates from streams, rivers, and soils.

Site	Mean N_2O Emission Rate (μg N m^{-2} h^{-1})	Reference
Agricultural/ urban canals, Mexico	165.00	*Harrison and Mattson* [2003]
Platte River	62.00	*McMahon and Dennehy* [1999]
LII River, New Zealand	171.00	*Clough et al. [*2006]
Nuese River, North Carolina	12.90	*Stow et al.* [2005]
Hudson River, New York	6.40	*Cole and Caraco* [2001]
Agricultural drains, Japan	7440.00	*Hasegawa et al.* [2000]
USA headwater streams	35.20	*Beaulieu et al.* [2008]
Suburban and agricultural rivers	420.21	*Laursen and Seitzinger* [2004]
Boreal river	37.94	*Silvennoinen et al.* [2008]
River estuary	13.45	*LaMontagne et al.* [2002]
Riparian soil	798	Machefert *et al.* [2003]
Riparian soil	109	*Machefert et al.* [2003]
Riparian soil	4.45	*Weller et al. [*1994]
Un-grazed steepe soil	8.2	*Holst et al.* [2008]
Soil near Cobb Mill Creek	<29.9	*Funk* [2011]
Cobb Mill Creek	119	This study

Emission factor 5 (EF5) is a value designated by the International Panel on Climate Change in order to predict the amount of N_2O produced for every kilogram of NO_3^- leached from an agricultural area (Eggleston *et al.*, 2006). There has been much debate over the correct value

to assign to EF5-g, the aquifer component of EF5 (Nevison, 2000; Reay *et al.*, 2005) as well as the suggestion that riparian zones be represented separately within the calculation of EF5 (Hefting *et al.*, 2003). Hefting (2003) suggested that an EF5-rip value might be on the order of 0.016 to 0.058 in comparison to the suggested downgrade value for EF5-g of 0.001 by Nevison [2000]. Currently EF5-g is set at 0.0025 based on suggested revisions and the addition of more observations (Eggleston *et al.*, 2006). EF5-g values calculated for the present sediment column experiments and field samples are 0.007 and 0.003 respectively which are well within the range of uncertainty of 0.0005 to 0.025 for EF5.

The EF5-g value for the columns of 0.007 is larger than the IPCC established value of 0.0025, however the former value is based on a large range of different environmental conditions representing 36 combinations of flow, temperature, and NO_3^- input. It is important to encapsulate a large variety of environmental conditions especially in order to predict future changes in this emission factor. The results from the column study have shown that increasing NO_3^- inputs results in higher N_2O yields. In addition, both the field and column results have shown an increase in N_2O production as the result of increased temperature. These results suggest that we might expect to observe overall increases in N_2O fluxes to the atmosphere as groundwater NO_3^- loading and temperature increase.

Predictions of increasing NO_3^- loads to aquifers and waterways on the ESVA are expected to cause an increase in NO_3^- concentration in shallow aquifers of close to 0.5 mg N L^{-1} per year (Böhlke & Denver, 1995; Flewelling, 2009). The increase of NO_3^- to the shallow aquifer is not expected to level off until 40 years after fertilizer application rates plateau (Flewelling, 2009). Assuming no other environmental changes, we speculate that by the year 2050 the average groundwater concentration of NO_3^- beneath CMC would reach 26 mg N L^{-1}.

Using the model that was developed to simulate changes in N_2O fluxes with changing groundwater NO_3^- concentration and temperature we are able to predict the magnitude of change we could expect to observe in N_2O emissions in 2050. In 2013 annual mean flux of N_2O was 9.00 µg N m^{-2} h^{-1} (disregarding an outlier of 3322.9 µg N m^{-2} h^{-1}). Using average conditions measured in the field of 15 ^oC groundwater temperature, 8 mg N L^{-1} groundwater NO_3^- concentration, and a pore water velocity of 0.7 cm h^{-1} the model predicts a flux of 9.62 µg N m^{-2} h^{-1}. For the whole stream reach this flux equates to an annual emission of 435.9 g N_2O-N per year. If we were to extrapolate our model to the predicted change in groundwater NO_3^- concentration of 26 mg N L^{-1} by 2050 the annual emission would rise to 4076.2 g N_2O-N per year, effectively raising the annual emissions by 835%. In addition, rising stream water temperatures in North America have been observed on the range of 0.009 to 0.077 °C per year (Kaushal *et al.*, 2010). Applying an increase in groundwater and stream water temperature of 1.5 ^oC by 2050 without a change in the current groundwater NO_3^- concentration annual emissions would increase to 491.8 g N per year only a 12.8% increase from current annual emissions. Applying both an increase in groundwater NO_3^- concentration and temperature annual emissions would be predicted to be 4599.5 g N per year increasing the 2013 annual emissions by 955%. While increase in water temperatures are expected to be minimal compared to the predicted increase in groundwater NO_3^- concentration on the ESVA, together these changes are estimated to drastically increase the emissions of N_2O at CMC. The model created here could be of much use for predicting changes of annual emissions at stream sites similar to that of CMC where we see significant denitrification occurring in shallow streambed sediments.

5 Conclusion

Nitrate leached from agricultural fields and denitrified along a groundwater flow path results in indirect N_2O emissions estimated to be between 0.13 to 7.7 Tg N per year and are a significant contributor to global N_2O emission budgets (Nevison, 2000). Through the use of data collected from field work performed in four seasons and sediment column experiments we have been able to discern physicochemical controls on N_2O production and removal in the streambed sediments of a second order agricultural stream. The column study showed that NO_3^- fluxes are dominantly defined by the input NO_3^- concentration and the residence time, where longer residence times allow for more denitrification to occur reducing NO_3^- fluxes. N_2O fluxes have large variance, but they are dominantly controlled by inflowing NO_3^- concentrations. Increasing NO_3^- concentrations had a significant impact on increasing the N_2O yield of the sediment columns and concomitant N_2O fluxes.

A seasonal signal of N_2O fluxes was observed at Cobb Mill Creek that reflected a seasonal lag in groundwater temperature. Measurements at depth allowed quantification of the denitrification and N_2O reactions beneath the sediment surface where a zonation of denitrification reaction steps occurring around the carbon rich depth of 30 to 5cm was observed. In many sample profiles N_2O was removed by denitrification prior to effluxing at the sediment surface, however not all N_2O was reduced and a few singular sample locations were responsible for up to 97% of the N_2O flux in the sample area. Ultimately, streambed sediments in low relief coastal streams can be a site of significant denitrification, however in an open system with advective fluxes, N_2O is not fully reduced to N_2 and substantial N_2O emissions result. While riparian zones are afforded high accolades for providing the ecosystem service of denitrification of agricultural nitrate, this service comes at a cost of N_2O emissions. This cost will increase with

the increasing pressures we put on riparian zones through increasing NO_3^- loading and rising stream temperatures.

References

Ambus P (1993) Control of denitrification enzyme activity in a streamside soil. *FEMS Microbiology Letters,* **102**, 225-234.

Angier JT, Mccarty GW (2008) Variations in base-flow nitrate flux in a first-order stream and riparian zone. *Journal of the American Water Resources Association,* **44**, 367-380.

Beaulieu JJ, Arango CP, Hamilton SK, Tank JL (2008) The production and emission of nitrous oxide from headwater streams in the Midwestern United States. *Global Change Biology,* **14**, 878-894.

Beaulieu JJ, Tank JL, Hamilton SK *et al.* (2011) Nitrous oxide emission from denitrification in stream and river networks. *Proceedings of the National Academy of Sciences of the United States of America,* **108**, 214-219.

Bergaust L, Bakken L, Frostegård A (2011) Denitrification regulatory phenotype, a new term for the characterization of denitrifying bacteria. *Biochemical Society Transactions,* **39**, 207-212.

Blackmer AM, Jbremner JM (1978) Inhibitory effect of nitrate on reduction of N_2O to N_2 by soil microorganisms. *Soil Biology & Biochemistry,* **39**, 187-191.

Böhlke JK, Denver JM (1995) Combined use of groundwater dating, chemical, and isotopic analyses to resolve the history and fate of nitrate contamination in 2 agricultural watersheds, Atlantic Coastal- Plain, Maryland. *Water Resources Research,* **31**, 2319-2339.

Bolster CH, Jr. (2000) Effect of heterogeneity on bacterial transport and deposition. Ph.D. Dissertation, University of Virginia, Charlottesville, 173 pp.

Bouwman AF (1996) Direct emission of nitrous oxide from agricultural soils. *Nutrient Cycling in Agroecosystems,* **46**, 53-70.

Bouwman AF, Beusen AHW, Griffioen J *et al.* (2013) Global trends and uncertainties in terrestrial denitrification and N_2O emissions. *Philosophical Transactions of the Royal Society B-Biological Sciences,* **368**.

Bouwman AF, Stehfest E, Van Kessel C (2010) Nitrous oxide emissions from the nitrogen cycle in arable agriculture: Estimation and mitigation. In: *Nitrous Oxide and Climate Change.* (ed Smith K) pp Page. London, Earthscan, Ltd.

Boyer EW, Alexander RB, Parton WJ *et al.* (2006) Modeling denitrification in terrestrial and aquatic ecosystems at regional scales. *Ecological Applications,* **16**, 2123-2142.

Bredehoeft JD, Papadopolous SS (1965) Rates of vertical groundwater movement estimated from the Earth's thermal profile. *Water Resources Research,* **2**, 325-328.

Christensen PB, Sorensen J (1988) Denitrification in sediment of lowland streams - regional and seasonal-variation in Gelbaek and Rabis-Baek, Baek, Denmark. *FEMS Microbiology Ecology,* **53**, 335-344.

Clough TJ, Bertram JE, Sherlock RR, Leonard RL, Nowicki BL (2006a) Comparison of measured and EF5-r-derived N_2O fluxes from a spring-fed river. *Global Change Biology,* **12**, 477-488.

Clough TJ, Bertram JE, Sherlock RR, Leonard RL, Nowicki BL (2006b) Comparison of measured and EF5-r-derived N_2O fluxes from a spring-fed river. *Global Change Biology,* **12**, 352-363.

Cobb PR, Smith DW (1989) Soil Survey of Northampton County, Virginia. (ed U. S. Department of Agriculture SCS) pp Page, U. S. Department of Agriculture, Soil Conservation Service.

Cole JJ, Caraco NF (2001) Emissions of nitrous oxide (N_2O) from a tidal, freshwater river, the Hudson River, New York. *Environmental Science & Technology*, **35**, 991-996.

Crutzen PJ (1981) Atmospheric chemical processes of the oxides of nitrogen, including nitrous oxide. In: *Denitrification, Nitrification, and Atmospheric Nitrous Oxide.* (ed Delwiche CC) pp Page. New York, NY, John Wiley & Sons.

Dawson RN, Murphy KL (1972) Temperature dependency of biological denitrification. *Water Research*, **6**, 71-&.

Debrewer LM, Ator SW, Denver JM (2007) Factors Affecting Spatial and Temporal Variability in Nutrient and Pesticide Concentrations in the Surficial Aquifer on the Delmarva Peninsula. pp Page, Reston, VA, U.S. Geological Survey.

Deurer M, Von Der Heide C, Bottcher J, Duijnisveld WHM, Weymann D, Well R (2008) The dynamics of N_2O near the groundwater table and the transfer of N_2O into the unsaturated zone: A case study from a sandy aquifer in Germany. *Catena*, **72**, 362-373.

Dillow JJA, Greene EA (1999) Groundwater Discharge and Nitrate Loadings to the Coastal Bays of Maryland. pp Page, Baltimore, U.S. Geological Survey.

Eggleston S, Buendia L, Miwa K, Ngara T, Tanabe K (eds) (2006) *2006 IPCC Guidelines for National Greenhouse Gas Inventories, Prepared by the National Greenhouse Gas Inventories Programme*.

Fetter CW (2001) *Applied Hydrogeology*, New York, Macmillan Publishing Company.

Firestone MK, Smith MS, Firestone RB, Tiedje JM (1979) Influence of nitrate, nitrite, and oxygen on the composition of the gaseous products of denitrification in soil. *Soil Science Society of America Journal*, **43**, 1140-1144.

Flewelling SA (2009) Nitrogen storage and removal in catchments on the Eastern Shore of Virginia. Unpublished Ph.D. Ph.D. Dissertation, University of Virginia, Charlottesville, VA.

Forster P, Ramaswamy V, Artaxo P *et al.* (2007) Changes in atmospheric constituents and in radiative forcing. In: *Climate Change 2007: The Physical Science Basis.* (eds Solomon S, Qin D, Manning M, Chen Z, Marquis M, Averyt KB, Tignor M, Miller HL) pp Page., Cambridge University Press.

Foster NW, Nicolson JA, Hazlett PW (1989) Temporal variation in nitrate and nutrient cations in drainage waters from a deciduous forest. *Journal of Environmental Quality*, **18**, 238-244.

Funk C (2011) Factors contributing to spatial variability of N_2O fluxes in a Virginia Salt Marsh. Unpublished MS Thesis, University of Virginia, Charlottesville, VA.

Galavotti H (2004) Spatial profiles of sediment denitrification at the ground water - surface water interface in Cobb Mill Creek on the Eastern Shore of Virginia Unpublished MS MS, University of Virginia, Charlottesville.

Galloway JN, Aber JD, Erisman JW, Seitzinger SP, Howarth RW, Cowling EB, Cosby BJ (2003) The nitrogen cascade. *Bioscience*, **53**, 341-356.

Galloway JN, Dentener FJ, Capone DG *et al.* (2004) Nitrogen cycles: past, present, and future. *Biogeochemistry*, **70**, 153-226.

Garcia-Ruiz R, Pattinson SN, Whitton BA (1998) Kinetic parameters of denitrification in a river continuum. *Applied and Environmental Microbiology*, **64**, 2533-2538.

Groffman PM (1994) Denitrification in freshwater wetlands. *Current Topics in Wetland Biogeochemistry*, **1**, 15-35.

Groffman PM, Butterbach-Bahl K, Fulweiler RW *et al.* (2009a) Challenges to incorporating spatially and temporally explicit phenomena (hotspots and hot moments) in denitrification models. *Biogeochemistry*, **93**, 49-77.

Groffman PM, Davidson EA, Seitzinger S (2009b) New approaches to modeling denitrification. *Biogeochemistry*, **93**, 1-5.

Groffman PM, Gold AJ, Kellogg DQ, Addy K (2002) Mechanisms, rates and assessment of N_2O in groundwater, riparian zones and rivers. In: *Non-CO_2 Greenhouse Gases.* (eds Van Ham J, Baede APM, Guichert R, Williams-Jacobse JGFM) pp Page. Rotterdam, Millpress.

Gu C (2007) Hydrological control on nitrate delivery through the groundwater surface water interface. Unpublished Ph.D Ph.D., University of Virginia, Charlottesville, 250 pp.

Gu C, Hornberger GM, Mills AL, Herman JS (2008a) The effect of freshets on the flux of groundwater nitrate through streambed sediments. *Water Resources Research*, **doi:10.1029/2007WR006488**.

Gu C, Hornberger GM, Mills AL, Herman JS (2008b) Influence of stream-aquifer interactions in the riparian zone on nitrate flux to a low-relief coastal stream. *Water Resources Research*, **44**.

Gu C, Hornberger GM, Mills AL, Herman JS, Flewelling SA (2007) Nitrate reduction in streambed sediments: effects of flow and biogeochemical kinetics. *Water Resources Research*, **43**, W12413, doi:12410.11029/12007WR006027.

Harrison J, Matson P (2003) Patterns and controls of nitrous oxide emissions from waters draining a subtropical agricultural valley. *Global Biogeochemical Cycles*, **17**.

Hedin LO, Von Fischer JC, Ostrom NE, Kennedy BP, Brown MG, Robertson GP (1998) Thermodynamic constraints on nitrogen transformations and other biogeochemical processes at soil-stream interfaces. *Ecology*, **79**, 684-703.

Hefting MM, Bobbink R, De Caluwe H (2003) Nitrous oxide emission and denitrification in chronically nitrate-loaded riparian buffer zones. *Journal of Environmental Quality*, **32**, 1194-1203.

Hefting MM, Bobbink R, Janssens MP (2006) Spatial variation in denitrification and N_2O emission in relation to nitrate removal efficiency in a N-stressed riparian buffer zone. *Ecosystems*, **9**, 550-563.

Hefting MM, Clement JC, Bienkowski P *et al.* (2005) The role of vegetation and litter in the nitrogen dynamics of riparian buffer zones in Europe. *Ecological Engineering*, **24**, 465-482.

Hill AR (1996) Nitrate removal in stream riparian zones. *Journal of Environmental Quality*, **25**, 743-755.

Hirsch AI, Michalak AM, Bruhwiler LM, Peters W, Dlugokencky EJ, Tans PP (2006) Inverse modeling estimates of the global nitrous oxide surface flux from 1998-2001. *Global Biogeochemical Cycles*, **20**.

Holst J, Liu C, Yao Z, Brueggemann N, Zheng X, Giese M, Butterbach-Bahl K (2008) Fluxes of nitrous oxide, methane and carbon dioxide during freezing-thawing cycles in an Inner Mongolian steppe. *Plant and Soil*, **308**, 105-117.

Holtan-Hartwig L, Dorsch P, Bakken LR (2002) Low temperature control of soil denitrifying communities: kinetics of N_2O production and reduction. *Soil Biology and Biochemistry,* **34**, 1797-1806.

Hubbard SS, Chen J, Peterson J *et al.* (2001) Hydrological characterization of the South Oyster bacterial transport site using geophysical data. *Water Resources Research,* **37**, 2431-2456.

Hutchinson GL, Davidson EA (1993) Processes for production and consumption of gaseous nitrogen oxides in soil. In: *Agricultural Ecosystem Effects on Trace Gases and Global Climate Change.* (eds Rolston DE, Duxbury JM, Harper LA, Mosier AR) pp Page. Madison WI, American Society of Agronomy.

Hutchinson GL, Guenzi WD, Livingston GP (1993) Soil-water controls on aerobic soil emission of gaseous nitrogen-oxides. *Soil Biology & Biochemistry,* **25**, 1-9.

Hynes RK, Knowles R (1984) Production of nitrous-oxide by *Nitrosomonas-europaea* - effects of acetylene, pH, and oxygen. *Canadian Journal of Microbiology,* **30**, 1397-1404.

Kaushal SS, Likens GE, Jaworski NA *et al.* (2010) Rising stream and river temperatures in the United States. *Frontiers in Ecology and the Environment,* **8**, 461-466.

Lindsey BD, Phillips SW, Donnelly CA *et al.* (2003) Residence times and nitrate transport in ground water discharging to streams in the Chesapeake Bay watershed. pp Page, New Cumberland, PA, US Department of the Interior, US Geological Survey.

Lowrance R, Altier LS, Newbold JD *et al.* (1997) Water quality functions of riparian forest buffers in Chesapeake Bay watersheds. *Environmental Management,* **21**, 687-712.

Ludwig B, Jager N, Priesack E, Flessa H (2011) Application of the DNDC model to predict N_2O emissions from sandy arable soils with differing fertilization in a long-term experiment. *Journal of Plant Nutrition and Soil Science,* **174**, 350-358.

Maag M, Vinther FP (1996) Nitrous oxide emission by nitrification and denitrification in different soil types and at different soil moisture contents and temperatures. *Applied Soil Ecology,* **4**, 5-14.

Machefert SE, Dise NB (2004) Hydrological controls on denitrification in riparian ecosystems. *Hydrology and Earth System Sciences,* **8**, 686-694.

Malhi SS, Mcgill WB, Nyborg M (1990) Nitrate losses in soils - effect of temperature, moisture and substrate concentration. *Soil Biology & Biochemistry,* **22**, 733-737.

Marxsen J, Fiebig DM (1993) Use of perfused cores for evaluating extracellular enzyme-activity in stream-bed sediments. *FEMS Microbiology Ecology,* **13**, 1-11.

Mcclain ME, Boyer EW, Dent CL *et al.* (2003) Biogeochemical hot spots and hot moments at the interface of terrestrial and aquatic ecosystems. *Ecosystems,* **6**, 301-312.

Mills AL, Herman JS, Anutaliya A (2011) Sediments as filters of applied nitrogen from discharging groundwater to low-relief coastal streams. In: *Coastal and Estuarine Research Federation.* pp Page, Daytona Beach, FL.

Mills AL, Hornberger GM, Herman JS (2008) Sediments in low-relief coastal streams as effective filters of agricultural nitrate. In: *AWRA Specialty Conference on Riparian Processes.* pp Page, Norfolk, VA, American Water Resources Association.

Molstad L, Dorsch P, Bakken LR (2007) Robotized incubation system for monitoring gases (O_2, NO, N_2O,N_2) in denitrifying cultures. *Journal of Microbiological Methods,* **71**, 202-211.

Mosier A, Kroeze C, Nevison C, Oenema O, Seitzinger S, Van Cleemput O (1998) Closing the global N_2O budget: nitrous oxide emissions through the agricultural nitrogen cycle -

OECD/IPCC/IEA phase II development of IPCC guidelines for national greenhouse gas inventory methodology. *Nutrient Cycling in Agroecosystems,* **52**, 225-248.

Mulholland PJ, Hill WR (1997) Seasonal patterns in streamwater nutrient and dissolved organic carbon concentrations: Separating catchment flow path and in-stream effects. *Water Resources Research,* **33**, 1297-1306.

Murray AE, Hollibaugh JT, Orrego C (1996) Phylogentic compositions of bacterioplankton from two California estuaries compared by denaturing gradient gel electrophoresis of 16S rRNA fragments. *Applied and Environmental Microbiology,* **62**, 2676-2680.

Murray JP, Parks GA (1980) Poliovirus adsorption on oxide surfaces. In: *Particulates in Water.* (eds Kavenaugh MC, Leckie JO) pp Page. Washington, DC, American Chemical Society.

Nevison C (2000) Review of the IPCC methodology for estimating nitrous oxide emissions associated with agricultural leaching and runoff. *Chemosphere - Global Change Science,* **2**, 493-500.

Nixon SW (1995) Coastal marine eutrophication - a definition, social causes, and future concerns. *Ophelia,* **41**, 199-219.

Nommik H (1956) Investigations on denitrification in soil. *Acta Agricultura Scandinavia,* **6**, 195-228.

Ocampo CJ, Oldham CE, Sivapalan M (2006a) Nitrate attenuation in agricultural catchments: Shifting balances between transport and reaction. *Water Resources Research,* **42**.

Ocampo CJ, Oldham CE, Sivapalan M, Turner JV (2006b) Hydrological versus biogeochemical controls on catchment nitrate export: a test of the flushing mechanism. *Hydrological Processes,* **20**, 4269-4286.

Ocampo CJ, Sivapalan M, Oldham C (2006c) Hydrological connectivity of upland-riparian zones in agricultural catchments: Implications for runoff generation and nitrate transport. *Journal of Hydrology,* **331**, 643-658.

Ocampo CJ, Sivapalan M, Oldham CE (2006d) Field exploration of coupled hydrological and biogeochemical catchment responses and a unifying perceptual model. *Advances in Water Resources,* **29**, 161-180.

Parkin TB (1987) Soil microsites as a source of denitrification variability. *Soil Science Society of America Journal,* **51**, 1194-1199.

Pina-Ochoa E, Alvarez-Cobelas M (2006) Denitrification in aquatic environments: A cross-system analysis. *Biogeochemistry,* **81**, 111-130.

Ravishankara AR, Daniel JS, Portmann RW (2009) Nitrous oxide (N_2O): The dominant ozone-depleting substance emitted in the 21st century. *Science,* **326**, 123-125.

Reay DS, Smith KA, Edwards AC, Hiscock KM, Dong LF, Nedwell DB (2005) Indirect nitrous oxide emissions: revised emission factors. *Environmental Sciences,* **2**, 153-158.

Richardson DL (1992) Hydrogeology and analysis of the groundwater flow system of the Eastern Shore, Virginia. pp Page, Reston, VA, U.S. Geological Survey.

Ronen D, Magaritz M, Almon E (1988) Contaminated aquifers are a forgotten component of the global N_2O budget. *Nature,* **335**, 57-59.

Seitzinger S, Harrison JA, Bohlke JK *et al.* (2006) Denitrification across landscapes and waterscapes: A synthesis. *Ecological Applications,* **16**, 2064-2090.

Seitzinger SP, Kroeze C, Styles RV (2000) Global distribution of N_2O emissions from aquatic systems: natural emissions and anthropogenic effects. *Chemosphere: Global Change Science,* **2**, 267-279.

Sheibley RW, Duff JH, Jackman AP, Triska FJ (2003) Inorganic nitrogen transformations in the bed of the Shingobee River, Minnesota: integrating hydrologic and biological processes using sediment perfusion cores. *Limnology and Oceanography,* **48**, 1129-1140.

Silvennoinen H, Liikanen A, Torssonen J, Stange CF, Martikainen PJ (2008a) Denitrification and N_2O effluxes in the Bothnian Bay (northern Baltic Sea) river sediments as affected by temperature under different oxygen concentrations. *Biogeochemistry,* **88**, 63-72.

Silvennoinen H, Liikanen A, Torssonen J, Stange CF, Martikainen PJ (2008b) Denitrification and nitrous oxide effluxes in boreal, eutrophic river sediments under increasing nitrate load: a laboratory microcosm study. *Biogeochemistry,* **91**, 105-116.

Simek M, Cooper JE (2002) The influence of soil pH on denitrification: progress towards the understanding of this interaction over the last 50 years. *European Journal of Soil Science,* **53**, 345-354.

Simek M, Jisova L, Hopkins DW (2002) What is the so-called optimum pH for denitrification in soil? *Soil Biology & Biochemistry,* **34**, 1227-1234.

Sinnott A, Tibbetts Jr. GC (1968) Ground-water Resources of Accomack and Northampton Counties, Virginia. pp Page, Charlottesville, VA, Department of Conservation and Economic Development, Division of Mineral Resources, Commonwealth of Virginia.

Smith KA (1997) The potential for feedback effects induced by global warming on emissions of nitrous oxide by soils. *Global Change Biology,* **3**, 327-338.

Smith KA, Crutzen PJ, Mosier AR, Winiwarter W (2010) The global nitrous oxide budget: A reassessment. In: *Nitrous Oxide and Climate Change.* (ed Smith K) pp Page. London, Earthscan, Ltd.

Smith MS, Firestone MK, Tiedje JM (1978) Acetylene inhibition method for short-term measurement of soil denitrification and its evaluation using n-13. *Soil Science Society of America Journal,* **42**, 611-615.

Tesoriero AJ, Liebscher H, Cox SE (2000) Mechanism and rate of denitrification in an agricultural watershed: Electron and mass balance along groundwater flow paths. *Water Resources Research,* **36**, 1545-1559.

Tesoriero AJ, Saad DA, Burow KR, Frick EA, Puckett LJ, Barbash JE (2007) Linking ground-water age and chemistry data along flow paths: Implications for trends and transformations of nitrate and pesticides. *Journal of Contaminant Hydrology,* **94**, 139-155.

Tesoriero AJ, Spruill TB, Mew Jr. HE, Farrell KM, Harden SL (2005) Nitrogen transport and transformations in a coastal plain watershed: Influence of geomorphology on flow paths and residence times. *Water Resources Research,* **41**.

Tiedje JM (1988) Ecology of denitrification and disimilatory reduction of nitrate to ammonia. In: *Biology of anaerobic microorganisms.* (ed Zehnder AJB) pp Page. New York, Wiley-Liss.

Tiedje JM (1994) Denitrifiers. In: *Methods of Soil Analysis. Part 2. Microbiological and Biochemical Properties.* (ed Page AL) pp Page. Madison, WI, Soil Science Society of America.

Tilman D (1987) Secondary succession and the pattern of plant dominance along experimental nitrogen gradients. *Ecological Monographs,* **57**, 189-214.

Toride N, Leij FJ, Van Genuchten MT (1995) The CXTFIT code for estimating transport parameters from laboratory or field tracer experiments, Version 2.0. pp Page, Riverside, CA, Agricultural Research Service, USDA.

(2009) 2007 Census of Agriculture. U. S. Department of Agriculture. http://www.agcensus.usda.gov/Publications/2007/.

Vitousek PM, Aber JD, Howarth RW *et al.* (1997) Human alteration of the global nitrogen cycle: Sources and consequences. *Ecological Applications,* **7**, 737-750.

Von Der Heide C, Bottcher J, Deurer M, Weymann D, Well R, Duijnisveld WHM (2008) Spatial variability of N_2O concentrations and of denitrification-related factors in the surficial groundwater of a catchment in Northern Germany. *Journal of Hydrology,* **360**, 230-241.

Wayne RP (2000) *Chemistry of Atmospheres,* Oxford, Oxford University Press.

Weier KL, Doran JW, Power JF, Walters DT (1993) Denitrification and the dinitrogen nitrous-oxide ratio as affected by soil-water, available carbon, and nitrate. *Soil Science Society of America Journal,* **57**, 66-72.

Well R, Weymann D, Flessa H (2005) Recent research progress on the significance of aquatic systems for indirect agricultural N_2O emissions. *Environmental Sciences,* **2**, 143-151.

Weller D, Correll DL, Jordan TE (1994) Denitrification in riparian forests receiving agricultural discharges. In: *Global Wetlands: Old World and New.* (ed Mitsch WJ) pp Page. Amsterdam, Elsevier.

Weymann D, Well R, Flessa H *et al.* (2008) Groundwater N_2O emission factors of nitrate-contaminated aquifers as derived from denitrification progress and N_2O accumulation. *Biogeosciences,* **5**, 1215-1226.

Wilhelm E, Battino R, Wilcock RJ (1977) Low-pressure solubility of gases in liquid water. *Chemical Reviews,* **77**, 219-262.

Willems HPL, Rotelli MD, Berry DF, Smith EP, Reneau RB, Mostaghimi S (1997) Nitrate removal in riparian wetland soils: Effects of flow rate, temperature, nitrate concentration and soil depth. *Water Research,* **31**, 841-849.

Woodside W, Messmer J (1961) Thermal conductivity of porous media, I, Unconsolidated sand. *Journal of Applied Physics,* **32**, 1688-1699.

Wuebbles DJ (2009) Nitrous Oxide: No Laughing Matter. *Science,* **326**, 56-57.